Relative changes of the biomechanical properties of living rabbit brain tested under controlled physiologic conditions with stress-relaxation indentation

by

Colin John Kazina

A Thesis submitted to the Faculty of Graduate Studies of

The University of Manitoba

in partial fulfilment of the requirements of the degree of

DOCTOR OF PHILOSOPHY

Department of Biosystems Engineering

University of Manitoba

Winnipeg, Canada

ABSTRACT

Mechanical testing of living brain with control or measurement of all potential sources of variability is difficult and not often or consistently performed. The primary objective of the current work is to compare mechanical properties of the living rabbit brain across relatively high and low groupings of arterial blood partial pressure of carbon dioxide (pCO_2) and mean arterial pressure (MAP), with control or measurement of all deformation, anatomical, and other physiological variables. It is hypothesized that there are significant differences in relative viscoelastic properties of the living rabbit brain under different combinations of pCO_2 and blood pressure.

Stress-relaxation brain indentations were performed on seven consecutive anesthetized living rabbits, with control or measurement of all possible variables.. Five indentations were performed on each animal, with 15 minute periods of rest between each indentation, with the following relative physiological parameters:

Indentation 1. Low MAP and low pCO_2.

Indentation 2. High MAP and low pCO_2.

Indentation 3. Low MAP and high pCO_2.

Indentation 4. High MAP and high pCO_2.

Indentation 5. Low MAP and low pCO_2.

The data were fitted to a generalized Maxwell model that incorporated two viscoelastic terms and one equilibrium elastic term. The relative stress-relaxation

coefficients and material properties were determined, and compared using statistical analysis. Peak stresses encountered with relative step-loading ranged from approximately 2-4 x 10^3 Pa, with corresponding “instantaneous” elastic moduli approximating 4-8 x 10^3 Pa. A short and long Time of Relaxation was determined for each viscoelastic term of the model, and ranged from 0.03 – 1.72 s and 9.92 – 32.55 s respectively.

Comparison of stress-relaxation coefficients and material properties reveals statistically significant differences in the stress coefficients and their respective elastic moduli across different combinations of pCO_2 and MAP, and between the last indentation group and previous indentations. There were no significant differences found in Time of Relaxation coefficients.

In conclusion, mechanical properties of step-loaded living rabbit brain are relatively dependent on pCO_2 and MAP, and repetitive deformations. This may be important for further understanding of the brain in different physiological states and accurate mechanical characterization of the brain. It also highlights the need to control for these parameters during the mechanical testing of brain.

ACKNOWLEDGEMENTS

SUPERVISORS

Stefan Cenkowski

Marc Del Bigio

PHD ADVISORY COMMITTEE

Stefan Cenkowski

Marc Del Bigio

Michael West

Qiang Zhang

EXTERNAL EXAMINER

Lynne Bilston

TECHNICAL AND LABORATORY SUPPORT

Beatrice Buzahora

Terry Enno

Drew Griffin

Xiaoyan Mao

Alex Shulyakov

FUNDING

Operating:	Natural Sciences and Engineering Research Council of Canada grant to Dr. Del Bigio
Equipment:	Canadian Foundation for Innovation grant to Dr. Del Bigio
Student support:	Manitoba Health Research Council
	Manitoba Medical Services Foundation
	University of Manitoba Department of Surgery
	University of Manitoba Faculty of Medicine
	University of Manitoba Graduate Students Association

TABLE OF CONTENTS

FIGURES

TABLES

ABBREVIATIONS

ABBREVIATION	FULL TEXT
CSF	cerebral spinal fluid
CT	computed tomography
E	elasticity modulus
ICP	intracranial pressure
LVDT	linear variable differential transformer
MRE	magnetic resonance elastography
MRI	magnetic resonance imaging
MAP	mean arterial pressure
m	meter
MHT	Micro Hardness Tester
mL	milliliter
mmHg	millimeter of mercury
mN	millinewton
N	Newton
pCO_2	partial pressure of carbon dioxide
Pa	Pascals
TRel	Time of Relaxation
η	dynamic viscosity
σ	stress

1. INTRODUCTION

1.1. Rationale and objective of current work

Detecting relative changes in the mechanical properties of brain across different physiological and pathological states may help further understanding of the brain. Identification of these changes may also provide variables in which to compare effects of therapeutic interventions used to alter the brain's physiological parameters or treat pathologies (Aoyagi et al., 1982; McHedlishvili et al., 1989). This may not only prove applicable in the experimental setting, but also potentially result in the development and refinement of tools that can be used to measure or compare the brain's mechanical properties in the clinical setting. Examples include Magnetic Resonance Elastography (MRE) (Murphy et al., 2013b) force and displacement recording surgical retractors for brain, pressure-sensing surgical implants, and force-measuring aspiration during stereotactic biopsy.

Pathologies of the brain that conceivable may have different mechanical properties compared to normal include traumatic brain injury, edema formation (as a result of any etiology), encephalomalacia (as a result of any etiology), all spectrums of hydrocephalus, the aging brain, and tumors. However, there are physiological variables that can range in both the normal and abnormal brain,

and may also affect the mechanical properties of the brain. These include pCO_2 and cerebral blood volume, cerebral perfusion pressure, serum sodium concentration, and temperature. Although these physiological parameters can vary, they also can be measured and relatively controlled.

Mechanical property testing requires deformation of the object of interest in as otherwise as natural its state as feasible. For a viscoelastic characterization, the deformation must be performed with measurement or control of the geometry of the deformation, the forces incurred, and all time-related variables such as rate of application of deformation and length for which the deformation is applied. Anisotropic tissues will differ in their mechanical properties depending on the direction in which the deformation is applied. Therefore, this must also be a consideration, with extrapolation of data stated only within the context of the direction of deformation tested (Abolfathi et al., 2009).

With respect to the investigation of in-vivo brain, this not only provides the opportunity to compare relative differences between pathological or physiological states, but also contributes information useful to the overall mechanical characterization of brain, including that which can be used for the development of rheological models and constitutive equations describing behavior of living brain. Although precise characterization of brain is very difficult due to the number of assumptions required of its anatomy, materials of composition, dynamic physiology, and the available methods for testing, it is none-the-less important to the improvement of a number of medical technologies such as surgical simulation (Delorme et al., 2012), the prediction of brain shift in image-guided

surgical systems (Kuhnt et al., 2012), and convection-enhanced delivery of drugs into the brain (Elder and Chiocca, 2012).

The living brain has been shown to exhibit change in its mechanical characterization and material properties with changes in testing (deformation), anatomical, and physiological variables. Control or monitoring of all variables is required to make meaningful conclusions of experimental results. There is limited investigation into the mechanical properties of the brain that controls for all the variables previously identified, in a consecutive series of samples under the same conditions. Therefore, any series of experiments in which all variables are accounted for is invaluable, and can be used primarily to relatively compare testing results across controlled physiological or pathological states, but also can make contributions to the overall characterization of brain.

It is logical to exhaust comparison of physiological variables prior to pathological states, as these variables can contribute to the further understanding of the mechanics of normal brain, can still vary in pathological states of brain, and in the clinical realm are often manipulated. The most compatible method of conducting direct in-vivo testing of the brain in as close to its natural state as possible is via indentation of the brain surface through a craniectomy. The indentation testing parameters that would preserve the brain in as natural its state as possible, and provide data not only for comparison across manipulated physiological variables but also useful for mechanical characterization of the brain, would be in the form of step-loaded stress-relaxation testing. The depth of indentation should respect the boundary

conditions and length of time of deformation should be applicable to conceivable clinical applications.

The primary objective of the current work is to compare mechanical properties of the living rabbit brain across relatively high and low groupings of the arterial partial pressure of carbon dioxide (pCO_2) and mean arterial pressure (MAP). Other goals include developing a rheological model that describes the behavior of living rabbit brain under step-loaded stress-relaxation indentation, with validation of the model against the experimental data, and identification of any relative mechanical property changes in the living rabbit brain as a result of repeated step-loaded stress-relaxation indentations with 15 minute periods of recovery between indentations.

It is the hypothesis of this dissertation that there are significant differences in relative viscoelastic properties of the living rabbit brain under different combinations of arterial pCO_2 and blood pressure, when all deformation, anatomical, and other physiological variables are controlled.

1.2. Biomechanics and the brain

1.2.1. An introduction to biomechanics

Biomechanics is an interdisciplinary area of study that applies engineering and physical principles to biological objects and systems. The term "mechanics" is used to describe force, motion, and strength of materials and particles and their interrelation. “Biomechanics” refers to mechanics applied to biological systems, and aims to explain the mechanics of living processes.

Understanding and describing an object in mechanical terms requires knowing the relationship of governing physical laws to the object’s geometry, materials of construction, physical response to forces imposed on it, and environment and boundary conditions (Fung, 1990; Tenti et al., 2008). When the object or system is a living one, physiologic and dynamic process must also be considered. Therefore, biomechanics, as an area of study, requires understanding of detailed physical and biological principles, and the ability to communicate in both areas effectively.

Rheology is the study of deformation and flow of matter under the influence of an applied load (i.e. force). The term "strain" refers to a change per unit length in a linear dimension in the direction of the force applied, and "normal stress" is the load divided by the area through which it acts perpendicularly (N/m^2). Poisson’s ratio is the ratio of transverse contraction strain to axial (or

longitudinal) strain of an object being deformed. “Elasticity" refers to recovery of original shape and dimensions upon removal of the deforming force. A perfectly incompressible elastic material (e.g. rubber) at small strains has a Poisson’s ratio of 0.5. "Plasticity" is the failure to return to original position after removal of the deforming force, and "viscosity" is the resistance to flow in response to the force.

“Poroelasticity” is the study of elastic porous materials whose coupling between the pore fluid diffusion and the matrix deformation influences the overall behavior of the composite material. "Viscoelasticity" is material behavior that exhibits both viscous (dependent on time) and elastic characteristics when undergoing deformation. It is characteristic of biological materials. The loading and unloading velocities (rates), pauses or holds of stress or strain, and the history of deformation affect a viscoelastic substance's response to deformation. (Cheng and Bilston, 2007; Fung, 2004; Goldsmith, 2001; Mchedlishvili et al., 1981).

Typical analysis of biomechanical testing includes the plotting of force-deformation or force-time curves and the mathematical determination of rheological parameters and coefficients. (Cheng et al., 2008; Fung, 2004) These data can further be compared with those obtained under a different set of conditions, looking for relative differences or similarities in mechanical properties between conditions. Constitutive equations may be formulated, integrating physical quantities of the material with general equations representing the laws of physics. This forms the basis for creating mathematical models of the material or system, which consist of a set of related mathematical functions whose purpose

is to simulate the response of the material or system to particular changes (e.g. deformations) (Cowin, 2007; Tenti et al., 2008).

Modeling deformation behavior can take either an analytical form involving generalized time derivatives of stress and strain, or else a physical representation of these quantities in terms of masses, springs, and dashpots (Goldsmith, 2001; Mchedlishvili et al., 1981). It is natural to expect that most biological materials, including the brain, display both elastic or solid-like properties and viscous or dissipative properties, as they often continually absorb and damp out a variety of transient loads (Engin and Wang, 1970; Fung, 2004; Tenti et al., 2008; Wang and Wineman, 1972). Non-linearity is inferred when the stress-deformation ratio also depends on the magnitude of the stress.

Understanding a biological system, including brain, from a mechanical perspective is key to characterizing and quantifying its mechanical properties. This facilitates the ability to compare and contrast mechanical properties under different physiologic and pathologic conditions. Relative differences of mechanical properties within a living system may correlate to diagnostic and prognostic information relating to those physiological or pathological processes, and methods or therapeutic interventions used to alter them.

1.2.2. The brain: an overview

The brain is arguably the most important and complex human organ, with regulatory input of essentially every function of the body. The essence of brain tissue on a cellular level is comprised of neurons and glia, in addition to the usual cells found in blood vessel walls. Neurons are the information-processing and signaling elements, with glial cells providing the majority of imperative neuronal support and other important roles. Both neurons and glia are structurally diverse, but in general consist of a cell body with radially projecting axon(s). The overall water content of the normal brain is estimated at 75-80%. (Kiernan, 2005; Trapp and Herrup, 2011)

Glial cells are numerous and diverse. Within the brain, astrocytes are present throughout, oligodendrocytes are found next to the cell bodies of some neurons, and ependyma mostly line the ventricular cavities within the brain. The brain consists of gray and white matter. Gray matter contains the cell bodies of neurons, embedded in a neuropil made up predominantly of delicate neuronal and glial processes. White matter consists mainly of weaving long processes of neurons, the majority being surrounded by myelin sheaths. Both gray and the white matter contain large numbers of neuroglial cells and a network of blood vessels. (Kiernan, 2005; Trapp and Herrup, 2011)

The human brain resides within the rigid skull, and is further enveloped by membranous coverings. The most outer covering is the dura, which is the

thickest and leather-like, and contains the entire brain (if the skull was removed) (Figure 1.1).

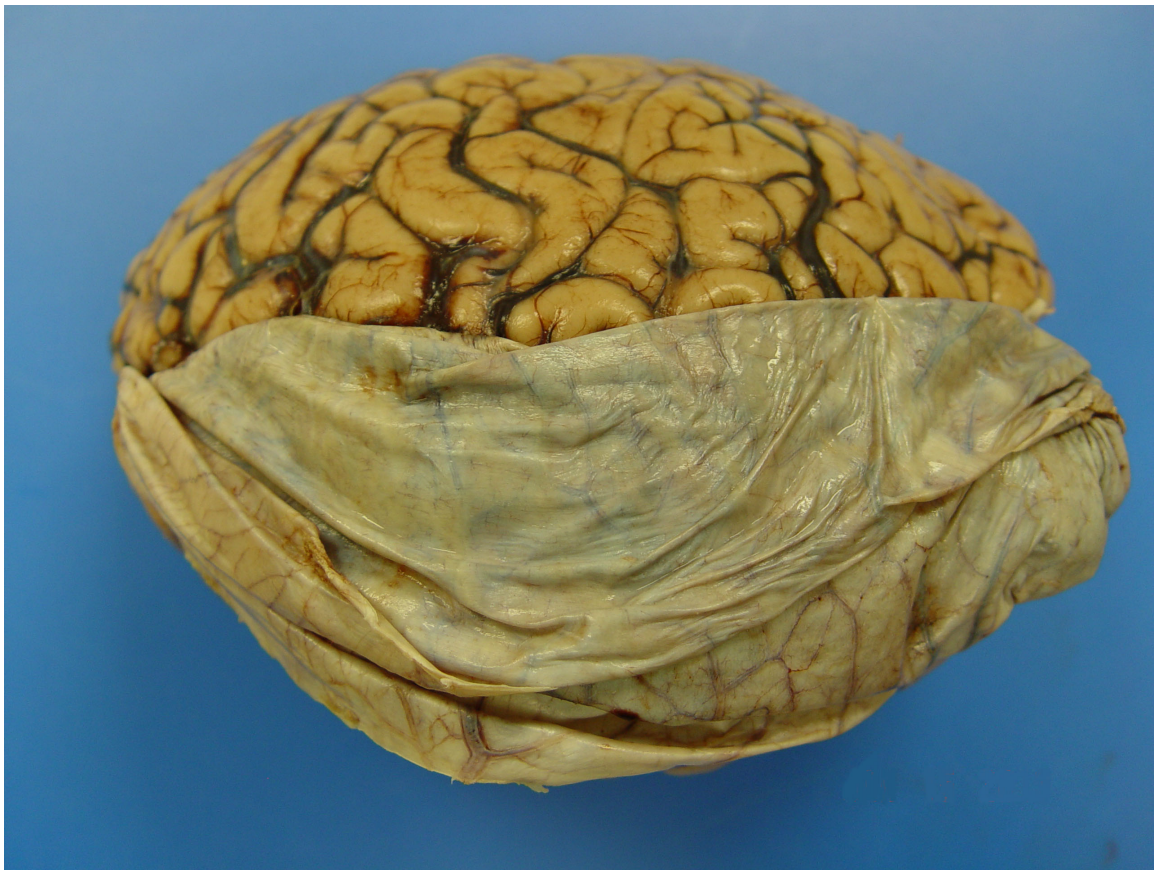

Figure 1.1. Human brain specimen, with dura, viewed from the convexity. The dura is seen covering the brain, with reflection of the dura off the right hemisphere (and turned over onto left hemisphere to show the undersurface of the right-sided dura).

Next is the arachnoid, which is more flimsy and lines the brain and blood vessels in a manner which resembles a thin plastic shrink wrap (Figure 1.2). The pia mater is a very thin layer that adheres to the surface of the brain. The

subarachnoid space, which contains cerebral spinal fluid (CSF) and delicate trabeculae (Kiernan, 2005).

Figure 1.2. Human brain specimen, with dura removed but arachnoid intact, viewed from the convexity. The mainly transparent arachnoid is best appreciated wrapping the sulcal veins, which run in the subarachnoid space.

The adult human brain weighs approximately 1200 to 1400 grams and occupies a volume of approximately 1100 to 1300 cm^3. The brain is divided into two cerebral hemispheres (right and left) by the falx cerebri, an extension of the dura inward. The brain surface is gyrated, and the general shape and

morphology of the brain can be viewed in Figures 1 through 3. The hemispheres are each divided into four lobes: frontal, parietal, occipital and temporal. In the most posterior-inferior area of the skull lies the cerebellum (Figure 1.3).

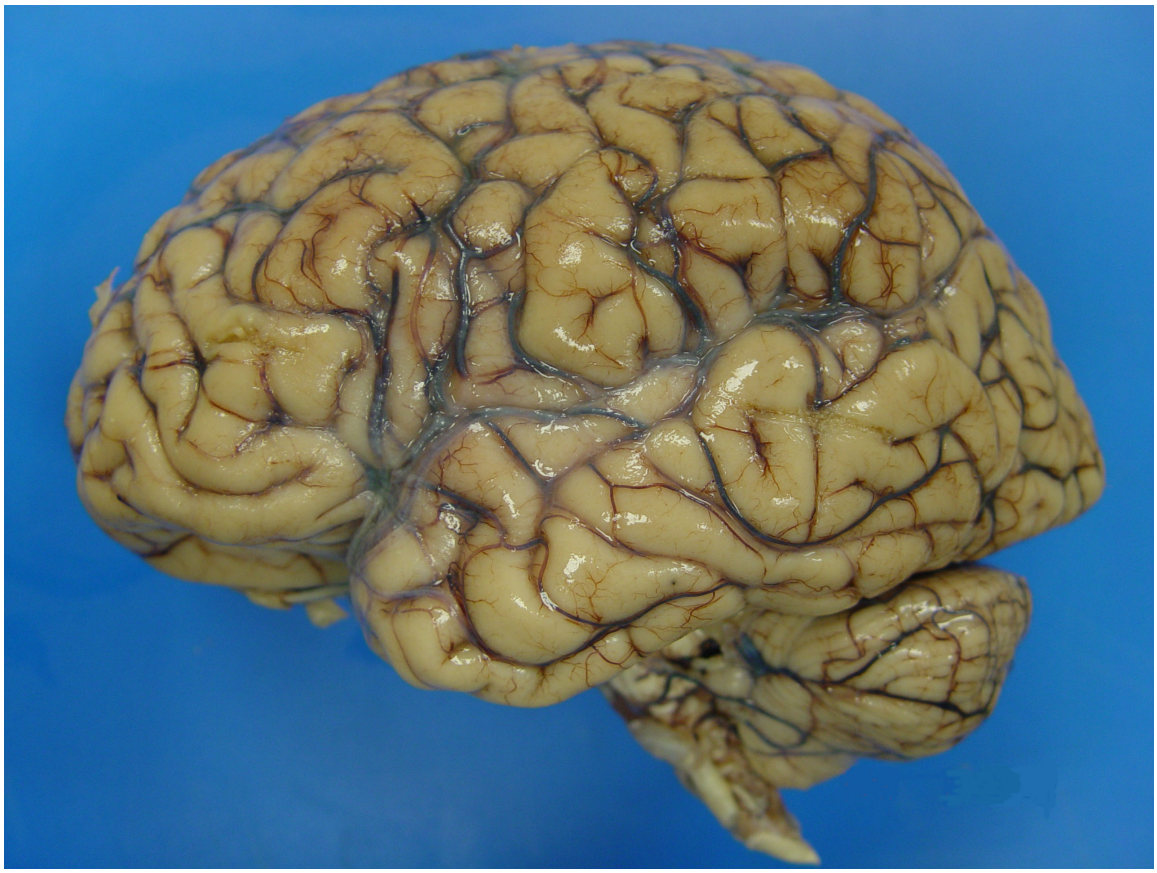

Figure 1.3. Human brain specimen, viewed from the left side.

Anterior to the cerebellum are the brainstem structures (midbrain, pons, and medulla), which in essence are the structures of connection between the brain and spinal cord. The cerebral peduncles at the midbrain are large corrugated columns of white matter that converge at the pons, and the fiber tracts of the spinal cord are continued in the medulla. In addition to the ascending

and descending fiber tracts to and from the cerebral cortex, diencephalon, cerebellum, and spinal cord, the brainstem also contains many nuclei, including those of the cranial nerves. The transition from the medulla to the spinal cord occurs at the foramen magnum of the skull (Figure 1.4) (Allen et al., 2002; Kiernan, 2005; Montemurro and Bruni, 1988).

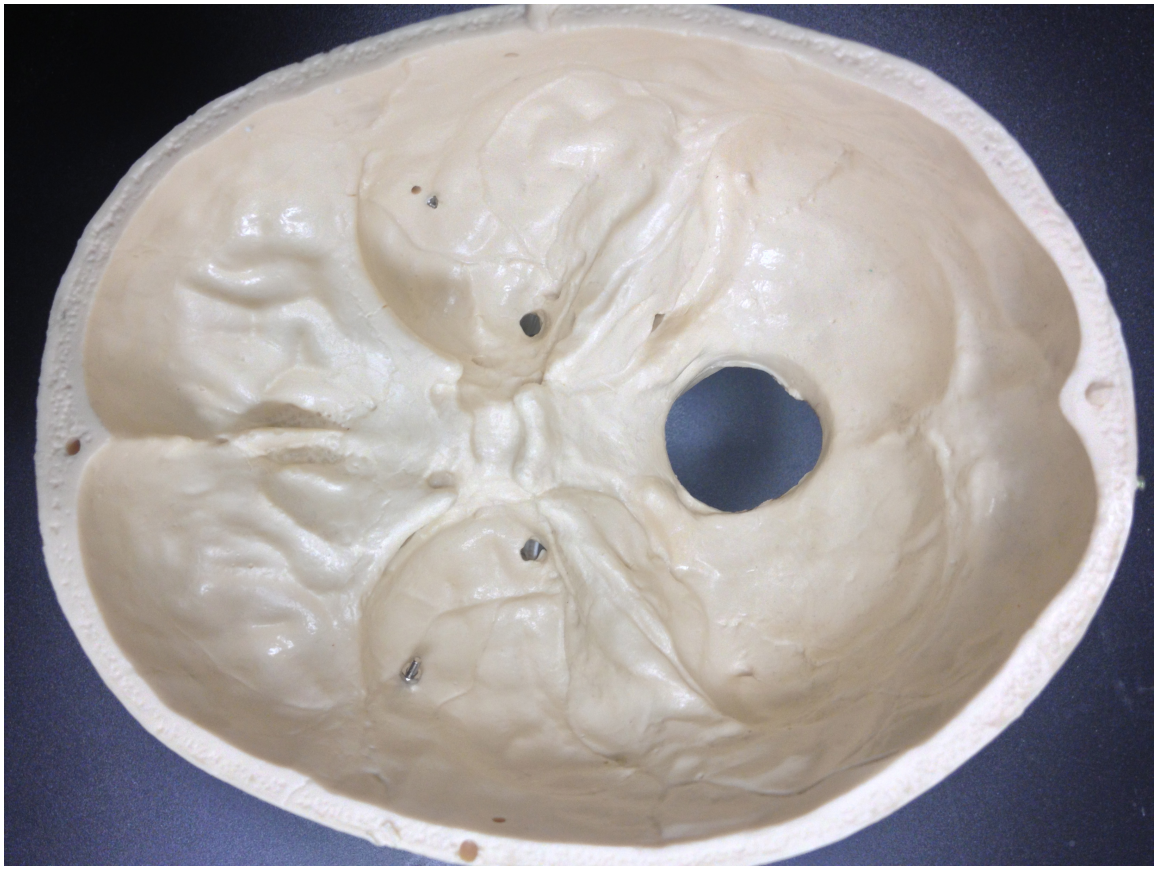

Figure 1.4. Human skull base model. The opening in the base of the skull is the foramen magnum.

Evident on cross-section of the brain are cavities, termed ventricles (Figure 1.5), that in-situ are filled with CSF. Cerebral spinal fluid is normally clear

and colorless with a density of 1.003 to 1.008 grams per cm^3. It is principally produced by choroid plexus within the ventricles and has a circulatory system that sees it flow through the ventricles, then out of the brain through specific outlets, to surround the central nervous system (subarachnoid with respect to the brain). In human, CSF is primarily reabsorbed through dural venous sinuses at the convexities of the brain. The total volume of CSF ranges from 80 to 150 mL, with approximately 15 to 40 mL residing in the ventricles. A higher hydrostatic pressure in the subarachnoid space drives the bulk flow of fluid in the forward direction, therefore draining CSF volume through absorption into the sinuses (Cutler et al., 1968; Marmarou et al., 1978; Tanna et al., 1991).

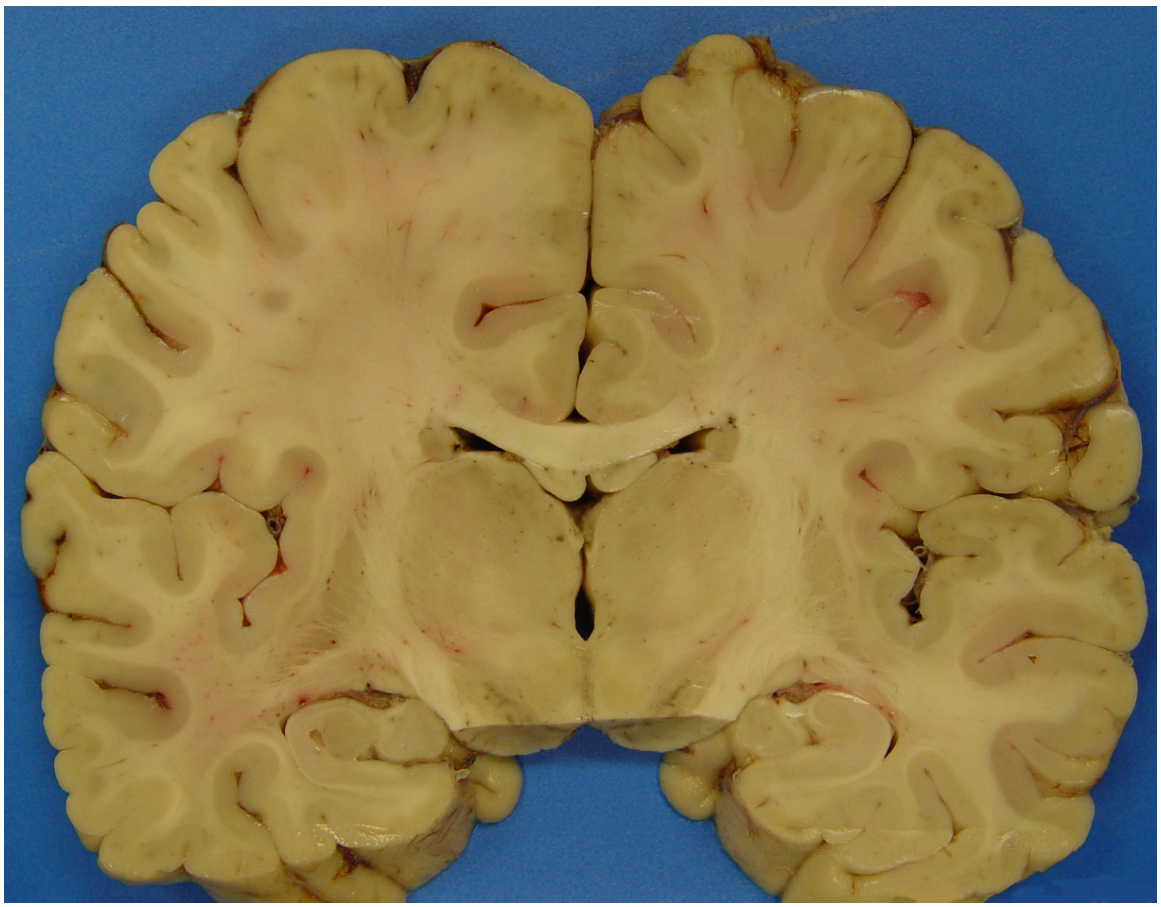

Figure 1.5. Human brain specimen, cut into a coronal slice at the anterior-posterior level of the cerebral peduncles. The cavities deep and central to the cortices are the ventricles (note: the location and morphology of the ventricles change with different anterior-posterior and superior-inferior orientations). Also evident are the regional locations of gray and white matter.

Brain anatomy is specific to species. The rabbit brain, for example, is relatively lissencephalic (relatively smooth cortical surface, without complex gyration) and has a relatively flat cortical surface at top of its hemispheres, compared to the human brain. Figure 1.6 illustrates these differences.

a) 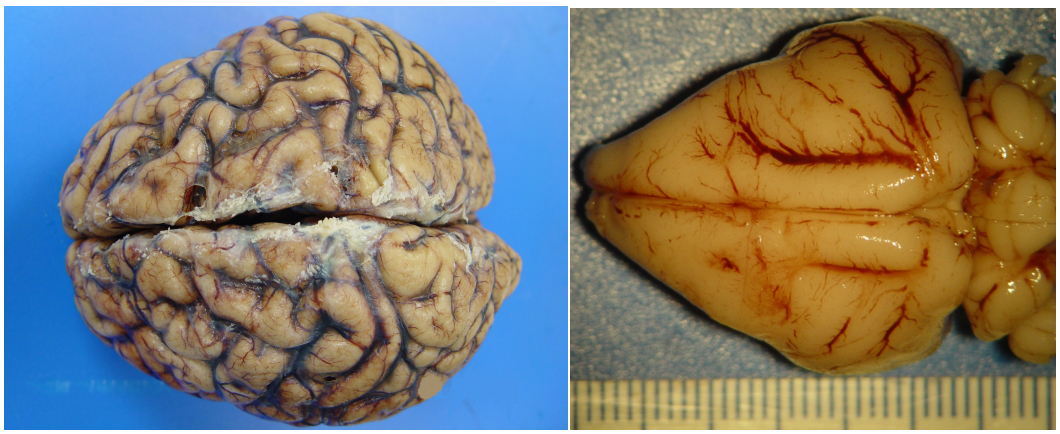

b) 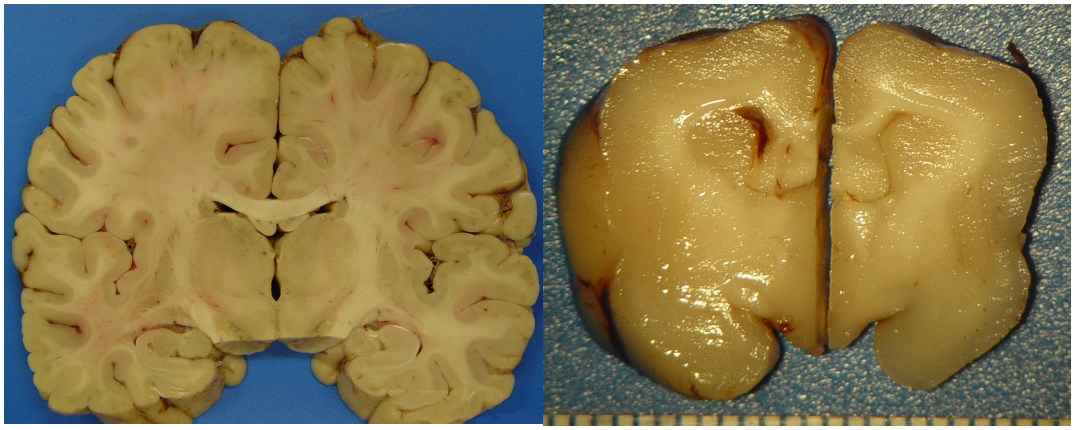

Figure 1.6.

a) Superior views of the convexities of the human (left) and rabbit (right) brain. The rabbit brain is relatively lissencephalic in comparison to the human brain. In the picture of the rabbit brain, each ruler division mark is 1 mm.

b) Coronal sections of the human (left) and rabbit (right) brain. The rabbit brain is relatively flat at the top of each hemisphere, in comparison to the human brain. In the picture of the rabbit brain, each ruler division mark is 1 mm.

The brain is composed of more than just neural-glial tissue. A vast network of blood vessels also exists, and contributes to the brain's structure and morphology. In addition, these vessels introduce blood volume and pressure into

the brain and intracranial space. Cerebral blood volume and cerebral blood flow are essentially functions of the cerebral arteriovenous pressure difference and cerebrovascular resistance. Approximately 80% of the resistance is found in the arterial system (and most specifically within the penetrating pre-capillary arterioles), with the venules and veins providing 20% (Hurm and Traystman, 1997). Mean arterial pressure (MAP) is normally 65 to 100 mmHg, and there is a progressive fall in blood pressure moving distally from the common carotid artery, with the capillary pressure in the brain approximating 50% of aortic pressure. In humans, subarachnoid venous pressure approximates 35 mmHg. These factors are largely determined by vessel caliber, and are normally maintained within narrow limits. The brain has the ability to regulate the transmission of blood pressure to the intracranial pressure (ICP) primarily through the dilation and constriction of resistance vessels in response to pressure (termed autoregulation) and pCO_2 (Guyton and Hall, 1996; Hurm and Traystman, 1997; Marmarou and Beaumont, 2011).

The proposed mechanisms of autoregulation include intrinsic changes in the vasomotor tone and the release of a variety of vasoactive substances from the endothelium or periadventitial nerves (in response to changes in transmural pressure). Perivascular nerve fibers branch throughout the adventitial layer of cerebral arteries and release a wide variety of neurotransmitter substances. The sources of cerebrovascular innervation may be either from remote neurons such as autonomic ganglia or nuclei, or involve local neurons. The sympathetic system results in vasoconstriction, and the parasympathetic results in vasodilation.

Catecholaminergic release results in vasodilation (specifically, by norepinephrine effect on β2 receptors) and serotoninergic release can result in both vasodilatative and vasoconstrictive effects (Branston, 1995; Tan et al., 2011; ter Laan et al., 2013). As pial arterioles penetrate the brain parenchyma, they gradually lose innervations from extracellular nerves originating from the peripheral ganglia. In addition to the neuronal control of vasomotor actions, there are various signaling modalities by which activation of astrocytes leads to vasodilation and vasoconstriction of parenchymal arteries (Filosa and Iddings, 2013). Regulation of cerebral blood flow is also performed by blood gases, with carbon dioxide (CO_2) considered to be the most important physiologic variable. Increased pCO_2 causes vasodilation and decreased pCO_2 caused vasoconstriction (Traystman, 1997). Much of our understanding of the regulation of cerebral blood flow comes from experimental investigation in animal models, including the rabbit. This includes the recognition that commonly used anesthetic agents, which are pertinent to the clinical entities of severe brain injury and brain surgery, may affect the regulation of cerebral blood flow (Aksenov et al., 2012; Reicher et al., 1987).

The brain is delicate. Despite the rigid and protective skull, it is susceptible to trauma through transmission of energy. It is also susceptible to tumor formation, both “benign” and malignant, as well as a variety of pathologies relating to the arteriovenous and CSF systems. There is no accurate way to extract the total personal and economic toll of brain pathologies on society. It not

only includes direct healthcare costs but also the indirect and opportunity costs of work missed by patients and informal caregivers. Estimates from the latest Economic Burden of Illness in Canada periodical report the cost of diseases or disorders of the nervous system approximate $8.3 billion in Canada in 1998, excluding mental health problems (Canada, 2002).

1.2.3. Relevance of the mechanical properties of brain

The brain is subject to the laws of mechanics just as any other structure or substance. Therefore its mechanical properties may change with alteration in its composition and environment. These alterations can be due to dynamic physiological or pathological processes, such as extremes in pCO_2 and blood pressure, cerebral edema, hydrocephalus, and space-occupying lesions (e.g. hemorrhage or tumor).

Intracranial pressure depends on several parameters: the intracranial volume, the elastance of the system, the contribution from the atmosphere, and the orientation of the cranial axis relative to the gravitational vector. Three different pressures contribute to ICP: atmospheric pressure, hydrostatic pressure, and filling pressure.

The filling pressure of the system is determined by the volume of the intracranial contents and the elastance of the enclosing structures. The intracranial contents consist of blood, brain and associated tissues, CSF, and

any pathologic masses. Elastance is a system parameter that is defined by the pressure change per unit of volume change namely, the corresponding pressure change for any given volume increase in cranial contents. Compliance is the inverse of elastance. Elastance arises as a combined result of both distention and displacement. In other words, as volume is added to the system, there are two principal routes for compensation, expansion or loss of volume (Lanier and Warner, 1992).

The skull is rigid and unyielding, and the ability of dura to distend within the skull is very limited. Therefore, any change in volume of the intracranial components or addition of a new volume must occur at the expense of other volume if ICP is to be maintained. Cerebral spinal fluid and venous blood can be displaced into their extracranial compartments, but brain through the foramen magnum (herniation) and dampening of arterial blood pressure are less resistant to displacement, and if they do occur usually result in brain injury. Hemorrhage, tumor, hydrocephalus, and cerebral edema can be associated with pathological additions in intracranial volume. The relationship between intracranial volume and ICP is not linear after a period of relative spatial compensation, and as volume is further added the pressure change per unit volume becomes increasingly large (Marmarou and Beaumont, 2011).

In the realm of medical practice, the extent of consideration of physical principles as they relate to brain is limited to measuring ICP. “ICP monitoring” involves the placement of a catheter coupled with a pressure transducer inside the brain. The pressure is mostly contemplated on an instantaneous basis, with a

normal range considered 8-15 mmHg. A pressure of greater than 20 mmHg is considered a trigger to institute therapeutic measures to attempt to lower the pressure, with the intention of maintaining cerebral perfusion and preventing herniation of brain (Brain Trauma et al., 2007; Marmarou and Beaumont, 2011; Razumovsky and Hanley, 1992).

Detecting relative changes in mechanical properties that characterize the brain may prove very important. The fact that pressure and volume changes are observed in the brain with varying physiological and pathological entities suggest that change in the mechanical properties of the brain are also possible. Characterization of the living brain from a mechanical perspective introduces a new set of variables in which to compare against physiological extremes and pathological states. Relative differences in material properties may help correlate to the detection and diagnosis of potential abnormal processes of the brain, the quantification and prognosis of the process, and the effect and measurement of an attempted therapeutic intervention (Cheng et al., 2008; Kyriacou et al., 2002; Shulyakov et al., 2012).

Modern neuroscience has a relative paucity of representation by the field of mechanics. This is likely due to the expertise required in both medical and physical sciences, and the inherent difficulties in performing mechanical testing on brain. Therefore, any number of important correlations between mechanical properties of brain, its pathologies, and therapeutic interventions remain relatively unexplored in this underrepresented area of study. However, before this is

attainable, the mechanical properties of living brain and its variable physiological states needs further characterization through direct testing.

1.3. Investigating the biomechanical properties of brain

1.3.1. Motivation

Determining the mechanical properties of a biological tissue is often difficult, due to the unnatural settings in which tissue usually must be tested, compounded by the complex physical property behaviors inherent to biological tissues (Fung, 2004). This is especially true for brain, which has the added difficulty of being very soft and fragile.

Regardless, there has always been interest in biomechanics and the brain. Over several decades, research concerning the biomechanical properties of the brain has mainly been motivated by the desire to understand forces involved in traumatic brain injury (e.g. motor vehicle collisions and physical assaults) (Arbogast and Margulies, 1998; Hosey and Liu, 1982; King et al., 1995; Kuijpers et al., 1995; Margulies and Thibault, 2000; Ommaya, 1968; Ommaya et al., 2002; Prange et al., 2003; Ruan et al., 1994; Voo et al., 1996; Walsh and Schettini, 1976; Zong et al., 2006). Studying the brain from this perspective has helped identify injury threshold levels and subsequently resulted in developing protective and diagnostic equipment, such as sports helmets and magnetic resonance elastography (MRE) respectively (Di Ieva et al., 2010; McIntosh et al., 2011)

More recently, biomechanical research has shifted to attempts at quantifying physical parameters and mathematically modeling the response of

brain to other stresses, as these are requirements for the development of a number of medical technologies (Brown et al., 2002; Delingette et al., 1999; Hartkens et al., 2003; Lim et al., 2005; Miller, 1999a; Nathoo et al., 2005). Diagnostic imaging has advanced significantly since the introduction of computed tomography (CT) and magnetic resonance imaging (MRI), to which clinical medicine has become dependent on. As refinements of imaging techniques are continuously introduced, the potential of imaging biomechanical properties such as elasticity, stiffness, and pressure should has also been investigated (Alperin et al., 2000; Di Bona et al., 2003; Fan et al., 2002; Manduca et al., 2001; McCraken et al., 2005). Imaging from this perspective may be the precursor to the developing a technique to non-invasively measure and monitor ICP and tissue stiffness (Alperin et al., 2000; Ueno et al., 2005; Yamamoto et al., 2004) or identify mechanical properties that change in a pathological state.

Magnetic resonance elastography (MRE) is a developing tool, with respect to the brain, that can provide unique information of brain material properties. This is done by imaging alterations of the magnetic spin density caused by mechanical vibration (Di Ieva et al., 2010; Glaser et al., 2012; Manduca et al., 2001; McCraken et al., 2005; Murphy et al., 2013a). However, little is known about the actual physical properties of the brain in pathological states that affect this function. By defining tissue elasticity with high-quality experimental data obtained via detailed mechanical testing, MRE can be compared to this data, possibly resulting in unique information regarding brain material properties. This

may pave the way for more applied clinical studies where therapeutic interventions could be systematically studied.

Further applications of imaging the brain's biomechanical properties are related to surgical robotics, automated surgical instruments, and surgical navigation techniques (Carter et al., 2005; Hagemann et al., 2002; Miga et al., 2000; Scholz et al., 2005). The brain is being recognized as uniquely suitable for the surgical application of robotics: it is symmetrically confined within a rigid structure and easily damaged by minor excursions of surgical instruments (Miller and Chinzei, 2002; Nathoo et al., 2005). There are many possible surgical applications of robotics. Examples in neurosurgery are brain retraction for surgical exposure, stereotactic placement through brain (e.g. functional procedures and deep brain biopsies), neurosurgical simulation tools, and microsurgical technique augmentation. Precise representation of boundary and loading conditions, geometry, and material properties are required to create mathematical models of brain tissue, which in turn are required for registration and predicting deformation in a surgical robot control system.

Significant difficulty in modeling the response of brain to forces in related to surgical technology arises from the brain's lack of rigidity. Images (or information derived from them) are registered to a patient before a surgical procedure, with the possibility of providing spatial navigation and guidance. However, deformation of the brain takes place during most surgical procedures, resulting in a mismatch between preoperative images and surgical presentation. Thus, the precise accuracy of the spatial guidance required, is degraded (Carter

et al., 2005; Hagemann et al., 2002; Ji and Margulies, 2005; Nathoo et al., 2005; Scholz et al., 2005; Taylor and Miller, 2004). Efforts in further detailed modeling are needed to address this issue, which may result in better predictions of brain shift.

Characterization of the mechanical properties of brain with the objective of developing end-application technologies requires the development of precise mathematical models and constitutive equations to represent the brain. The accuracy of such models is entirely dependent on the assumptions and approximations made regarding biological characteristics (i.e. anatomy and physiology). Perhaps more practically, biomechanical testing of brain could reveal new measures in which to effectively compare, or even prognosticate and differentiate, physiological variability or pathologies (Glaser et al., 2012; Kyriacou et al., 2002). In essence, this would be measuring the overall mechanical response of the cranial contents, which is how the brain is viewed clinically. Interestingly, this is the less often stated objective for publications involving experimentation involving the mechanical properties of brain, with the majority of research in this area conducted with the intention of quantifying mechanical constants exactly and defining constitutive equations for brain.

1.3.2. Methods of investigation: principles

Determining the mechanical properties of the brain requires investigation with applied forces, and there are a number of ways in which a deformation can be applied. Control and/or monitoring of stress, deformation, time-dependent factors (e.g. loading rates, pauses), and friction is required as these are the variables from which mechanical properties are determined. The deforming load can be applied perpendicularly to the sample surface, termed compression, or with a degree of shear (tangential or torsional), where the combined energy of a pair of opposing parallel forces cause the stress. In addition, volumetric strains (e.g., hydrostatic pressure, confined compression, space-occupying deformation within a sample) can be used. Testing can be static or dynamic. Regarding dynamic testing, there are two main categories: the decay of free oscillations and forced oscillation (continued application of an oscillating force, with the resulting displacement of the sample measured) (Fung, 2004).

Viscoelasticity can be studied with dynamic testing. It can also be studied by applying a constant load and measuring deformation change over time. This is known as the test of creep. Similarly, applying a constant deformation allows for the analysis of load change over time, known as stress-relaxation. If these tests are performed with an initial "instantaneous" load, the time-dependent retardation and relaxation functions, as well as the instantaneous elastic moduli, can be determined.

Repetitive or cyclic loading can have a more general purpose with respect to viscoelasticity. If a viscoelastic material undergoes deformation repeatedly, the force-deformation and stress-relaxation curves may shift. If the same deformation is repeated indefinitely, the difference between successive cycles decreases, and eventually a steady state is reached. This is thought to be attributed to the redistribution of fluid, and is referred to as preconditioning. It is thought appropriate to precondition before mechanical testing if the sample being tested is ex-vivo tissue that normally undergoes cyclic loading in-vivo (e.g. vascular pulsations). However, arbitrary preconditioning of biological tissues has been used to reduce variability of subsequent tests and to what degree this results in an inherent change in the tissue may vary. Also, in a poroviscoelastic material, where the objective may be to “precondition” out the fluid phase in order characterize the viscoelastic component, this objective is unlikely to be met in a well-hydrated tissue (Cheng et al., 2008; Gefen and Margulies, 2004; Shulyakov et al., 2012; Shulyakov et al., 2011).

1.3.3. Methods of investigation: experimental

The majority of head injury mechanisms are of an abrupt change in acceleration or deceleration of the head, in which the brain is damaged at its points of contact with the inner table of the skull or secondary to shear of the tissues upon itself. Investigation of these mechanisms most often consisted of

experiments that typically involved large indirect forces in an ex-vivo context. Much of this work has been previously reviewed in detail (Goldsmith, 2001). Studying the boundary conditions of the brain has been the major focus of the research on traumatic brain injury mechanics (Carter et al., 2005; Ji and Margulies, 2007; Kuijpers et al., 1995; Ommaya et al., 2002; Penn et al., 2005). After this type of impact, the injured portion of the brain undergoes a cascade of pathological changes that typically results in swelling and bleeding. However, the boundary conditions imposed by the skull are rigid, and the total volume the intra-cranial contents will remain constant. Therefore, any increase in abnormal brain tissue or clot necessitates a decrease in CSF and/or blood volume, followed by squeezing and herniation of the brain (all of which can quickly lead to clinically evident brain damage or death). This physical principal is key to the treatment of brain injuries and disorders.

Accelerating or decelerating the head near-instantaneously has limited application to the brain's response to lower stresses and strains. These may be encountered with other pathological processes that form in minutes (e.g. edema formation, extremes in physiological variables) to even years (e.g. tumor growth). The context of lower mechanical forces and a wide variety of strain rates is also necessary to consider with the refinement of medical technologies, as previously discussed. This necessitates testing of brain via direct deformation methods under controlled parameters.

The first published research of *direct* testing of brain is from 1954, and involved working out the driving point impedance of a vibrating rigid sphere in a

container of both whole and ground pig brains (Franke, 1954). However, the most common method of direct mechanical testing of brain has been the static unconfined compression of (ex-vivo) brain samples (Chatelin et al., 2012; Chinzei and Miller, 1997a; Dodgson, 1962; Galford and McElhaney, 1970; Hickman, 1965; Koeneman, 1966; Laksari et al., 2012; Mendis et al., 1995; Miller, 1999b, 2005; Morrison et al., 1998; Pamidi and Advani, 1978; Peters et al., 1997; Prange and Margulies, 2002; Shen et al., 2006; Wu et al., 2004a; Wu et al., 2004b). This first documented use of this method was performed by Dodgson, who loaded murine brain slices with a constant weight. He evaluated the creep, and the effects of soaking the samples in solutions of different pHs and at different temperatures (Dodgson, 1962). Shortly after, Koeneman published his observations of creep and relaxation of samples in unconfined compression, in a variety of species (Hickman, 1965; Koeneman, 1966). Although the samples were previously frozen, Koeneman first discussed and presented brain as a viscoelastic substance. He reported a compression modulus of 8.8 to 15 kPa.

Galford and McElhaney used unconfined compression of brain samples to conduct dynamic testing, proposing coefficient values suitable for modeling viscoelastic behavior (Galford and McElhaney, 1970). However, a number of assumptions regarding tissue geometry and heterogeneity and post-mortem effects were made, which was not uncommon to early biomechanical testing of brain in general. It was found that brain tissue was strain-rate sensitive, with increasing stiffness at higher loading rates, and increasing stiffness with applied strain, resulting in a concave upward non-linear stress-strain curve. Since then

similar qualitative results have been found, with continued observations of strain-rate sensitivity (Bilston, 2011).

More commonly for brain, dynamic means of testing have been conducted in the context of shear. A number of different groups have developed custom methods of parallel plate shear, and a few have conducted rotary and torsional shear (Fallenstein et al., 1969; Garo et al., 2007; Hrapko et al., 2008; Nicolle et al., 2005). An important consideration in evaluating a shear apparatus is the means in which slip is eliminated or accounted for between the compressive plates and the sample surface. Shear response of a viscoelastic material is characterized in terms of shear modulus, and represents the stress response to shear strain. The relaxation shear modulus represents the temporal stress response to a unit shear strain. The shear modulus for brain tissue (ex-vivo) has fallen within the order of kilopascals, increases with loading rate, and is dependent on strain as unit strain increases. Viscoelastic relaxation modulus has been found to range in orders of magnitude from 10^2 to 10^4, with the lower values obtained with higher strains (Bilston, 2011).

Fallenstein noted observations of increased shear moduli with drying of samples, and decrease in the storage modulus if the sample had been frozen (Fallenstein et al., 1969). The labs of Margulies and Bilston have put forth numerous publications relating to shear testing of brain samples. A sample undergoes oscillatory shear from one parallel plate, and the effect of a number of frequencies can be evaluated. This method and set-up is similar to ones used by

others). Shearing of brain samples has also been tested by simple static tests (Donnelly and Medige, 1997).

Unconfined deformation has also been adapted in an elongation form, by using an adhesive to fix the parallel plates to the sample (Lu et al., 2006; Miller, 2001a). This method effectively eliminates the friction issue that may complicate unconfined compression. It also allows for the evaluation of tensile strength of brain material. (Aimedieu and Grebe, 2004; Morrison et al., 2000).

The large majority of biomechanical testing published to date has been conducted ex-vivo. Cheng et al (Cheng et al., 2008) published a review encompassing a number of these works. Further review has been published by Bilston, 2011, who summarized that “characterization of brain tissue properties has been plagued by differences in results arising from differences in test methods”. Ex-vivo testing requires many assumptions regarding physiological distortions, including loss of blood perfusion, disruption in hydration and temperature regulation, post-mortem tissue degeneration, and possible sample preparation artifacts, and any one of these variables may be a significant factor in differences in reported data. Regardless, consideration of the summative findings of ex-vivo is warranted, considering the relative paucity of mechanical testing of brain tissue in general, and certainly within spectrum of in-vivo testing. Brain tissue has been found to be a very soft, non-linearly viscoelastic solid material, and in isolation has a low linear viscoelastic strain limit. Brain tissue is strain-rate sensitive, with increasing stiffness with increasing strain rate. Failure occurs at

moderate strains, of the order of 25-100%, depending on the loading type. (Bilston, 2011; Cheng et al., 2008).

1.4. Direct In-vivo Mechanical Testing of Brain.

1.4.1. Rationale and specific methods

With methods for material testing and computational modeling evolving, the desire has further evolved to study mechanical properties of brain in finer detail with respect to stages of development, anatomical variation, physiology, and pathology. This requires the brain to be tested in its natural state. Whether testing brain in the ex-vivo setting is relevant to the end goal of understanding and characterizing living brain is a valid question (Bilston, 2011). The number of variables that can, in theory, require consideration comparing the in-vivo to ex-vivo are very large, and in the works published to date most are not addressed.

The indentation method allows direct mechanical property testing of brain in-vivo. Animal experiments typically necessitate the use of anesthesia and indenting through a craniectomy. With this exception, the brain remains close to its natural state. However, it is necessary that the numerous anatomical, compositional, and physiological variables that may influence measured mechanical properties be controlled or accounted for. Furthermore, considerations of species, age, weight, and health status of the animal should also be given. Relating to the influence of cerebral perfusion pressure on testing results, the mean arterial blood pressure, autoregulation capability, pCO_2, cerebrospinal fluid pressure, and sources of transferred pressure or venous

congestion (e.g. body positioning, mechanical ventilation, vascular occlusion) should ideally be controlled for or at least accounted for. So must the following anatomic and geometric details: exact location of testing and angle of indentation, tissue heterogeneity and anisotropy (e.g. grey vs. white matter), and boundary conditions (e.g. dural, meningeal and vascular compliance and tethering; mechanical influence of pia and glia limitans at the brain surface and subcortical structures). In conjunction with accounting for anatomic and physiologic variables, all testing parameters including force, deformation (including direction), and time (e.g. rate of loading, type of loading, pause lengths) must be either be pre-defined or measured.

In order to test the mechanical properties of brain without performing a craniotomy, one must use an indirect method. One indirect technique that has often been used to obtain information for the purpose of determining the compliance of brain is injecting or withdrawing known amounts of fluid into the CSF space, and recording the CSF pressure. Although the resulting information approximates the volumetric buffering capacity within the CSF compartment, this includes the extracranial portion where the elastic properties of the dura are not confined by the skull. Also, it does not factor the compressibility of the vascular structures and the brain tissue itself. Therefore this method requires a significant number of assumptions regarding anatomical detail, boundary conditions, and mechanical properties of a number of heterogeneous materials.

As previously described, MRE enables non-invasive measurement of elasticity, and can provide unique information on brain material properties.

However, it remains an indirect method of acquiring information on biomechanical properties and itself requires validation by direct methods of testing brain. In addition, the deformations are very limited in both absolute value as well as available range with MRE (Bilston, 2011), and not within the spectrum of deformations that may be caused by physiological or pathological processes.

1.4.2. Review of literature

Mechanical testing and characterization of brain, including the work done with living brain, has been inconsistent in its methods and results. It is therefore very difficult to draw comparisons across different works, and each set of published work needs consideration in its own right and context.

1.4.2.1 Specific experiments

The first publication of in-vivo mechanical testing of brain was produced by Fallenstein et. al. in 1969. A small driving point impedance device was constructed, consisting of a sinusoidally-driven flat-ended, cylindrical probe ($0.1cm^2$ cross-sectional area) attached to an impedance head and associated electronic equipment for signal conditioning and display. The device allowed for accurate monitoring of force and acceleration at a given frequency. Eight

anesthetized 4.5 - 5.5 kg young adult rhesus monkeys were tested. Mechanical ventilation and pCO_2 monitoring were not specified, however the internal carotid artery was cannulated for blood pressure monitoring and the internal jugular vein cannulated for saline infusion and drug administration. The animals were placed in sitting position with head fixation, and had holes trephined over the medial area of the precentral gyrus. After removal of dura, reportedly without disruption of the arachnoid, the impedance probe tip was placed in direct contact with the arachnoid. While at a specified static deformation the probe was driven with a small sinusoidal amplitude and the force and acceleration signals from the probe recorded. Testing parameter values, for the most part, were not identified. The only results shown were two "typical" unitless Lissajous figures at different amplitudes (2.5×10^{-3} and 30×10^{-3} cm), revealing a loss of symmetry in the plot of the higher amplitude (Fallenstein et al., 1969). At lower amplitudes, without specifics of the depth or frequency named, decreasing blood pressure was stated to correlate with a decrease in the ratio of loss to storage shear modulus ratio.. Unfortunately the raw data were not published and there was no monitoring of physiologic parameters aside from intracarotid pressure.

In 1970, Metz et al. (1970) published a set of experiments using a deformation probe consisting of a 15-gauge hypodermic tube closed at one end. Slots in the tube near this end were covered with a thin cylindrical rubber membrane. Introduction of a given volume of fluid into the probe causes a measurable increase in the radius of the rubber cylinder. The "pumping modulus"

was defined as the incremental pressure change necessary to displace an additional 0.002 cm^3 per unit length of probe (i.e. a measure of mechanical resistance of the tissue to expansion of the balloon). Volume pumped was read off a micrometer dial on a burette holder, with pumping modulus recorded. The system was normally filled with water. To check the probe expansion, X-ray films were taken after the water was replaced with a radio-opaque agent. It was reported that "three identical sets of experiments were performed at different sites in each brain of a series" of anesthetized rhesus monkeys during life (under anesthesia), immediately after death, and after fixation. The animals were placed in a stereotactic frame, and the probe, "held in the micromanipulator arm of the apparatus, was inserted vertically through a drill hole in the skull into a lobe of the brain and the hole sealed with bone wax". In their published manuscript, examples of data were shown indicating that in one animal, the right frontal, right occipital, and left occipital lobes were used. X-ray and post-mortem examination confirmed that the balloon lay entirely within brain tissue. A series of equal volumes, increasing from approximately 4-14 x 10^{-3} cm^3, were pumped into the probe while recording the pressure in the probe. The monkey was then sacrificed and further testing performed. Although raw data were not shown, plots of the elastic modulus suggested that elasticity increased from in-vivo to ex-vivo and from ex-vivo in-situ to an extracted fixed brain (over the same range of strain). (Metz et al., 1970) However, the details or impact of repetitive insertion of the probe into variety of locations were not considered.

Walsh and Schettini authored a number of publications involving in-vivo brain indentation. The brain surface pressure of living dogs through the intact dura was measure using a coplanar ring transducer (Schettini et al., 1971; Schettini and Walsh, 1974). Physiologic variables were reported to have been controlled or monitored.. The cisterna magna was cannulated for continuous pressure monitoring. The brain was loaded to the transducer by increasing intracranial volume via hypercapnic hypoxia and intravenous distilled water infusion (Majors et al., 1972; Schettini et al., 1972). Schettini and Walsh's work also included a series of experiments with seven sedated dogs in reclining position, with physiological conditions kept as normal as possible. The pressure transducer was rapidly inserted (manually) to a predetermined depth and held for approximately 2 s. After withdrawal, recovery was allowed for 10-15 min. Next the depth-control cylinder was repositioned a predetermined amount within the barrel, which resulted in a slightly greater insertion depth for subsequent measurement. The exact number of repeated tests and any details regarding testing parameters were again unreported, and the results and curves pertaining to only one dog were shown. Pressure-deformation curves, starting at the estimated point of brain contact, were displayed as single linear lines approximating best-fits to the experimental points. Although the degree of variability and outliers were not reported, the slopes of these curves ranged from 17.3 (peak pressure 30 mmHg and corresponding depth 1.2 mm) to 25.5 (peak pressure 25 mmHg and corresponding depth 1.4 mm) mmHg/mm. The elastic modulus was derived using the solution for indentation of a viscoelastic material

by a rigid, cylindrical, flat-ended punch, and relates the total force on the punch to the insertion depth in terms of the size of the indenter and the elastic properties of the material. With the value assumed for Poisson's ratio as 0.5, the range of calculated elastic moduli corresponding to the range of pressure-deformation slopes was 2.80×10^5 to 4.12×10^5 dynes/cm^2 (Walsh and Schettini, 1976).

The later works of Walsh and Schettini discussed the importance of relative comparison of in-vivo variables, in lieu of pursuing precise material characterization. They continued with the same testing apparatus and used the ratio of change in pressure to change in depth as their index of comparison, taken to represent an elastic response. Reported are ratios, albeit extrapolated in terms of assumptions in linearity and indirect measurement, that suggest changes in cerebral hemodynamics may result in changes in elasticity of the brain tissue itself. However, there data is reported in an observational manner, without statistical analysis. (Schettini and Walsh, 1984, 1988; Walsh and Schettini, 1984, 1990)

Pal'tsev and Sirovskii developed a unique apparatus for testing brain mechanical properties in anesthetized and ventilated live adult dogs. Pressures were monitored in the carotid artery, jugular vein, or sagittal sinus. Through a wide craniotomy and durotomy, two intraparenchymal pressure monitors were placed 5-10 mm deep to the cortical surface to be compressed. A single plate (dimensions not reported) fixed to a stereotaxic apparatus was lowered onto the

cortical surface, with depth known and pressure measured. Through a window in the plate, a second compressive plate of 1 mm^2 surface area indents further into the cortical surface, also with depth known and pressure measured (each plate recording pressure independently). This compression was to maximum depth of 3 mm, at an approximate loading rate of 0.05 mm/s. Testing was conducted under different physiological conditions, including high and low blood pressure and pCO_2. They reported a change in mechanical properties that correlated increasing pCO_2 but did not provide quantitative information. (Sirovskii et al., 1981)

Mchedlishvili et al. performed in-vivo mechanical testing on the cortical surface of the parietal lobes of anesthetized, paralyzed, and ventilated adult rabbits. Their stereotaxic indentation apparatus was load controlled, with a 6.8 mm diameter spherical tip that contacted the cortical surface through a broad trephination. It is assumed that indentations were conducted directly on the arachnoid layer. Creep tests with step loading to 0.053 N for 12 seconds were performed, with the resulting deformation depth analyzed dynamically. The left common carotid artery and external jugular vein were cannulated for recording of blood pressure. An iliac artery, or the cannulated common carotid artery, and blood pressure was controlled. Brain edema formation, in which the presence was confirmed upon completion of the experiment by determination of cerebral water content increase (by 15.5 ± 2.7 % compared to normal rabbit brain), was initiated via hypotension. Three minute long ischemic episodes were created by

lowering arterial pressure to near zero, and performed three times over 40 minutes in one group and four times over 60 minutes in the another group, with each subsequent resumption in pressure being lower than the previous. In response to the step loaded force, instantaneous elastic response, viscoelastic delayed deformation, and slow linear viscous flow were material behavior characteristics exhibited by the brains tested, as reported by the authors (depth-time curves not shown). In first group of animals, brain tissue compliance (as defined as the sum of the instant and delayed deformations) and hysteresis gradually decreased consistently. In the second group, transient increases were seen in both parameters after 45 minutes and attributed to the early development of brain edema. (Itkis and Mchedlishvili, 1979; McHedlishvili et al., 1989; Mchedlishvili et al., 1981). This group's work was the first to highlight relative differences in mechanical properties of brain to in relation to alterations within the vasculature.

Aoyagi et al. (1980, 1982) used anesthetized young adult dogs that were intubated and mechanically ventilated to keep pCO_2 between 25 and 40 mmHg. Large bilateral craniotomies and durotomies were performed and the arachnoid was left intact. The indenter tip was a flat cylindrical steel piece of 5 mm radius. Predetermined cortical gyri were indented to a depth of 2 mm over 0.06 seconds. The exact number of repeat indentations at specific areas and under specific physiological conditions is not clear, however a 3-minute period was documented as the interval of time considered by the authors to be suitable to consider repeat

indentation without necessitating consideration of the effects of previous indentations (Aoyagi et al., 1980; Aoyagi et al., 1982).

Testing was conducted in normal brain, as well as cold lesioned brain. In all states of brain, testing was conducted in combination with variables known to affect cerebral perfusion pressure, including post mannitol administration and subsequent rehydration with 5% glucose solution. Also, in normal brains, indentation data was gathered at a wide range of blood pressures, and compared to post-mortem testing. Brain was assumed to be viscoelastic and its response to deformation comparable to the Maxwell model. Accordingly, relaxation was evaluated and E and η were calculated. E was calculated using the tangent line at 20% of the indentation distance. Analysis of different locations of indentation confirmed differences in E and η, with the overall range for E being 18,000 - 38,000 Pa. In one dog, with indentations conducted in a number of locations, E was found not to vary widely between two groups blood pressures, one with MAPs ranging from 113-163 mmHg and the other from 33-77 mmHg. This was believed to reflect autoregulation in the normal brain. Respectively, means for E and η were 32,146 Pa and 17,053 Pa·s for edematous brain, and 15,681 Pa and 8,037 Pa·s for necrotic brain. Following dehydration by 20% mannitol, one area of one brain showed an increase in E of approximately 20%. In edematous brain, E was seen to decrease with dehydration and significantly increase after rehydration, but this was also limited to a specific location in what appears to be one animal. After death, generally E increased and η decreased (Aoyagi et al., 1980; Aoyagi et al., 1982). The limitations of this work mainly relate to the small

sample size for each variable tested (which were numerous, often in combinations). Therefore it is not appropriate to take values for E and η literally.

In contrast to the sophisticated equipment used by predecessors, Fukuhara et al. (1994, 1996) used a simple ophthalmodynamomometer, an instrument used to determine the relative pressure in the retinal arteries via compression of the eye, to conduct in-vivo cortical surface indentations. They interpreted the compression pressure as brain elastance. In experiments with anesthetized and paralyzed adult cats, they indented through small circular holes onto intact arachnoid. The pressure-deformation curve of one cat indented in 1 mm increments every minute, showed slightly increasing pressures required to complete each successive step. After 60 min intervals, repeated indentations produced pressures very similar at all increments to the first indentation. Approximately 11,733 Pa was required to reach 5 mm depth. The results were similar with rat and dog brain (note, however, that the number of animals were not identified) until the 4 mm increment, at which point the elastance was 8199 Pa in cat, 5600 Pa in dog, and 4266 Pa in rat (Fukuhara et al., 1996; Fukuhara et al., 1994). In a separate experiment, six cats underwent 3 mm deep indentations into the frontal, parietal, and occipital lobes, bilaterally. The averaged equivalent stress was approximately 5 kPa, however, the elastance in the parietal cortex was approximately 39% higher, which was statistically significant. Subsequently, 5 mm diameter metal cylinders were placed in the skull holes and held for 3 hours, compressing the cortical surface 3 mm. Ten minutes after removal of the

cylinder, elastance was measured, revealing that it was significantly elevated in every region compared to the initial measurements. Following a 60 min rest interval, another series of in-vivo measurements showed no significant differences from the initial measurements.

In-vivo brain surface ophthalmodynamometry was also performed on 14 human patients (aged 51-83 years) immediately after evacuation of chronic subdural hematoma via a hole located 6 cm above and 1 cm anterior to the external auditory meatus. The measurement was taken at 5 mm depth onto the intact arachnoid and any subdural hematoma capsule (if present). Patients were given local anesthetic for the operation, and $PaCO_2$, PaO_2 and blood pressure were kept within normal ranges. One month after surgery, CT scan revealed that in 6 patients where the space was greater than 3 mm the elastance had been significantly higher: 3720 ± 1080 Pa compared to 2480 ± 1027 Pa (approximately 50% increase). There was a correlation between age and elastance, but no analysis of the relationship between age and size of subdural space. Despite the limitations of the works and data reported, Fukuhara et al were the first to publish in-vivo mechanical testing of human brain, and also provided context regarding a number of species.

Miller and Chinzei, to aid development of mathematical models of tissue deformation for robotic applications (Chinzei and Miller, 1997b; Miller, 1997; Miller, 1999b, 2001b; Miller and Chinzei, 1997), performed in-vivo indentation on the brains of two anesthetized and ventilated 50 kg pigs (Chinzei and Miller,

1997a, 1998; Chinzei, 1997; Miller et al., 2000). A right frontal craniectomy and durectomy was performed leaving an 25 x 20 mm oval area of exposed cortex into which one indentation was made at 1 mm/s to a depth of 3.9 mm with a 10 mm diameter flat punch indenter. Other earlier publications suggest more than one indentation with interval times of a few minutes, examining the relationship between load depth, rate, and force. One published force-deformation curve reveals a fairly linear relationship of approximately 0.1 N increase for every millimeter indented. Although a relaxation component to the indentation is reported and evident from the force-time curve, it was not further discussed or analyzed. Using 0.499 for the value of Poisson's Ratio, the instantaneous E was calculated to be 3,240 Pa. The range of E appears to be 1,300 to 4,400 Pa. MRIs were acquired approximately 3 hours after the animal was euthanized, for the purpose of identifying geometric information necessary for mathematical modeling. The main shortcoming of their work the use of only two animals, and absence of published physiologic parameters.

Margulies et al. indented with a 4 mm diameter half-sphere into 10 four week old piglet brain, in both in vivo and ex vivo conditions (Gefen and Margulies, 2004). During the in-vivo experiments, animals were anesthetized, paralyzed, and mechanically ventilated, with physiological parameters controlled. Bilateral craniectomies were performed, approximately 2.5 by 5 cm each, followed by durotomy. Friction between the indenter tip and the cortical surface was negated by lubrication. The brain was then indented in anterior, middle, and posterior

locations in both hemispheres (order of indentation randomized), at a rate of 1 mm/second on the right and 3 mm/s on the left. A depth of 4 mm was held for 90 s. Each indentation was performed six times per site, with a 45 s rest interval.

During the first, fifth, and sixth indentations of each set, ventilation was stopped twice, for 15-20 s during the ramp and early hold period (when peak forces are produced), and again at the last portion of measurement (when long-term loads were recorded). A presumed representative photograph of indenter - brain interface during testing was published, with the angle of contact being quite tangential and in a sulcus. This is an important consideration when interpreting the results of parameter calculations, which are based on perpendicular indentation of a homogenous and isotropic sample. Following in-vivo testing, ex-vivo in-situ indentations were conducted. Centre-points of these indentations were "within ~5 mm" of those used for in-vivo measurements, as were subsequent in-vitro indentations. In-situ testing and in-vitro testing both took approximately 2.5 hours each to complete, therefore the effects of post-mortem biological changes in brain tissue should be considered when interpreting results. A short-term shear modulus (Gs) was calculated, substituting an instantaneous peak force with a finite rise time of 1.3 or 4 s (for rates of 3 and 1 mm/s respectively), as well as a long-term shear modulus (Gl), which was calculated from the average plateau portion of the relaxation decay between 85 and 90 seconds.

Six "typical" relaxation curves were presented (Gefen and Margulies, 2004), Shear moduli were significantly dependent on the testing mode and test

number in series, but neither modulus depended on speed of indentation or site. Hence, the data was averaged across speed and across site. Subsequently, an ANOVA for mode and fifth and sixth cycles was performed separately for Gs and Gl. The effect of mode was still significant, but the shear modulus was not significantly affected between the fifth and sixth runs. Hence, the moduli measured at fifth and sixth cycles were averaged together and defined as the "fully preconditioned" moduli values. Gl was 100-150% greater than Gs for all testing modes, and first-run moduli were greater than preconditioned moduli for all cases except the in-vivo Gl. In-vivo values for Gs and Gl were statistically indistinguishable from those in-situ. The design of the study was adequate to determine differences between in-vivo and in-situ properties for all but the preconditioned Gs. Values of Gs and Gl were indistinguishable between in-vivo and in-vitro on the first indentation run. However, after preconditioning the in-vivo properties were significantly stiffer than in-vitro.

The time course of brain tissue relaxation between the in-vivo, in-situ, and in-vitro experimental modes was compared. Differences across test modes were significant for the long-term time constant of relaxation, which decreased between in-vivo and in-situ in all cases except the first-cycle 1 mm/s indentations. In-vivo with the same preconditioning status, the faster loading rate consistently increased the long-term relaxation time and decreased its coefficient G2.

Shulyakov and Del Bigio have performed in-vivo indentation of rat brain, using the same indenter apparatus as the work completed for this thesis (and

detailed later) (Shulyakov et al., 2009). Physiological monitoring, including intracranial pressure, arterial blood pressure, and cerebral blood flow, was performed. With indentation of 1.5 mm depth of a 2 mm radius flat punch indenter tip. Elasticity was not found to change after death. Creep deformation over 15 s was 7.96±1.6% in live brain and 27.9±0.24% after death, indicating that viscous properties change. Further comparisons were made of live rats at different ages, showing significant increase in elastic properties as the animals age through to 180 days, and creep behavior that decreased in the postnatal period to stabilize at 21 days. These mechanical property changes corresponded to a decrease in brain water content and increase in total protein content (Shulyakov et al., 2011). On a separate cohort of animals, when tests of creep at 100 mN, and 100 oscillations of 20 to 100 mN were performed gradual deformation of the intracranial contents was observed. Following cisternal kaolin injection to create hydrocephalus, after 7-9 days there was a transient increase in intracranial stiffness, and viscoelastic strain during application of a constant force significantly increased by >50% (Shulyakov et al., 2012). In a separate experiment, the pathological variable of traumatic contusion was explored for it's effect on the in-vivo mechanical response of rat brain to indentation. Testing was performed 2 hours to 21 days after the contusing force was delivered. Initially, edema and tissue necrosis led to the brain becoming less elastic and less viscous. Later, along with undergoing reactive cellular changes, the brain became stiffer than normal (Alfasi et al., 2013).

1.4.2.2 Interpretation and meaning

In summary, direct in-vivo mechanical testing of brain has been performed across an inconsistent set of variables relating to physiologic control and testing conditions, and from which the data accrued is reported in a non-standard manner. This has made it difficult to determine the validity of individual works, compare them, and summate the results of in-vivo mechanical testing of brain as a whole. The variety of species, anatomical consideration, physiological parameter measuring, deformation methods, and data analysis make literal interpretation of material coefficients or properties, put forth as numerical values, inappropriate. Regardless, the data consistently shows the very soft, viscoelastic nature of brain, that has been generally agreed upon, and shown in ex-vivo experimentation. Also, different anatomical locations and regions of a brain tested continue to show differ from each other.

It is the differences shown between in-vivo and ex-vivo testing, as well as the differences within variables specific to the in-vivo state, where the contribution of direct in-vivo testing has been large. Although not well quantified, the majority works detailed above reveal that elastic and viscos components of brain are affected by whether they were tested in the in-vivo and ex-vivo state. Furthermore, works in which variations in physiological parameters, including those which relate to cerebral blood volume and perfusion pressure, and

pathologic states (e.g. edema, inured brain) have been compared have revealed differences in the mechanical response to similar testing conditions.

This leads to a natural conclusion that mechanical testing of brain should be done in the living state where possible, considering the numerous variables that may affect the results, including a number of which may be counteracting and not readily apparent. When conducting direct in-vivo mechanical testing of brain, all physiologic variables should be controlled for which relate to intracranial pressure, water content, and temperature. Practically, this means controlling blood gases (pCO_2, H^+, and O_2), blood pressure, CSF loss, brain surface moisture, serum sodium, body temperature, and exposed brain surface temperature. The testing conditions must also be conducted within the context of specific anatomy, including geometry (angle of deformation), material composition (specific region of brain), and anisotropy (relationship to white matter fibers). Analysis of the data from such testing should be reported in as simple and straightforward a manner as possible, within the consideration of the brain being viscoelastic. Conducting and reporting testing results as summarized will eliminate a number of potential confounding variables, and allow confidence in subsequently comparing each variable under otherwise the same testing conditions. This is the basis and philosophy under which the methods were developed for this current work.

1.4.3. Potential tools of investigation

All medical research, including the study of the mechanical properties of the brain, is performed with the overall philosophy and end goal of improving the health of humans. Therefore, although directly testing the mechanical properties of a living human brain has not yet been performed under controlled and replicable conditions, the applicability of investigational tools currently used in a laboratory environment to the clinical realm should always be considered. Modification of existing clinical tools to be able to perform mechanical testing is equally warranted.

Hand-held devices resembling indenters have been developed for applicability in clinical medicine, and although do not measure time-related parameters, have the ability to measure force and degree of deformation. These tools provide information which is useful in describing the tissue tested in mechanical terms. These tools require relatively large forces and are useful for tissue that is clearly stiffer than brain, such as skin and muscle (Hansma et al., 2009; Zheng et al., 1999). There are no devices described in the literature that would be safe to test on a living human brain. However, the fact that hand-held devices for testing mechanical properties exists highlights possibility that more sophisticated and fine-measurement instruments can be developed in the future. It can be envisioned that an instrument such as this could one day find itself inside an operating room where brain surgery is performed. The development of tools to measure mechanical properties inside the body are currently underway

for other tissues (e.g. liver, prostate) both to aid in diagnosis as well as surgical techniques (Ahn et al., 2012; Beccani et al., 2013).

Developing a device to test the mechanical properties of a brain in a living human is very difficult, as it must be safe and carry no risk of damaging brain. This will always be the limiting factor in the development of such a tool and method. The brain is perceived to be more easily damaged by direct deformation forces than any other issue in the body, and carries the highest functional value. As direct mechanical testing is invasive, the feasibility of developing acceptance for an investigational tool will rely on the ability to build on and extrapolate from established invasive therapies, which are surgical techniques and their associated instruments. Examples of these include brain retraction, aspiration of brain tissue and, ultrasound use on the cortical surface of brain to confirm the presence of deeper pathology (Carter et al., 2005; Schiavone et al., 2009).

2. METHODS

The primary objective and hypothesis of this dissertation necessitates control of all mechanical, anatomic, and physiological variables during step-loaded stress-relaxation indentation of living rabbit brain under specific and pre-defined groupings of MAP and pCO_2. A large amount of time and resources were required to develop and refine the animal model, the step-loaded in-vivo indentation test, and the ability to control all physiological parameters in order to meet the objectives and evaluate the hypothesis of current work. The methodology used for the currently presented work, detailed in the remaining sections of this chapter, was the result of a number of pilot experiments.

All aspects of the current work and the specific methodology were novel to the writer and the laboratory environment. Furthermore, there is no published methodology that approaches the same degree of sophisticated mechanical testing on living brain with control of all physiological variables, and on a consecutive series of animals with the same testing parameters.

2.1. Animal model

Seven consecutive young adult male New Zealand white rabbits (2.8 to 3.5 kg) underwent in-vivo brain indentation stress-relaxation testing under the same anatomic, physiologic, mechanical testing conditions. This species was chosen in part because of its brain size and relative lissencephaly (Figure 1.6). The exposure of the frontal lobe of this species can be performed on a large enough area to allow testing with consistency between animals, while respecting boundary conditions and without damaging the tissues. Also, this animal's size allows for physiologic monitoring and manipulation not technically possible in smaller mammals such as mice or rats.

The University of Manitoba approved an animal care protocol relating to the ethical treatment of research animals as per the Canadian Council on Animal Care. The rabbits were obtained from a local breeder, and administered a subcutaneous injection of diluted enrofloxacin (Baytril) on arrival followed by addition of enrofloxacin to the drinking water one week prior to experimentation to control for possible subclinical Pasteurella infection, which can affect pulmonary function. This step was initiated during the pilot experimentation, after a series of rabbits were found to be refractory to normal ventilatory settings and subsequently found to be harboring pulmonary exudate.

The animals were placed under a general anesthetic and a tracheotomy performed, with subsequent mechanical ventilation via a ventilator (Harvard Apparatus; Holliston, USA) and 3.5 mm (inner diameter) endotracheal tube.

Endotracheal intubation was found to be difficult to perform and less reliable in proper placement of the tracheal tube, and therefore abandoned in during pilot experimentation for the more direct tracheotomy approach.

A sedating cocktail of intramuscular acepromazine 1 mg / kg, ketamine 35 mg/kg, and xylazine 5 mg/kg was used for induction. Following intubation, anesthesia was maintained with inhalational isoflurane (concentration titrated to the minimum dose required to maintain clinical anesthesia; range 1.0 - 2.0 %), delivered with 99 % O_2. Isoflurane is an anesthetic commonly used in surgical procedures of animals and humans, but has been shown capable of lowering blood pressure and resulting in vasodilation of cerebral blood vessels, when concentrations of greater than 1% are maintained (Li et al., 2013; Van Aken et al., 1986). Therefore, the interpretation of any experimental results is strictly in relation to the context of inhalational isoflurane anesthesia. However, not only is it practical to use one of the most common methods of anesthesia, but the reality for this current work was that after the initial operative procedures at the beginning of each experiment the typical isoflurane concentration was never raised above 1%.

A pulse oximeter on a rectal probe was used to ensure that oxygen saturation remained above 92% (SurgiVet; Norwell, USA). This value is a generally regarded clinical standard, and ensures that arterial partial pressure of oxygen remains above 60 mmHg, which is above the threshold in which hypoxic conditions cause a response in cerebral blood flow. Oxygenated ventilatory support was based on supplementing volumes appropriate for animal mass. For

a 3 kg animal, the frequency is forty breaths per minute and the volume 18.82 cm^3. Arterial blood was monitored for pressure, and sampled for pCO_2 measurements. Further details regarding physiological manipulation methods are detailed later. Invasive procedures were performed under aseptic technique. Normothermia was maintained with a warming-cooling blanket (temperature of 37°C). The animal was positioned prone, and the scalp was shaved, cleansed with chlorhexidine, and draped to maintain aseptic conditions. After scalp excision, a surgical microscope was used to provide magnification.

A left frontal craniectomy was drilled meticulously, approximating a circle with diameter slightly exceeding 6 mm. A larger craniectomy would be associated with significant risk of damaging normal tissues and encroaching on boundary conditions (i.e. falx and rounding edges of the frontal lobe). The 6 mm diameter indentation site, included enough surface area to reasonably average slight variations in surface vasculature and sulci location and morphology, but remains a small enough to fit within the craniectomy. The dura was then removed, taking care to leave the arachnoid intact, which revealed the near-flat cortex within the craniectomy window. The exposed brain approximated 6 mm in diameter.

The field was irrigated with 37°C sterile 0.90% sodium chloride throughout the experiment. The animal was placed on a custom platform that included head fixation with a modified zygomatic arch - incisor clamp (David Kopf Instruments; Tujunga, USA). The platform was affixed to the indenter apparatus (Figure 2.1). The exact body platform and head position was manipulated to ensure the

trajectory of indentation deformation would be perpendicular to the cortical surface (Figure 2.2).

Figure 2.1. In-vivo rabbit brain indentation. The indenter tip is passing through the craniectomy window and in contact with the cortical surface. The rabbit is supported with its head affixed in relation to the indenter apparatus, using a zygomatic arch - incisor clamp (David Kopf Instruments; Tujunga, USA).

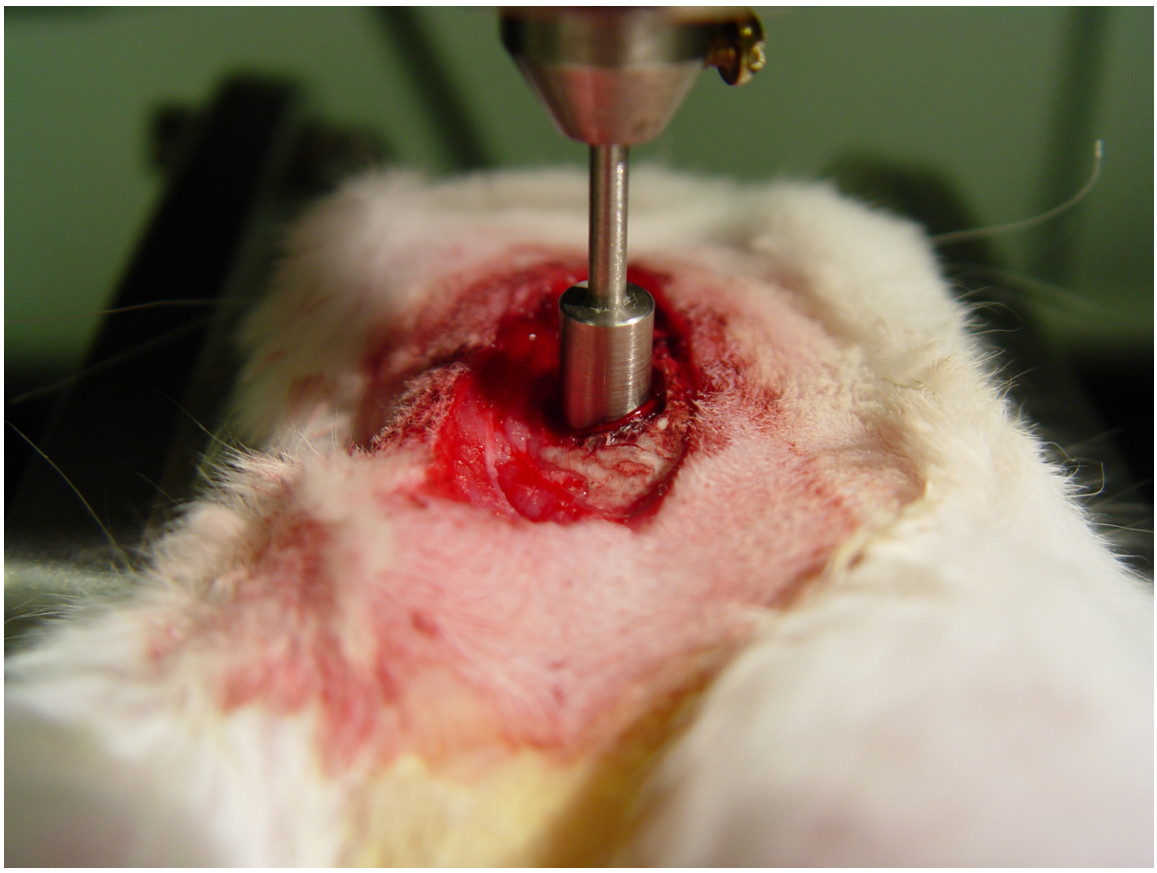

Figure 2.2. In-vivo rabbit brain Indentation. The indenter tip descends through the craniectomy window to indent the cortical surface of the brain.

Details of indentation apparatus and method will follow this section. After completion of testing, the animal was euthanized with an overdose of pentobarbital. The brain was removed from the skull en bloc and fixed in 10% formalin. Once fixed the brain was dissected in the coronal plane to ensure that there had not been any intracerebral hemorrhage or laceration of the brain due to the experimental methods, as these entities would affect the experimental results of mechanical property testing.

2.2. Indentation

The indenter used was a customized open platform Micro Hardness Tester (MHT) (CSM Instruments SA; Peseux, Switzerland). Aspects of its application have been previously described (Shulyakov et al., 2011; Shulyakov et al., 2009). Technical specifics are detailed in Appendix 1.

When choosing an indenter tip, one must consider the shape and size of the tip's surface that will be contacting the test sample. For a very soft sample, a relatively large radius flat-punch indenter tip will take more force to reach a pressure that deforms the sample compared to a smaller radius. With the MHT, the larger the contact area between the indenter tip and sample surfaces, the greater an averaging effect with respect to the surface it is indenting. This is especially important for something like the cortical surface of brain, as there are subtle differences from one brain to another in the details and arrangement of the leptomeninges and vessels. For in-vivo rabbit brain testing, a 3 mm radius steel flat punch indenter tip is used, chosen to accommodate the 6 mm craniectomy precisely. These are the largest sizes of indenter tip and craniectomy that maintain the brain in its normal state, and respect boundary conditions.

After the rabbit was placed in the head holder, the table position is moved so that, under direct visualization, the exposed cortical surface of the rabbit's brain is closely approximated to the indenting surface of the indenter tip. The MHT and its control unit are entirely computer controlled and menu driven. Indentation is initiated via controller command, and the indenter tip and brain

approach contact. Detection of 4.6 mN of force triggers an indentation. This value was determined through pilot experimentation. The indenter tip is in full contact with the brain surface at the initiation of indentation. Inertia is the limiting factor in actually attaining an “instantaneous” step-loaded indentation, and the maximum physical limit of depth is encountered before the set maximum force can be reached. With the MHT, this takes approximately 1 s and the depth of indentation is 1948 μ m.

For each rabbit, an indentation was performed five times, with fifteen minutes intervals of rest between each indentation, to allow for potential recovery of viscous properties and adjust physiological variables to the desired testing conditions. The indentation parameters were exactly the same, as described above, for each indentation. Manipulations of blood pressure and pCO_2 were performed for different indentations, and are described in detail below.

2.3. Physiologic manipulation

For each rabbit, five indentations were performed, each under physiologic conditions of relative difference:

Indentation 1. Low MAP and low pCO_2.

Indentation 2. High MAP and low pCO_2.

Indentation 3. Low MAP and high pCO_2.

Indentation 4. High MAP and high pCO_2.

Indentation 5. Low MAP and low pCO_2.

“High” and “low” refer to relative differences between the two for a particular parameter. Significant categorical differences were confirmed prior to further analysis, with the quantitative values found in the Results section of this manuscript (Chapter 3). The primary objective and targets for these physiological variables were that they be significantly different from each other where planned. Regardless, the quantitative values of the categories of high and low were intended to reflect states of relative hypercarbia and hypocarbia (for pCO_2) and hypertension and hypotension (for MAP), respectively. For the New Zealand White rabbit, wide ranges for MAP under normal conditions have been reported, but generally the range is 65 to 100 mmHg (Kurashina et al., 1994; Manning et al., 1994; Suckow and Douglas, 1996). For pCO_2, the range was been manipulated as wide as from 20 to 60 mmHg, with general acceptance that 35 to 45 is normal state range (Manning et al., 1994; Scheller et al., 1986; Suckow and Douglas, 1996)

Intra-arterial blood pressure was monitored using telemetric pressure monitors with fluid-coupled catheters (Data Science International; New Brighton, USA). A femoral artery surgical isolated, followed by cannulation of the artery with the catheter. The catheter was advanced to place the tip within the aorta. Pressure is viewed live and also recorded. The contralateral femoral artery was also exposed and cannulated, but with a 21-gauge angiocatheter for purpose of obtaining blood samples. Arterial blood was analyzed (IDEXX Laboratories; Westbrook, USA) specifically for pCO_2 value, and performed just prior to an indentation. A 25-gauge intravenous butterfly catheter was secured in a right marginal ear vein, for the purpose of administering 200 μm/min of 200 μg/mL phenylephrine. Phenylephrine is a selective α_1-adrenergic receptor agonist, and causes vasoconstriction, which in turn raises blood pressure (Thiele et al., 2011).

Relative hypotension was the baseline state of blood pressure of the animal under general anesthetic. Relative high blood pressure was induced with the phenylephrine bolus, delivered intravenously via a syringe pump. A relatively “high” blood pressure was deemed achieved, and indentation suitable to begin, once the pressure was seen to stabilize despite continued delivery of phenylephrine. Relative states of hypocarbia and hypercarbia were attained via increasing and decreasing ventilatory flow rate, respectively.

The order of the indentations was always performed as previously listed numerically. The rest period in between each indentation was 15 minutes. Indentation 1 and Indentation 5 were performed under the same relative physiological parameters, with the intention of determining if there are any

differences between two similar indentations that might be attributed to repeat indentations in which there is not more than 15 minute recovery periods in between. The 15 minute length of time is chosen for the rest period specifically, as it is longer than any pauses between repeated in-vivo brain deformations published previously.

2.4. Analysis

Force-time curves of indentations were captured and analyzed. Inspirations and expirations create intrathoracic pressure differentials that are transmitted to the brain via the venous system. On plots these appear as saw-toothed peaks and troughs. Figure 2.3 is a typical example of the raw data force-time curve, as presented by the MHT software.

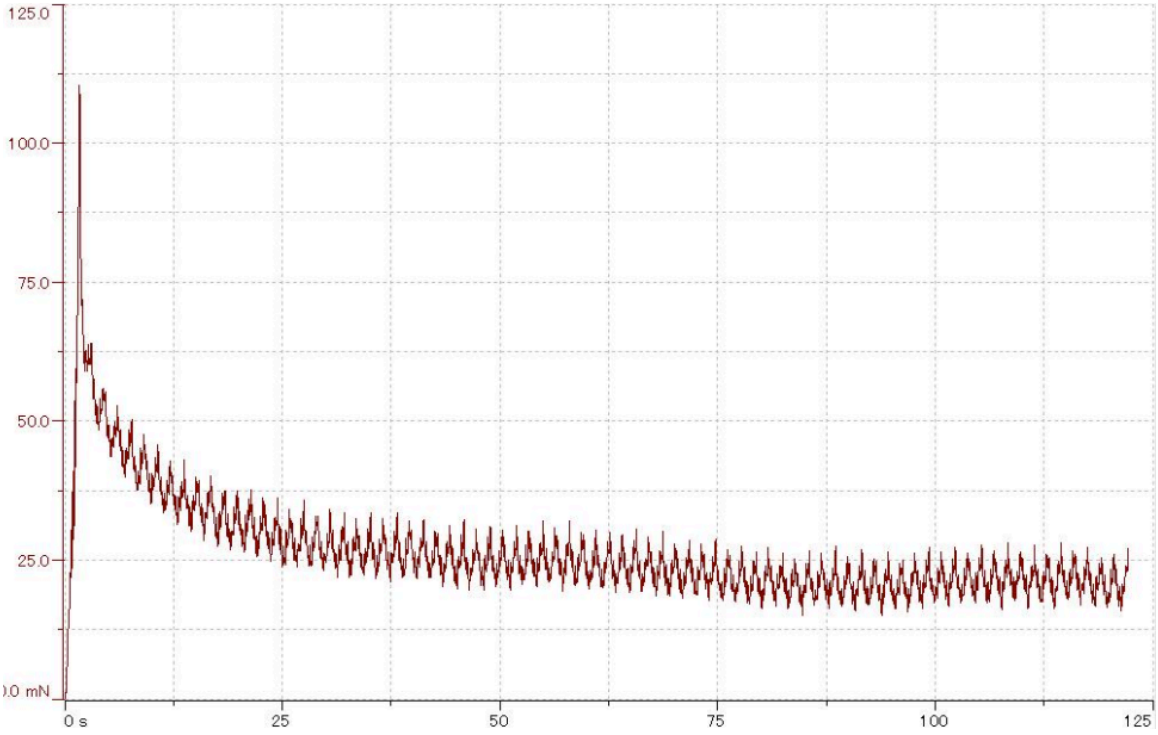

Figure 2.3. Example of MHT software presentation of data acquisition in a force-time curve, from an actual indentation (Rabbit #1; Indentation 1). X-axis: Time (s). Y-axis: Force (mN).

Within these pulsations are subtle “sub-pulsations” generated by the cardiac cycle (Figure 2.4).

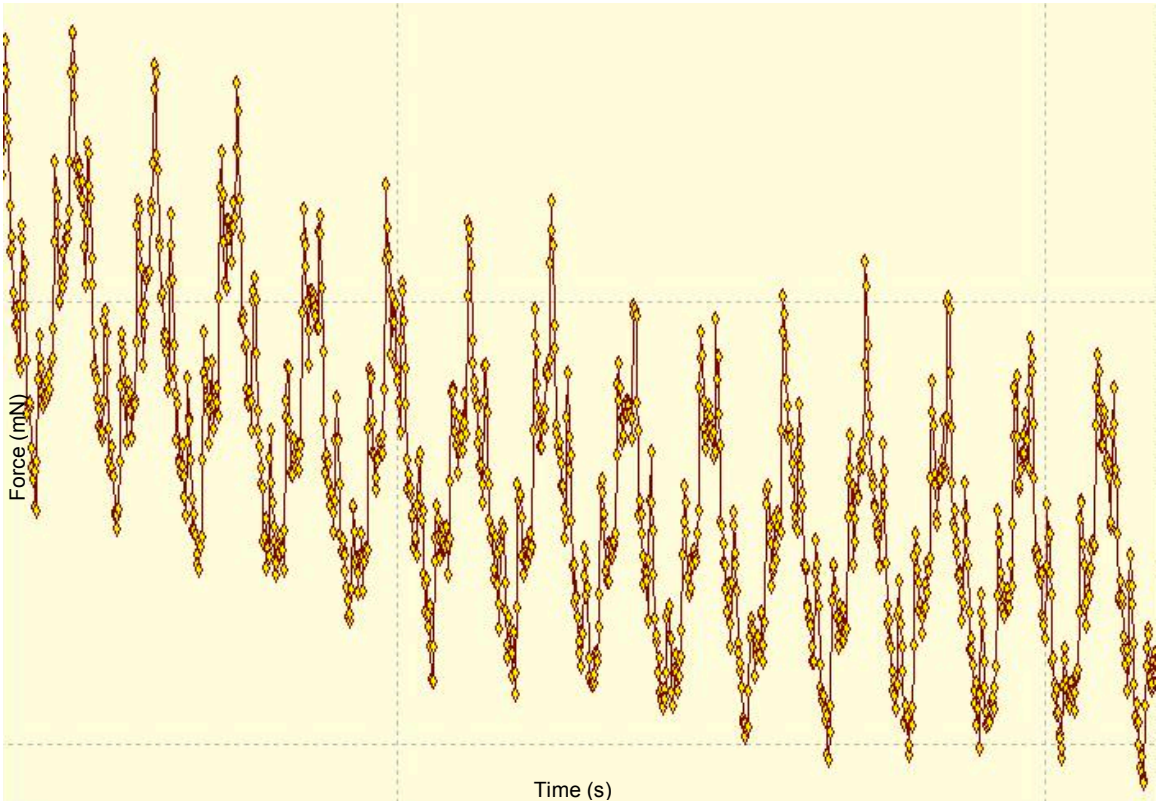

Figure 2.4. Zoomed-in portion of Figure 2.3, providing illustration of respiratory and cardiac transmitted pulsations.

For all indentations, all points corresponding to peak expirations and inspirations were transferred into new force-time plots, enabling evaluation of “peak” expiration and “peak” inspiration data points separately. The peak force immediately following step loading was considered as time 0 s. Force-time curves were converted to stress-time scatter plots, with stress calculated by

dividing force values over the cross-sectional area of the indenter tip (Equation 1):

$$\sigma = \frac{F}{A} \quad (1)$$

σ = stress (Pa), F = indenter force (N), A = area (m^2).

Continuing with the example shown in Figure 2.3 and 2.4, illustration of the subsequent stress-time curve in the form of expiration and inspiration can be seen in Figure 2.6. The plotting of the peak expiration and inspiration points form a relatively smooth curve for each.

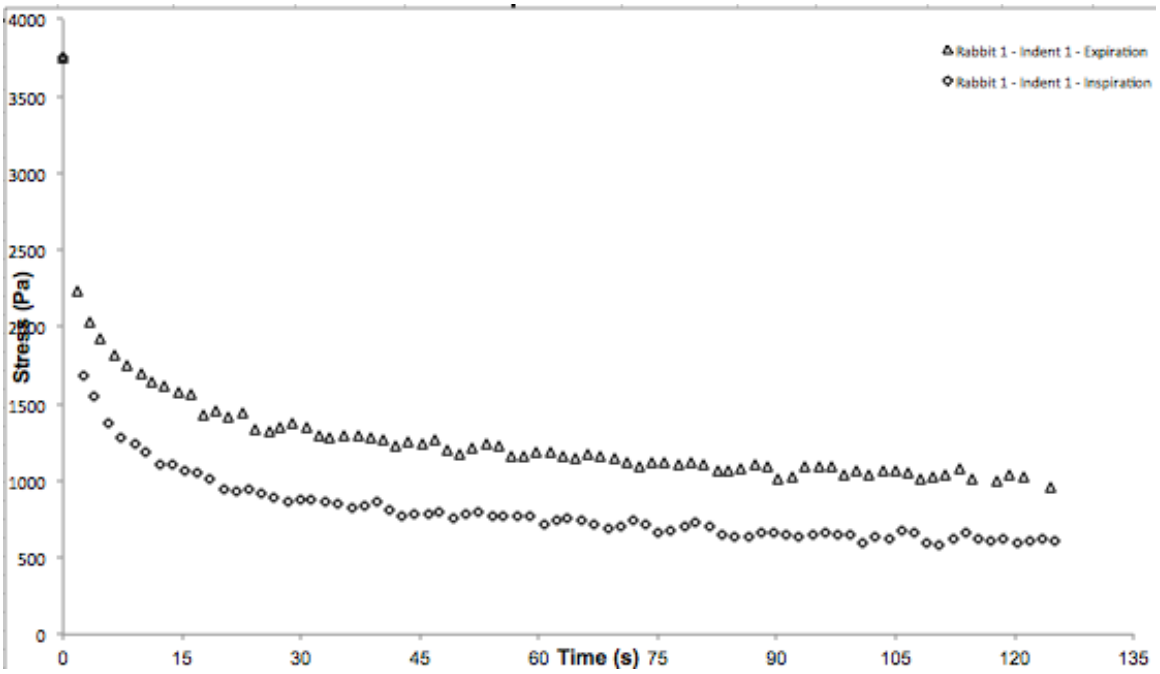

Figure 2.5. Plotting of the peak expiration and inspiration points from Figure 2.3 (Rabbit 1; Indent 1). Two curves are formed for the purpose of separate analysis.

The Maxwell model (Mohsenin, 1986) is used to model behavior of viscoelastic material and stress relaxation specifically. The experimental data were evaluated for fit to a generalized Maxwell model consisting of a spring (Hook's law) and dashpot (Newtonian fluid) in series, paralleled with another spring and dashpot in series, paralleled with a single spring (Figure 2.6). This is to represent a material with two viscoelastic elements, each with its own viscosity and elasticity moduli, and a stress equilibrium element. This model can be represented by Equation 2.

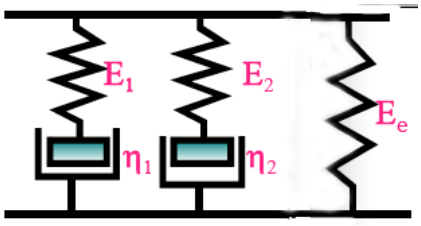

Figure 2.6. Spring and dashpot representation of the generalized Maxwell model used to fit the experimental data.

$$\sigma_P(t) = A_1 \exp\left(-\frac{t}{TRel_1}\right) + A_2 \exp\left(-\frac{t}{TRel_2}\right) + A_{Eq} \qquad (2)$$

$\sigma_P(t)$ = peak stress (Pa), $TRel_1$ and $TRel_2$ = time of relaxation constants (s), A_1 = intermediate stress coefficient (Pa) associated with $TRel_1$, A_2 = intermediate stress coefficient (Pa) associated with $TRel_2$, A_{Eq} = equilibrium stress coefficient (Pa), t = time (s).

MATLAB software (MathWorks; Natick, USA) was used to perform a least-squares curve fit to solve for the intermediate stress coefficients (A_1 and A_2), their respective decay constants (times of relaxation) ($TRel_1$ and $TRel_2$), and the equilibrium stress coefficient (A_{Eq}). The MATLAB equations and code used for this are found in Appendix 2.

The values for the elastic modulus, for peak and intermediate coefficients were calculated via the Boussinesq problem (Mohsenin, 1986) for die loading (Equation 3). This method of calculation was used specifically because the cortical surface of the rabbit brain is flat (Figure 1.6) and the indenter tip is a cylindrical flat punch. A Poisson's ratio of 0.45 was used (Brands et al., 2002; Soza et al., 2005), acknowledging that others have used or calculated values for brain ranging from 0.499 (Miller, 2000) to 0.35 (Guillaume et al., 1997). It is felt that brain is nearly incompressible, with a Poisson's ratio that approaches 0.5, but has been shown to yield values of less than 0.5 when loading conditions are not-instantaneous (Guillaume et al., 1997). "Instantaneous" loading is theoretical, as there is always the technical limitation of inertia with testing, and is directly related to the indentation method used in the current work. Therefore, a Poisson's ratio of 0.45 was chosen, as was previously discussed in other works (Shulyakov et al., 2009).

$$E_{P,1,2,Eq} = \frac{\left(\sigma_{P,1,2,Eq}\ (A)\right)\left(1-\mu^2\right)}{(d)(r)} \quad (3)$$

E = elastic modulus (peak stress, intermediate 1 stress coefficient, intermediate 2 stress coefficient, and stress equilibrium) (Pa), σ = stress (peak, intermediate 1 coefficient, intermediate 2 coefficient, equilibrium), μ = Poisson's ratio estimate for in-vivo rabbit brain (0.45), d = depth of indentation (m), r = radius of the indenter (m).

The viscosity coefficients for the viscoelastic elements of the model were then calculated from the rearranged definition of the relaxation time:

$$\eta_{1,2} = E_{1,2}(TRel_{1,2}) \quad (4)$$

η = viscosity coefficient (first and second) (Pa·s), E = the corresponding elastic modulus of the Maxwell model (Pa), TRel = relaxation time of the corresponding Maxwell element(s). Subscript 1 refers to the portion of the curve that has a longer time of relaxation and Subscript 2 refers to the portion of the curve with the shorter time of relaxation.

Statistical comparison of the stress-relaxation coefficients and mechanical properties was performed using JMP software (SAS Institute, Cary NC). All stress relaxation coefficients and material properties were expressed as mean ± standard error of the mean. Comparison across indentations were made using analysis of variance followed by post hoc intergroup comparisons with Tukey-

Kramer HSD. Statistical significance set at $p<0.05$. All statistical analysis detail is available, including with the results, in Appendix 3.

2.5 Assumptions

Analyzing and comparing mechanical testing data from in-vivo brain step-loaded stress-relaxation indentation requires a number of assumptions. These assumptions are necessary because many of the anatomical, physiological, and testing parameters are found on a continuum of variability, but need to categorized in order to make comparison possible.

The mechanical response of a viscoelastic object or material under deformation can be compared across the temporal relation of stress, strain, and time. However, in order to quantify and describe the data so that it can be compared across other testing conditions, the viscoelastic response needs to be fitted to a mathematical model. A Maxwell model is used for this purpose in the current work, and consists of a spring and dashpot in series, paralleled with another spring and dashpot in series, paralleled with a single spring. If the objective was to mathematically describe the response of the material literally, it must be assumed that the material is linear viscoelastic under the strain used. It is generally considered that brain tissue exhibits non-linear behavior. It is the assumption of the current work that using the Maxwell model as described is still warranted, as the goal of the current work is to present the data in as simple a model as possible, and not to mathematically describe brain literally, but provide a simple measure of the overall mechanical response of the cranial contents in which to compare physiological variables.

Calculation of stress, apparent elastic moduli, and apparent viscosity coefficients also required assumptions. The Boussinesq problem is appropriate for the context of flat-punch cylindrical die loading onto a flat infinite surface. Although this is the case in the current work, the brain surface can never be relied on to be perfectly flat or uniform. Regardless, it is much more so this than any other geometry. The assumption regarding the choice of Poisson's ratio as 0.45 has previously been discussed. As this value is used for all indents and animals, a choice of a slightly different value would not affect the detection of relative value changes amongst physiologic groupings. Specific technical assumptions relating to step-loaded indentation and analysis of relaxation have also been discussed, with degree in which the step load is "instantaneous" being of most importance. Delay in the loading rate can change the response and measurement of material relaxation. However, this a factor common to every indentation performed in the current work, and is not considered to limit the value of detecting differences when comparing groupings physiologic parameters.

The complexity of the surface anatomy of the brain is not only important in terms of geometry, but also in terms of variability. No two living rabbit brains are exactly the same, and subtle differences in the brain pia – arachnoid interface, including the presence of blood vessels, may affect direct measurements. This is the reality of biomechanical testing, and also applies to subcortical anatomical variability as well. In addition to anatomical variability, testing in a living system introduces physiological variables. pCO_2 and blood pressure are dynamic processes. However, they are easiest to consider when considered categorically.

It is assumed that the relative high versus low values for these parameters are suitable to represent clinical scenarios of hypo and hypercarbia, and hypo and hypertension. Also, the absolute effects of anesthetic agents on regulation of cerebral blood flow, and their interactive effects with the aforementioned physiologic variables, may impact the relaxation behavior of brain. However, the goal is to detect relative differences in mechanical properties (not absolute relaxation coefficients or material properties), and the anesthesia employed in this work was the same for each animal.

3. RESULTS

Seven consecutive rabbits had in-vivo brain indentation stress-relaxation testing performed under the same anatomic, physiologic, and mechanical testing conditions. Each rabbit had five indentations performed, in sequence with a specific set of physiological parameters, as described in the previous section.

Three indentations were eliminated from analysis due the inability to attain a relative and consistent increase in blood pressure, when that was the intended goal for that indentation: Rabbit 6 – Indentation 4, Rabbit 7 – Indentation 2, and Rabbit 7 – Indentation 4. In all three cases, technical difficulties with maintaining intravenous access in relation delivery of phenylephrine was the source of the problem.

As previously described, the indentations were performed under a specific and deliberate set of physiological variables:

Indentation 1. Low blood pressure and low pCO_2.

Indentation 2. High blood pressure and low pCO_2.

Indentation 3. Low blood pressure and high pCO_2.

Indentation 4. High blood pressure and high pCO_2.

Indentation 5. Low blood pressure and low pCO_2.

Where intended, statistical differences were attained between groups of physiological variables (Figures 3.1 and 3.2). Indents 1, 3, and 5 ranged in mean MAPs from 50 to 55 mmHg. Indents 2 and 4 had mean MAPs of 96 and 115

mmHg. Indents 1, 2, and 5 ranged in mean pCO_2 values from 30 to 34 mmHg, and Indents 4 and 5 both had a mean pCO_2 values of 54 mmHg.

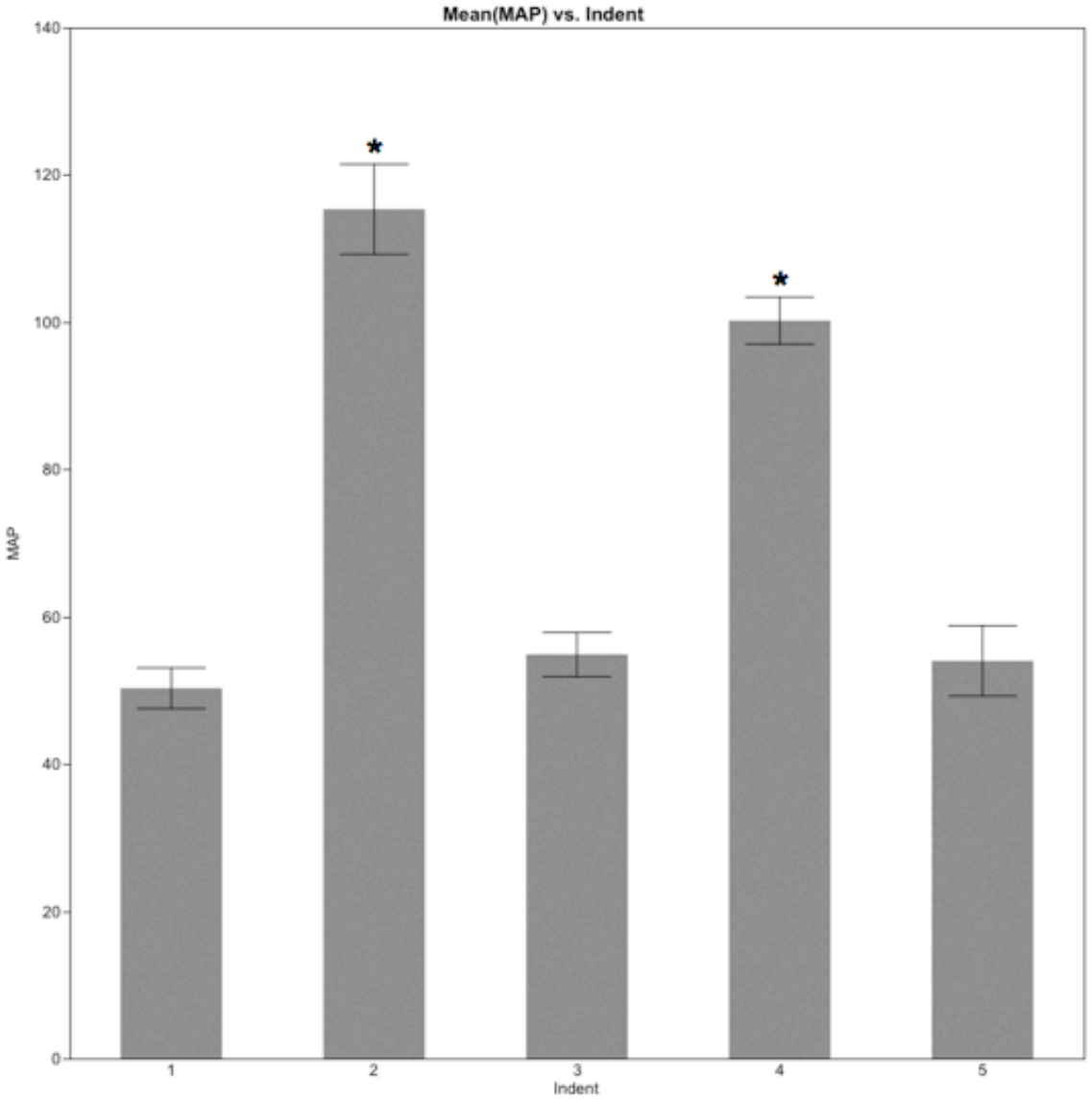

Figure 3.1. The bar graph (with SE bars) for the mean mean arterial pressure (MAP) (mmHg) per indentation group. The difference between the intended relatively low blood pressure groups (i.e. Indent 1, 3, and 5) is confirmed significant from the intended relatively high blood pressure groups (i.e. indent 2 and 4) (* $p<0.0001$).

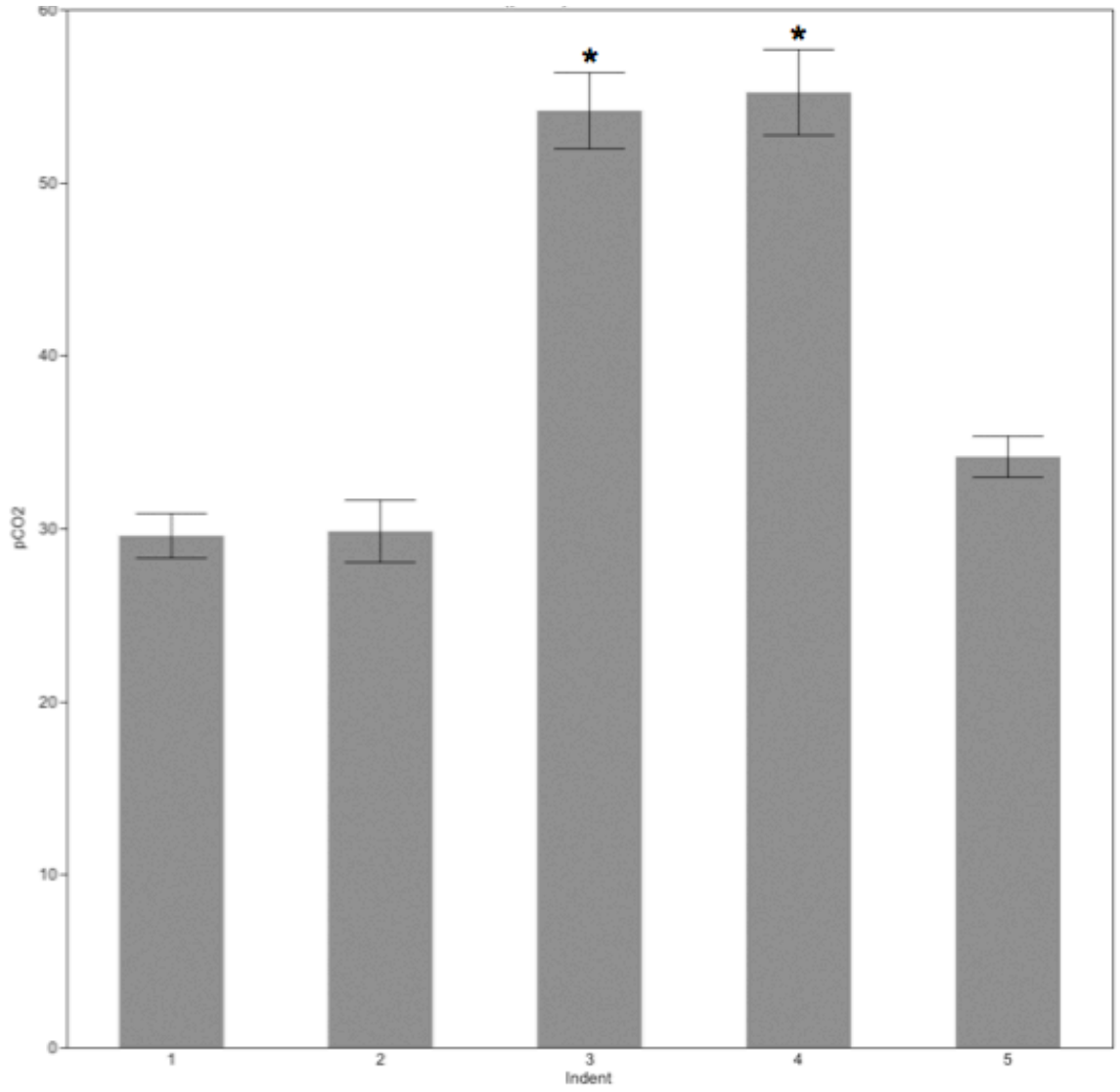

Figure 3.2. Presented is the bar graph (with SE bars) for the pCO_2 (mmHg) per indentation group. The difference between the intended relatively low pCO_2 groups (i.e. Indent 1, 2, and 5) is confirmed significant from the intended relatively high pCO_2 groups (i.e. indent 3 and 4) (* $p<0.0001$).

The original data curves for all indentations in both expiration and inspiration phases are viewable in Appendix 4 and 5 respectively.

Fitting of the generalized Maxwell model, as previously defined, to the data sets resulted in good fits. In keeping with the example indentation used in the previous section for illustration purposes, Figure 3.3 is the plot including the simulation line from the model, with the data points. In this case the R^2 value was 0.99.

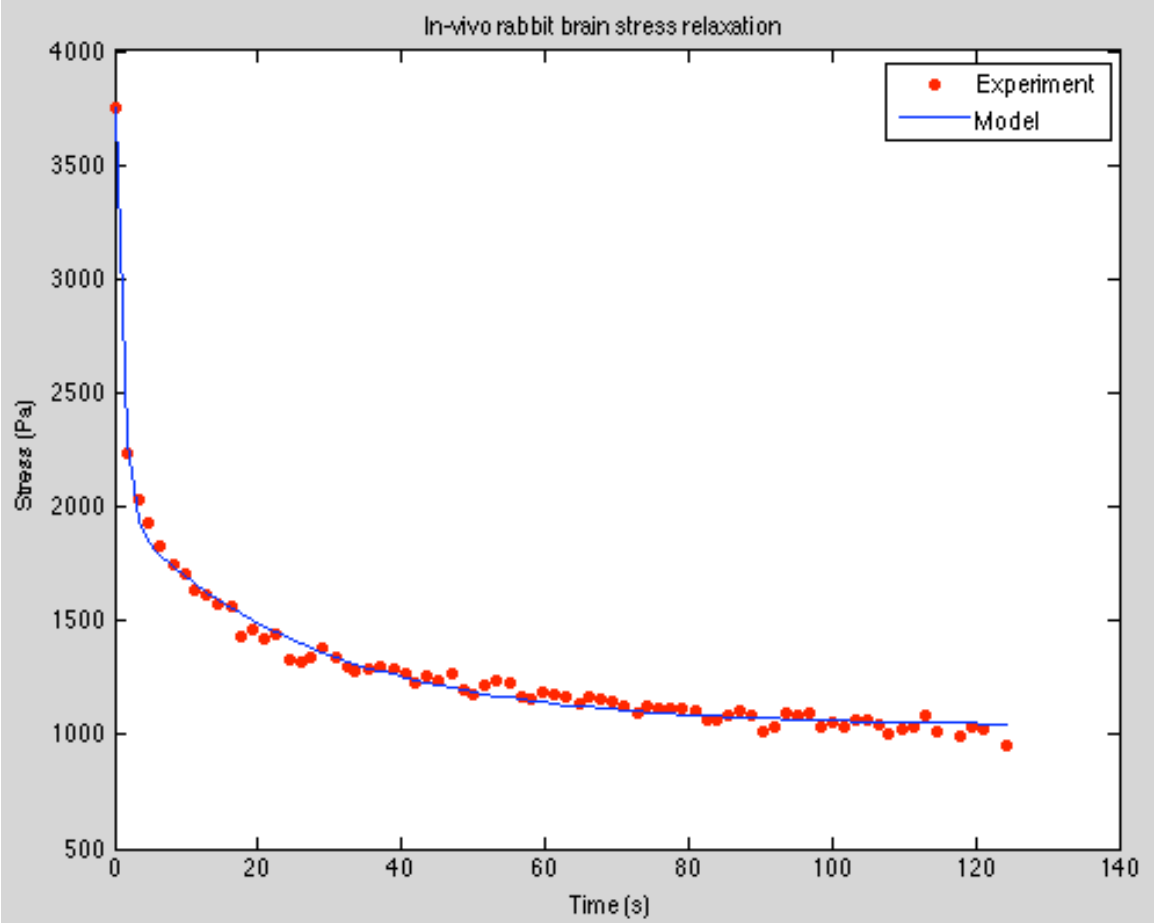

Figure 3.3. Plotting of a generalized Maxwell model with two viscoelastic components (each a Hookean spring and Newtonian dashpot in series) and an equilibrium stress, fitted to the data of Rabbit 1 – Indentation 1 – Expiration (continuing the illustrative example seen in Figures 7-9). R^2 = 0.99.

Table 1 shows all R^2-values for all indentations, as well as the differences in value between actual peak stress and model-derived peak stress. This information helps objectify the goodness of fit of the model to the experimental data. The latter is relatively small considering that the data peak stresses were of the order of magnitude of 10^3 to 10^4.

Table 1. R^2-values of the least-squares curve-fitting technique for the generalized Maxwell model fitted to the data, for all analyzed indentations. In addition, the differences in value between actual peak stress and model-derived peak stress are presented. This provides objective information in which to help evaluate the fit of the model to the data. The high R^2-values and small differences between the experimental and model peak stresses suggest a good fit.

Rabbit #	Indentation	data peak stress minus expiration simulation (Pa)	expiration model R2	data peak stress minus inspiration simulation (Pa)	inspiration model R2
1	1	5	0.99	4	0.99
	2	4	0.99	2	0.99
	3	8	0.99	-1	0.99
	4	6	0.99	1	0.99
	5	0	0.99	6	0.99
2	1	3	0.99	1	0.99
	2	3	0.99	3	0.99
	3	-12	0.99	0	0.99
	4	13	0.98	2	0.99
	5	2	0.99	1	0.99
3	1	4	0.99	4	0.98
	2	1	0.98	5	0.99
	3	0	0.99	1	0.99
	4	8	0.99	0	1.00
	5	0	0.97	4	0.98
4	1	1	0.99	1	0.99
	2	1	0.99	0	0.99
	3	0	0.95	0	0.99
	4	7	0.96	3	0.98
	5	16	0.96	2	0.96
5	1	0	0.98	0	0.99
	2	3	0.96	2	0.98
	3	9	0.92	0	0.97
	4	2	0.95	6	0.97
	5	0	0.98	2	0.98
6	1	5	0.98	6	0.99
	2	26	0.95	3	0.98
	3	4	0.97	0	0.99
	5	0	0.97	0	0.98
7	1	8	0.99	1	0.99
	3	-1	1.00	-1	1.00
	5	0	0.97	1	0.99

The peak stresses (σ_P) recorded at the time of the step load (t = 0 s) are shown in Table 2, along with the accompanying “instantaneous” elastic modulus (E_P) (calculated based on Equation 3). Again, “instantaneous” in this case is not literal, as previous described. In terms of order of magnitude, the values in Pa were between 10^3 to 10^4. Figure 3.4 presents the peak stresses in graphical form. Indent 4 was significantly greater than Indents 3 and 5, with the mean±SE for Indent 4 being 3707±175 Pa and for Indent 3 2823±175 Pa and Indent 5 2553±175 Pa.

Table 2. Measured peak stress (σ) and “instantaneous” modulus of elasticity (E) values associated with the step-load, for all analyzed indentations.

Rabbit number	Indentation number	Peak σ (Pa)	Instantaneous E (Pa)
1	1	3752	7237
	2	3106	5991
	3	3124	6025
	4	4000	7715
	5	2559	4936
2	1	3069	5919
	2	3174	6122
	3	2025	3906
	4	3164	6102
	5	3376	6511
3	1	4053	7817
	2	3321	6405
	3	3316	6396
	4	3878	7480
	5	2494	4810
4	1	3740	7213
	2	3870	7464
	3	3115	6008
	4	4014	7742
	5	2542	4903
5	1	2544	4907
	2	2647	5105
	3	2785	5371
	4	3479	6710
	5	2550	4918
6	1	3193	6158
	2	3128	6033
	3	3270	6307
	5	2371	4573
7	1	3702	7140
	3	2124	4097
	5	1982	3823

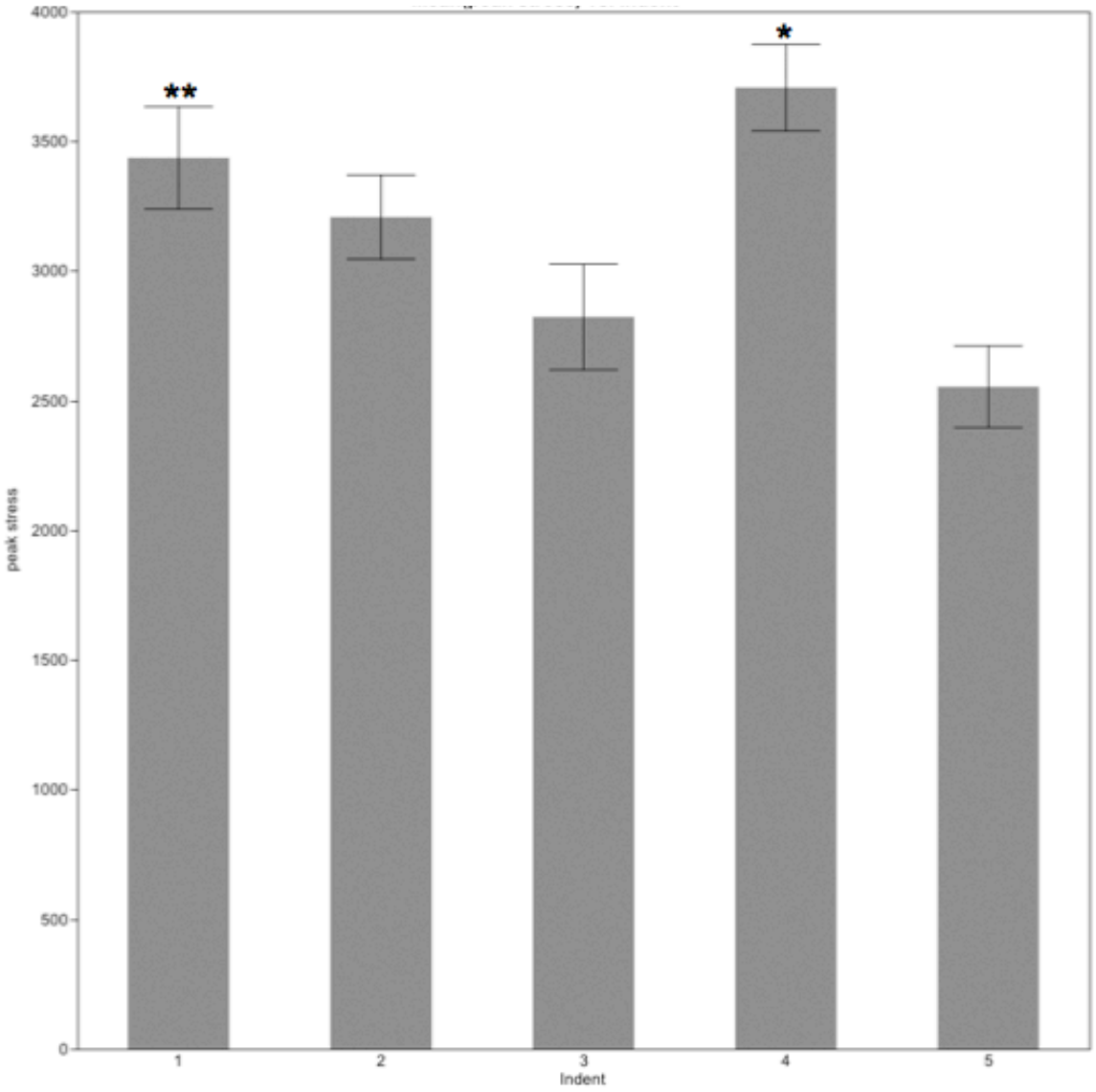

Figure 3.4. Bar graph for mean peak stress (Pa) (where t = 0 s) with standard error for each indentation group. Indent 4 was significantly larger than Indent 3 and 5 (* $p<0.05$ and $p<0.005$ respectively). Indent 1 was significantly higher than Indent 5 (**$p<0.05$).

The relaxation coefficients and material properties for all analyzed indentations are found in Tables 3 and 4, for expiration and inspiration phases respectively. A number of significant differences were identified in the stress coefficients, with these shown in Figures 3.5 to 3.9. For every significant difference in stress coefficient, there was a significant difference in the corresponding elastic modulus, an expected interaction as the elastic moduli are directly calculated from the stress (Equation 3).

Table 3. The relaxation coefficients and material properties for all analyzed indentations in the expiration phase.

A_2 = intermediate stress coefficient (Pa) associated with $TRel_2$

$TRel_2$ = shorter of the two decay constants (s) (relates to the first part of the stress-time curve)

E_2 = elastic modulus (Pa) calculated from A_2

η_2 = viscosity coefficient (Pa·s) calculated from $TRel_2$ and E_2

A_1 = intermediate stress coefficient (Pa) associated with $TRel_1$

$TRel_1$ = longer of the two decay constants (s) (relates to the second part of the stress-time curve)

E_1 = elastic modulus (Pa) calculated from A_1

η_1 = viscosity coefficient (Pa·s) calculated from $TRel_2$ and E_2

A_{Eq} = equilibrium stress coefficient (Pa).

Rabbit #	Indentation	A_2 (Pa)	TRel 2 (s)	E_2 (Pa)	η_2 (Pa-s)	A_1 (Pa)	$TRel_1$ (s)	E_1 (Pa)	η_1 (Pa-s)	A_{Eq} (Pa)
1	1	1770	1.08	3413	3686	939	27.25	1811	49357	1038
	2	1238	1.15	2388	2746	797	28.22	1537	43379	1067
	3	1189	1.24	2293	2844	901	21.43	1738	37240	1026
	4	2033	1.00	3921	3921	975	9.92	1880	18654	986
	5	1147	0.96	2212	2124	902	24.40	1740	42449	510
2	1	1629	0.75	3142	2356	855	18.19	1649	29996	582
	2	1621	0.89	3126	2783	886	21.03	1709	35937	664
	3	808	0.07	1558	109	659	32.55	1271	41372	570
	4	1466	1.06	2827	2997	700	23.29	1350	31444	985
	5	2077	1.49	4006	5969	814	17.97	1570	28212	483
3	1	1922	0.71	3707	2632	1022	20.86	1971	41118	1105
	2	1148	0.66	2214	1461	586	19.90	1130	22491	1586
	3	1173	0.70	2262	1584	857	13.00	1653	21488	1286
	4	1517	1.00	2926	2926	592	15.00	1142	17127	1761
	5	1275	0.64	2459	1574	546	20.48	1053	21567	673
4	1	1705	0.59	3288	1940	913	21.81	1761	38405	1121
	2	1797	0.78	3466	2703	777	19.92	1499	29852	1295
	3	1264	0.73	2438	1780	601	25.34	1159	29373	1250
	4	1686	1.17	3252	3805	662	30.38	1277	38789	1659
	5	1336	1.11	2577	2860	522	24.35	1007	24515	668
5	1	938	0.03	1809	54	697	17.54	1344	23579	909
	2	761	0.66	1468	969	530	14.91	1022	15241	1353
	3	979	1.03	1888	1945	626	21.25	1207	25657	1171
	4	1213	1.19	2340	2784	702	19.21	1354	26009	1562
	5	1237	0.69	2386	1646	555	18.71	1070	20028	758
6	1	1335	0.75	2575	1931	833	19.99	1607	32116	1020
	2	1343	1.13	2590	2927	632	26.41	1219	32192	1127
	3	1011	1.53	1950	2983	801	17.41	1545	26897	1454
	5	844	0.52	1628	846	608	12.66	1173	14846	919
7	1	1591	0.81	3069	2486	1202	19.06	2318	44187	901
	3	740	1.72	1427	2455	690	20.75	1331	27614	695
	5	1138	0.90	2195	1975	472	22.45	910	20437	372

Table 4. The relaxation coefficients and material properties for all analyzed indentations in the inspiration phase.

Rabbit #	Indentation	A_2 (Pa)	$TRel_{2\,(s)}$	E_2 (Pa)	η_2 (Pa-s)	A_1 (Pa)	$TRel_1$ (s)	E_1 (Pa)	η_1 (Pa-s)	A_{Eq} (Pa)
1	1	2333	1.43	4500	6435	794	28.60	1531	43798	621
	2	1657	0.50	3196	1598	857	20.50	1652	33865	591
	3	2570	0.42	4957	2082	684	19.43	1319	25633	-129
	4	2815	0.56	5429	3040	1033	12.64	1992	25183	151
	5	1453	0.69	2802	1934	825	23.82	1591	37902	275
2	1	2127	0.35	4102	1436	789	16.77	1522	25520	152
	2	2163	0.50	4172	2086	881	17.98	1699	30551	127
	3	1837	0.66	3543	2338	599	18.48	1155	21350	-411
	4	2734	0.57	5273	3006	607	19.66	1171	23016	-179
	5	2416	0.39	4660	1817	943	14.96	1819	27209	16
3	1	2141	0.57	4129	2354	1099	15.80	2120	33490	809
	2	1603	0.76	3092	2350	624	22.00	1204	26477	1089
	3	2050	0.58	3954	2293	840	12.57	1620	20365	425
	4	2316	0.47	4467	2099	738	10.69	1423	15216	824
	5	1603	1.00	3092	3092	496	22.39	957	21419	391
4	1	2177	0.41	4199	1722	873	19.92	1684	33541	689
	2	2245	0.37	4330	1602	860	17.96	1659	29790	765
	3	2099	0.04	4048	162	531	17.03	1024	17441	485
	4	2116	0.38	4081	1551	917	15.81	1769	27962	978
	5	1551	0.35	2991	1047	580	22.51	1119	25181	409
5	1	1246	0.45	2403	1081	633	19.80	1221	24173	665
	2	1018	0.30	1963	589	601	10.45	1159	12113	1026
	3	1871	0.02	3609	72	522	21.21	1007	21354	392
	4	1609	0.50	3103	1552	788	15.35	1520	23329	1076
	5	1454	0.65	2804	1832	546	14.68	1053	15459	548
6	1	1925	0.48	3713	1782	737	19.62	1421	27889	525
	2	1839	0.35	3547	1241	740	17.33	1427	24734	546
	3	2184	0.48	4212	2022	1225	9.27	2363	21902	-139
	5	1255	0.38	2421	920	661	9.45	1275	12048	455
7	1	1974	0.31	3807	1180	1208	16.71	2330	38932	519
	3	2006	1.02	3869	3946	661	19.16	1275	24427	-542
	5	1341	0.58	2586	1500	604	12.97	1165	15109	36

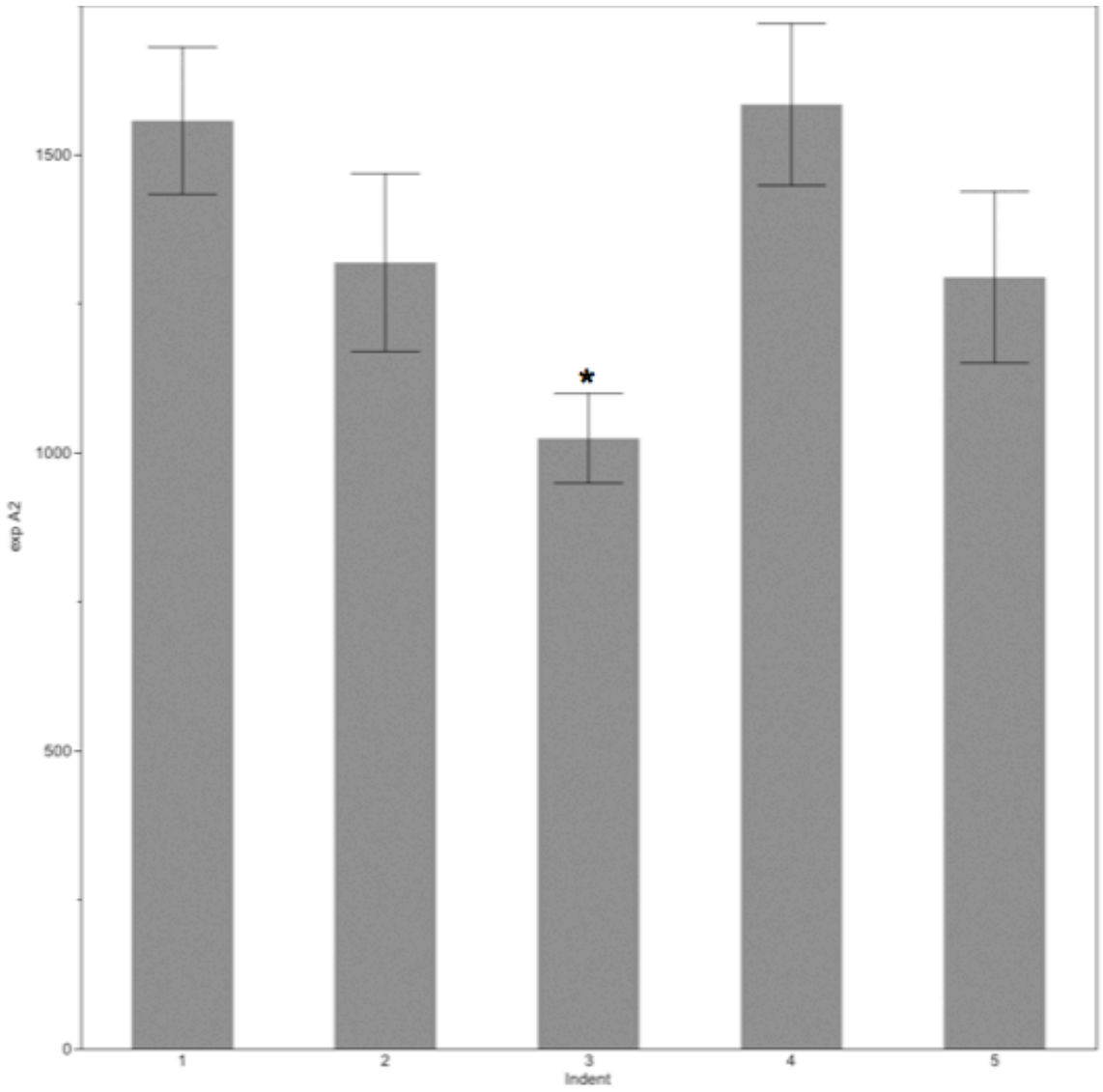

Figure 3.5. Bar graph for the expiration mean stress coefficient (Pa) associated with the faster time of relaxation coefficient (first part of curve), with standard error for each indentation group. Indent 3 was significantly lower than Indents 1 and 4 (* $p<0.05$).

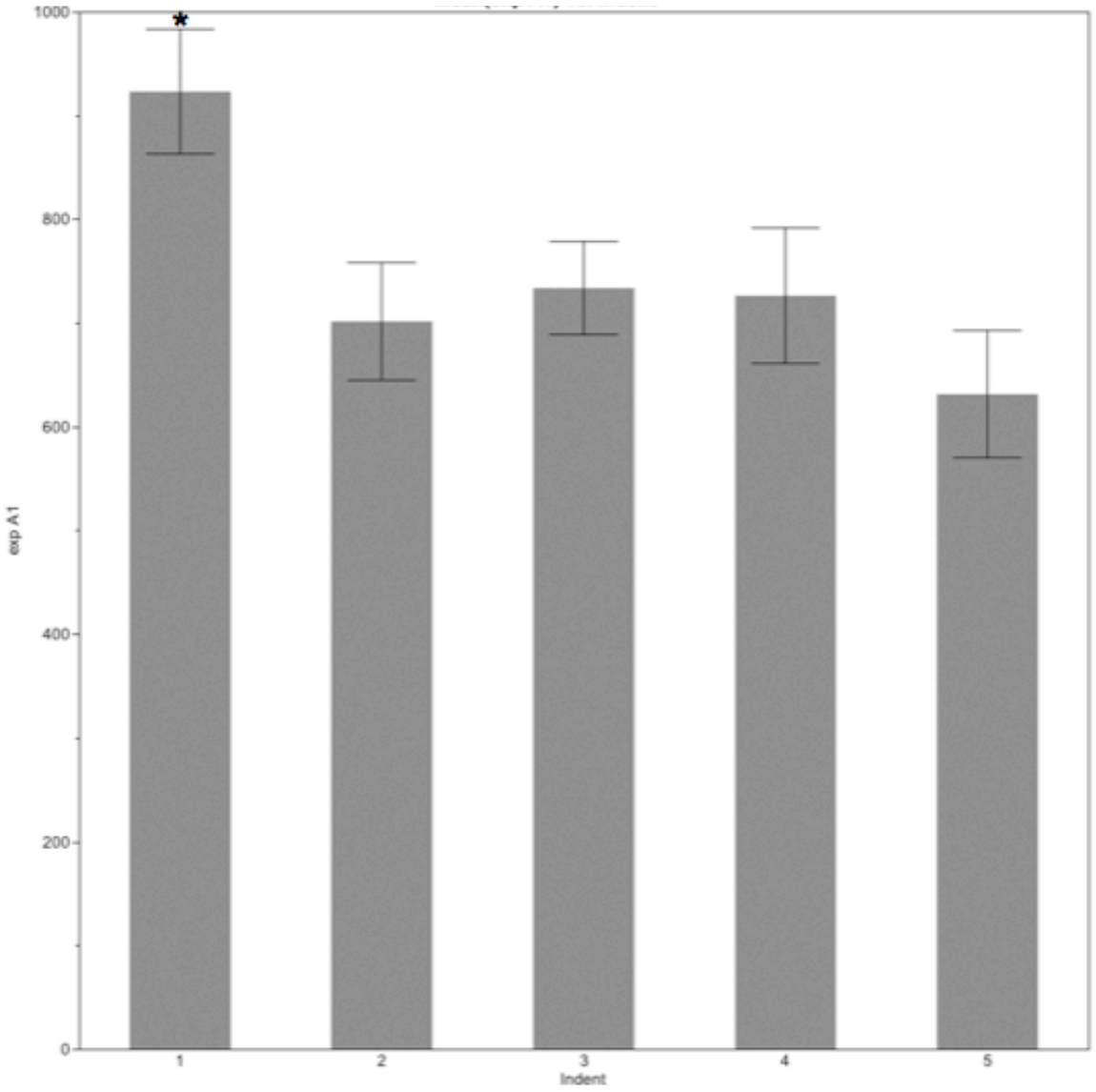

Figure 3.6. Bar graph for the expiration mean stress coefficient (Pa) associated with the slower time of relaxation coefficient (second part of curve), with standard error for each indentation group. Indent 1 was significantly higher than Indent 5 (* $p<0.01$).

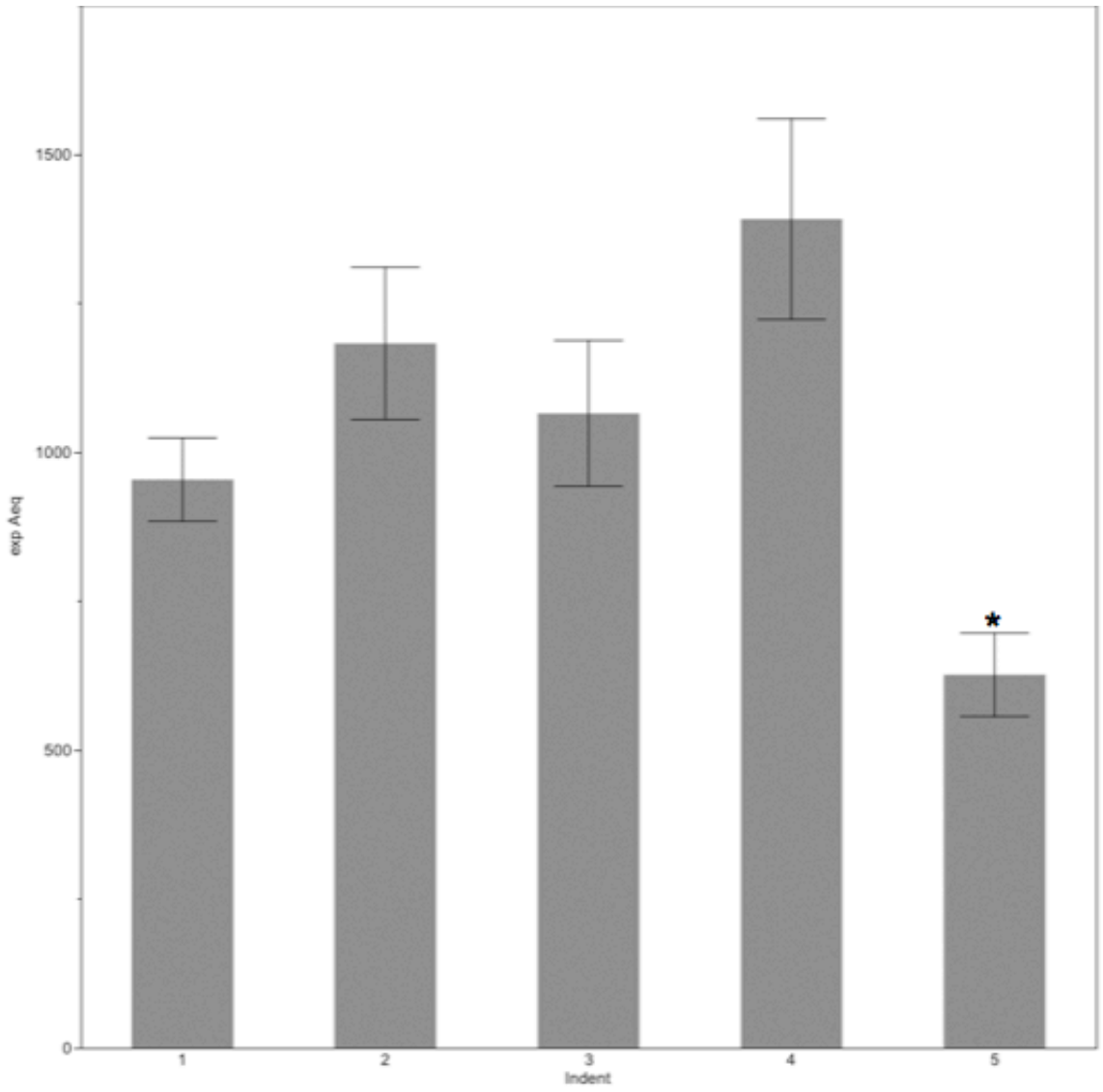

Figure 3.7. Bar graph for the expiration mean equilibrium stress coefficient (Pa) with standard error for each indentation group. Indent 5 was significantly lower than Indents 2, 3, and 4 (* $p<0.05$, $p<0.05$, $p<.001$ respectively).

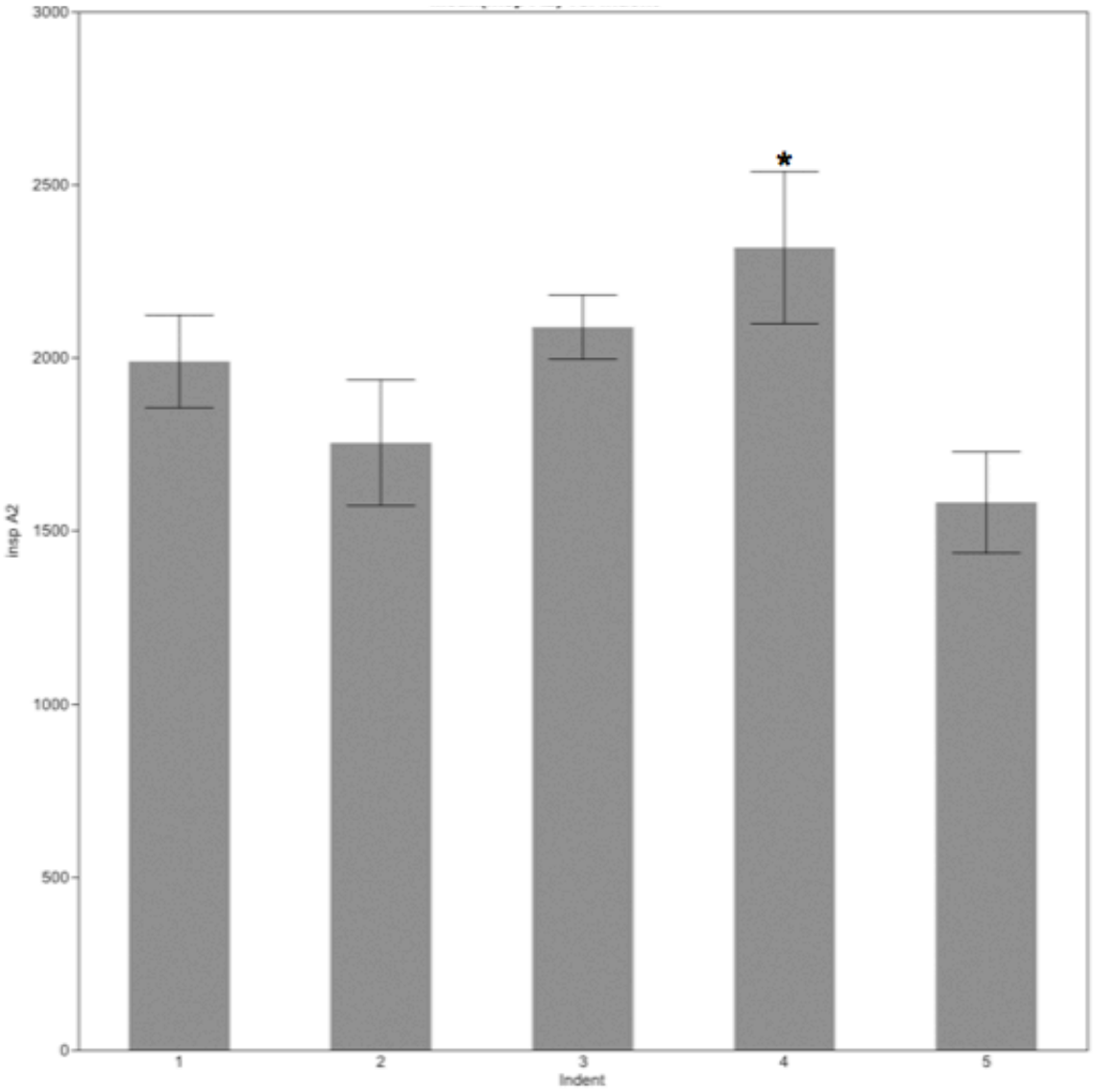

Figure 3.8. Bar graph for the inspiration mean stress coefficient (Pa) associated with the faster time of relaxation coefficient (first part of curve) with standard error, for each indentation group. Indent 4 was significantly higher than Indent 5 (*$p<0.05$).

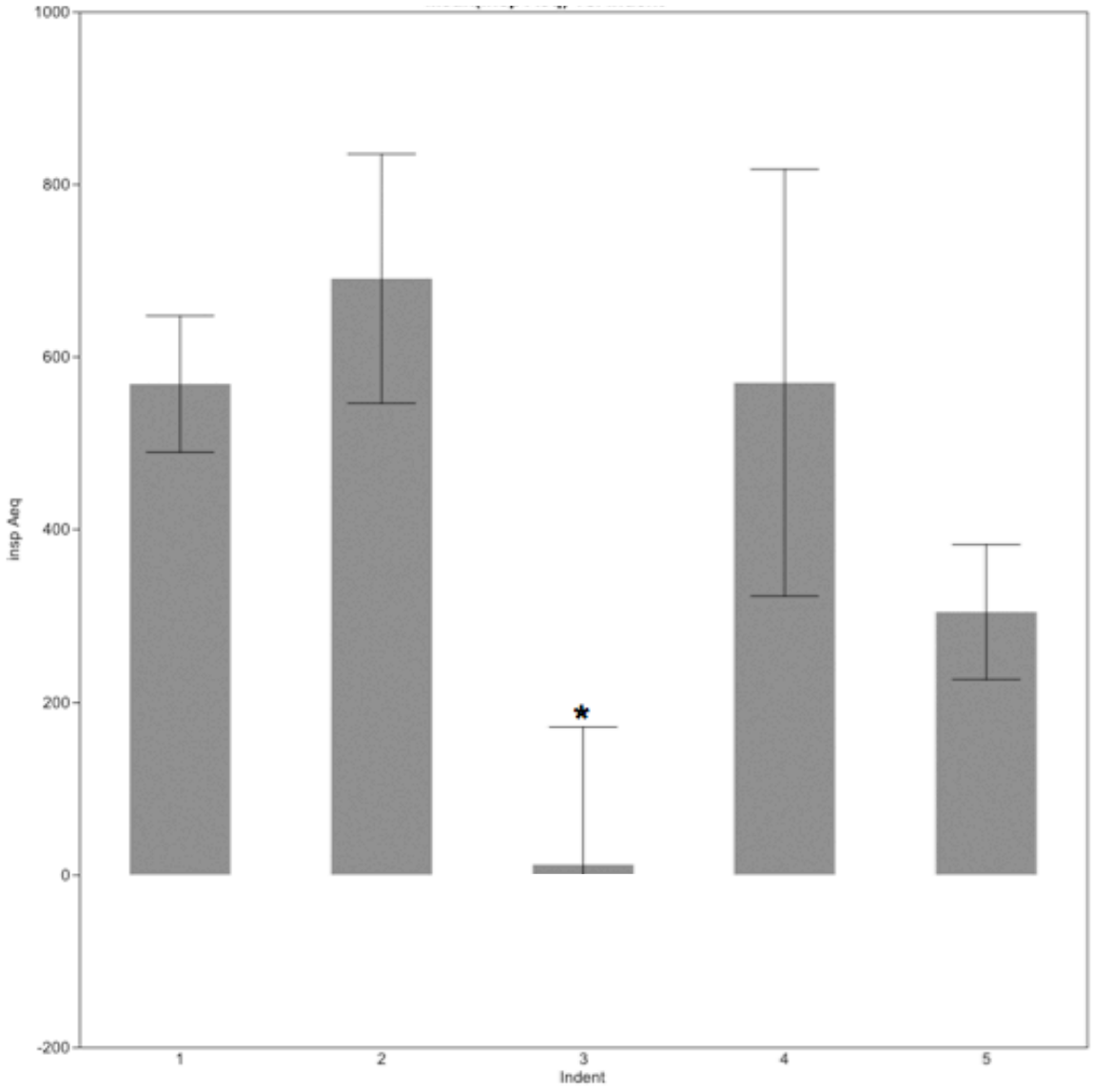

Figure 3.9. Bar graph for the inspiration mean equilibrium stress coefficient (Pa) with standard error, for each indentation group. Indent 3 was significantly lower than Indent 1 and 2 (* $p<0.05$).

4. DISCUSSION

The primary objective of this work was to perform stress-relaxation indentation on the living rabbit brain, with all variables of deformation, anatomy, and physiology controlled for or measured, and compare mechanical properties across relatively high and low groupings of pCO_2 and MAP. There has been no previous work published in which this has been performed, specifically with control of all possible variables related to mechanical testing, anatomic precision, and relative control of physiological parameters. This was performed successfully on seven consecutive rabbits. The preparation and undertaking of these experiments was complex and time-consuming, and reflects the difficulty in which in-vivo mechanical testing is performed with control of all variables.

Multidisciplinary expertise is required in both the planning and execution of successful experiments involving mechanical testing of living brain. Practically, performing these experiments requires technical knowledge and skill in the anesthetic delivery, mechanical ventilation, and physiological monitoring and manipulation, and the ability to make live-time adjustment of any of these features based on medical information. Lack of ability in any of these components may lead to loss of control or recognition of variables that may influence the mechanical properties of brain, and therefore affect the results of experimentation and the ability to compare them to other experiments that were intended to be the same.

A number of pilot experiments were necessary to attain consistency in performing in-vivo rabbit brain indentation while simultaneously controlling all relevant physiological parameters. Six animals were used in the initial design of the experimental set-up and methods. Eleven animals were required to perfect the process of general anesthetic delivery and control of normal physiologic parameters. In addition, 7 animals died under general anesthetic. Fifteen rabbits were used during the technical refinements of developing the indenter commands to attain step-loading and recording of other testing parameters. Finally, six animals were excluded from analysis because they were performed under variable or uncontrolled pCO_2 or blood pressure values.

An anesthesiologist is the ideal person to perform the precise physiological monitoring and manipulation required during in-vivo testing. A neurosurgeon is the ideal person to perform the craniectomy and durotomy, and introduce the deformation, as precise understanding of anatomy and skill to perfectly fashion the opening in a manner that respect the brain's natural state and boundary conditions are prerequisites to obtaining meaningful and reproducible data acquisition. It is often not feasible The role of the expert in mechanics is not as imperative during the actual experimentation, as the planning of the deformation parameters are made prior and analysis after.

Regardless of the level of experience and expertise invested in the experimentation and the control of all variables, there are factors common to in-vivo testing which are not controllable and may influence experimental results. These are limitations of this current work, as well as any other in-vivo testing.

Firstly, no two living entities are exactly the same, which applies to both anatomy and material composition. In the current work, the indentation was perform in the same location for every animal, with the same trajectory and depth. The indenter trajectory was chosen to be the visual right angle to the cortical surface, in order to maintain consistency in the evaluation of the known anisotropic conditions below the cortical surface. Regardless, variations in the exact gyral and sulcal pattern of the brain and vessel locations between animals may contribute to variation in any component of mechanical response of the cranial contents analyzed. Also, blood pressure and pCO_2 are dynamic processes, and although can be relatively manipulated and grouped into high and low (as done in this current work), they can not be titrated to an exact number consistently. This is a limitation of investigation, as the mechanical properties associated with even slight variations in pCO_2 or blood pressure may reciprocate those variations into the data obtained and used for further analysis. Future experimentation in which testing is performed in more ranges and combinations of blood pressure and pCO_2 may further recognition and understanding of the differences in mechanical properties of in-vivo brain and potentially highlight interactive effects.

The working hypothesis of this current work was that there are significant differences in relative viscoelastic properties of the living rabbit brain under different combinations of arterial pCO_2 and blood pressure, when all deformation, anatomical, and other physiological variables are controlled for. The experimental data was fitted to a generalized Maxwell model, and a least-squares curve-fitting

technique was used to solve for stress-relaxation coefficients. These coefficients and mechanical properties were compared across indentations. Although there were no statistically significant differences in the Time of Relaxation decay constants ($TRel_2$ and $TRel_1$), there were a number of significant differences in the peak, intermediate, and equilibrium stress coefficients (σ_P, A_2, A_1, and A_{Eq}) and the associated elastic moduli. Therefore the hypothesis is accepted.

The absolute values obtained in these experiments for relaxation coefficients and material properties are on the same orders of magnitude as previously published. There has not been publication of the version of the Maxwell model used in this current work, and thus there are no direct comparisons available for each of the elastic and viscous elements independently. Regardless, it is not the intention of these values to be interpreted as absolute representation the true mechanical property of brain tissue. They are intended serve as a quantitative representation of the overall mechanical response of the cranial contents, which is the way in which the brain is understood in the clinical realm, and in which different physiological states can be compared. Of note, the negative values obtained for the model-derived equilibrium stress coefficient in the inspiration phase likely represent that the this element becomes negligible (and balances that positive values), and do not warrant literal translation.

The mean peak stress (σ_P) and stress coefficient associated with the first part of the stress-relaxation curve (A_2), and their corresponding elastic moduli (E_P and E_2 respectively), were significantly higher in Indent 4 when compared to

Indent 3 in the expiration phase. Those indents differed physiologically by their MAP, with Indent 4 having a higher MAP, but were similar in pCO_2 values. The relatively high pCO_2 in both of these indentations correlate with known states of relative cerebral vasodilation and increased cerebral blood flow. With significant and similar degrees in vasodilation secondary to hypercarbia, the higher MAP in Indent 4 may be directly transmitting that pressure to the brain, resulting in a higher force of deformation required to displace the same relative volume and an overall increased stiffness of the brain. The fact that this increased stress coefficient is observed in the first part of the curve is compatible with the understanding that when the brain sustains a deforming force, it is blood and CSF that are first displaced. The differences in σ_P and in turn E_P is likely the summative result, as σ_P is composed of the stress coefficients (without A_1 or A_{Eq} having significant differences between Indents 4 and 3).

Another instance in which A_2 and E_2 were significantly lower in the expiration phase of Indent 3, was in comparison with Indent 1. In Indent 1 both the MAP and pCO_2 were low. In this scenario the higher A_2 is likely again related to the cerebral vasculature. However, as opposed to it being directly a result of increased arterial pressure transmission through a similarly dilated vasculature, it is likely due to an element of vascular smooth muscle tone and elastic wall tension. Vascular elasticity is related to vessel wall tension, which is the equilibrium of transmural pressure and passive wall tension. Passive wall tension is due to the elastic properties of the vessel wall, and is enhanced by contraction of vascular smooth muscle (active wall tension). With a low pCO_2 (and low MAP)

there is a state of relative vascular constriction, and with this a higher elastic component to the brain is conceivable secondary to contraction of vascular smooth muscle. There is no significant difference in the peak stress between the two indents as there was between 3 and 4. Mechanical property changes of brain secondary to specific changes in the property changes of the cerebral vessel walls has been theorized and observed previously (Schettini and Walsh, 1988). Specifically, Schettini and Walsh observed a decrease in an elastic component of brain, a component that they attributed to the initial part of a deformation, and correlated to a fall in cerebral blood flow.

The equilibrium stress coefficient (A_{Eq}) of the inspiration phase is another coefficient that was significantly lower in Indent 3, compared to both Indents 1 and 2 (where there was relative hypocarbia). This coefficient describes the remaining elastic element after relaxation has plateaued. In Indent 3 where high pCO_2 and low MAP result in maximal cerebral vasodilation, relative to the other physiologic groupings, A_{Eq} becomes a negligible term in the generalized Maxwell Model. This may be explained by attributing A_{Eq} as that which accounts for elements of vascular wall tone and transmural pressure, factors present in some form in the other Indentations and in the expiration phase.

A_{Eq} also shows significant differences in the expiration phase, but this time with Indentation 5 being lower than 2, 3, and 4. This coefficient was also notably lower in Indentation 5 compared to Indent 1 ($p = 0.08$). This may reveal an effect of repeated indentations (when the rest period in between indentations is less than 15 minutes). Indentations 1 and 5, where physiologic groupings were

relatively the same, also had significant differences in the stress coefficient associated with the second part of the stress-relaxation curve (A_1). This highlights the importance that an assumption that a rest period of 15 minute in between indentations assures complete return of the brain to its natural / pre-tested state may be oversimplified or incorrect. Future works are needed to definitively define and quantify the effect of repeat indentation in the living brain, starting with repeat indentations of the exact same testing, anatomic, and physiological variables.

In the current work, it is unknown to what degree the physiological manipulations that took place before Indentation 5 were contributory to the significant differences seen in the coefficients of that indentation. The forces incurred by the cortical surface with indentions were not felt to be large enough to injure the brain and stimulate a pathological process such as bleeding or edema. However, it is unknown to what degree a biphasic or poroelastic element contributes to the mechanical properties of the brain, and it is plausible that fluid is dispersed from the region of indentation after repeated tests. This highlights the importance of future testing evaluating the impact of preconditioning when investigation the brain's mechanical properties. Alternatively, or perhaps contributory, a prolonged (beyond 15 minutes) effect takes place in the processes of autoregulation and chemoregulation of the cerebrovasculature. Indent 4 is conducted under relative hypercarbia and hypertension, an uncommon combination in a normal animal. It is conceivable that this induced set of physiological parameters may result in regulatory factors that take longer than

15 minutes in which to return cerebral vascular tone and blood flow to the usual state of relatively lower pCO_2 and blood pressure, as found in Indent 5.

It was a secondary goal of this work to develop a rheological model that is suitable to describe the behavior of living rabbit brain under step-loaded stress-relaxation. A generalized Maxwell model consisting of a spring and dashpot in series, paralleled with another spring and dashpot in series, paralleled with a single spring, was fitted to the experimental data. This model represents a material with two viscoelastic elements, each with its own viscosity and elasticity moduli, and a equilibrium stress element. Both visually and objectively the generalized Maxwell model was shown to fit well to the experimental data. A least-squares curve-fitting technique was then used to solve for stress and decay coefficients, as previously detailed. Many biological materials, including brain tissue in isolation, are considered to be non-linear in their viscoelastic properties. This current work is not an attempt to quantify the absolute mechanical properties of brain tissue in isolation, but to explore a method in which to compare the overall mechanical response of the cranial contents in the in-vivo setting. This is the reality in which the brain is analyzed in the clinical environment, and in which physiological parameters are manipulated for therapeutic effects. The Maxwell model used does not consider the non-linear aspects of viscoelasticity which may be present in brain tissue, but did provide a straightforward method in which to obtain quantitative data to compare across physiological conditions.

Although a model can be applied to in-vivo data and mechanical properties extracted, the use of absolute values to mathematically describe the brain's behavior under deformation is applicable only to the set of testing conditions and variables encountered with that particular method of experimentation. This has been discussed previously, and highlights the difficulty in attaining a general mechanical characterization of brain (Cheng et al., 2008). There are a number of limitations inherent to testing living brain. This is regardless of how well the numerous controllable variables in anatomy, physiology, and testing are accounted for, and applies to the current work. Step-loaded stress-relaxation deformation is useful for evaluating properties of viscoelasticity. The step-load also has practical use in facilitating a constant deformation in a living object that pulses, such as living brain. In addition, small deformation step-loads have analogous clinical scenarios (e.g. surgical manipulation, depressed skull fractures, etc.). However, introducing a step-load to a precisely defined depth from an initial resting state, with measurement of force, is not actually "instantaneous". It approximates 1 second, and the difference between this and "instantaneous" may influence the peak stress attained (and calculated modulus) and subsequent relaxation. However, comparison of chosen and controlled variables, under otherwise the same testing conditions, will highlight important *relative* mechanical property changes.

In the current work, step-loaded stress-relaxation indentations were performed on living rabbit brain. Although it seems intuitive that in-vivo testing is

required for control of a number of physiological variables that may affect tissue properties, there have been results published that are contradictory (Gefen and Margulies, 2004). Regardless, when mechanical testing of brain is performed in a living subject, there is the ability to control and contrast physiological principles that are inevitably important to living patients in the clinical spectrum. In the current work, stress-relaxation was compared across groupings of MAP and pCO_2. Not only could further ranges and different groupings of these variables be examined with future testing, but so could other physiological variables already manipulated in the clinical setting to control ICP, such as serum sodium and temperature. Future work may then continue with evaluation of any number of pathological states found in the brain, as recently performed in hydrocephalic rats by Shulyakov et al. (2012), with and without comparing the effects of physiological manipulations or therapeutic interventions. The inevitable goal remains that with the continued accrual of mechanical property testing data and further mechanical characterization of brain, tools that can be used to measure or compare the mechanical properties in the living human brain in the clinical setting are developed and refined.

5. CONCLUSIONS

Stress-relaxation indentation can be performed successfully in the living rabbit brain with control or monitoring of anatomic, physiological, and mechanical testing variables. The step-loaded stress-relaxation response of the living rabbit brain is well-fitted to a generalized Maxwell model that includes two viscoelastic terms and an equilibrium elastic term. Comparison of stress-relaxation coefficients and material properties reveals statistically significant differences in stress coefficients across different combinations of pCO_2 and MAP, and after a sequence of indentations. The hypothesis of this thesis is accepted.

The differences observed might in part be due to the heterogeneous composition of the brain, including blood and blood vessels. Specifically, changes in vascular tone, cerebral blood volume, and cerebral perfusion pressure that accompany changes in pCO_2 and blood pressure, may contribute to the differences in stress coefficients and mechanical properties detected across the different physiologic groupings. This may be important for further understanding of the brain in different physiological states and accurate mechanical characterization of the brain. It also highlights the need to control for these parameters during the mechanical testing of brain.

6. FUTURE DIRECTIONS

Investigating the mechanical properties of brain has become an increasing focus of research. However, there are a large number of variables which require control and coordination to perform such testing in an accurate and meaningful way, and in turn there is a relative paucity in the published literature representing this area of research. A number of physiological variables dictate that conducting testing in the in-vivo state is preferred.

The dynamic nature of these variables, including cyclic pulsations, lend to two testing methods in which control of physiologic and testing parameters can be achieved: stress-relaxation indentation and MRE. The rabbit is a useful animal for conducting in-vivo stress-relaxation brain indentation, namely because of its size and brain geometry. MRE can be performed on any species, most notably human as it is a non-invasive method. Although this is not a direct rheological method of testing, it's ability for use in a non-invasive manner and on living humans is highly desirable. Continued research should take place with both methods. The categories of variables which are available for control, manipulation, and comparison are related to repetitive deformation, developmental status and age, physiology (e.g. pCO_2, blood pressure, temperature, and osmolality), and pathological conditions (e.g. brain injury, brain edema, hydrocephalus, intracerebral hematoma, and tumor). These categories of

variables should be exhausted in the order as listed, because assumptions regarding each is propagated into the next category.

Certain brain pathologies, relatively common in humans, may allow a unique opportunity to accrue stress-relaxation data from living human brains. Space-occupying lesions (e.g. tumors, intracerebral hematomas, and abscesses) and cerebrovascular aneurysms often necessitate brain surgery as part of their treatment. The surgeries conducted to help treat these pathologies often require the use of retractors to move and hold regions of brain, in order to provide optimal visualization and safety. Adapting surgical retractors to measure force, their position in space, and time could conceptually turn a commonly performed neurosurgical technique into a method in which to accrue living human brain relaxation data.

7. REFERENCES

Abolfathi, N., Naik, A., Sotudeh Chafi, M., Karami, G., Ziejewski, M., 2009. A micromechanical procedure for modelling the anisotropic mechanical properties of brain white matter. Comput Methods Biomech Biomed Engin 12, 249-262.

Ahn, B., Kim, Y., Oh, C.K., Kim, J., 2012. Robotic palpation and mechanical property characterization for abnormal tissue localization. Med Biol Eng Comput 50, 961-971.

Aimedieu, P., Grebe, R., 2004. Tensile strength of cranial pia mater: preliminary results. J Neurosurg 100, 111-114.

Aksenov, D., Eassa, J.E., Lakhoo, J., Wyrwicz, A., Linsenmeier, R.A., 2012. Effect of isoflurane on brain tissue oxygen tension and cerebral autoregulation in rabbits. Neuroscience letters 524, 116-118.

Alfasi, A.M., Shulyakov, A.V., Del Bigio, M.R., 2013. Intracranial biomechanics following cortical contusion in live rats. Journal of Neurosurgery 119, 1255-1262.

Allen, J.S., Damasio, H., Grabowski, T.J., 2002. Normal neuroanatomical variation in the human brain: an MRI-volumetric study. American journal of physical anthropology 118, 341-358.

Alperin, N.J., Lee, S.H., Loth, F., Raskin, P.B., Lichtor, T., 2000. MR-intracranial pressure (ICP): a method to measure intracranial elastance and pressure noninvasively by means of MR Imaging: baboon and human study. Radiology 217, 877-885.

Aoyagi, N., Masuzawa, H., Sano, K., 1980. [Compliance of the brain (author's transl)]. No to shinkei = Brain and nerve 32, 47-56.

Aoyagi, N., Masuzawa, H., Sano, K., Kihira, M., Kobayashi, S., 1982. [Compliance of brain--Part 2 Approach from the local elastic and viscous moduli (author's transl)]. No to shinkei = Brain and nerve 34, 509-516.

Arbogast, K.B., Margulies, S.S., 1998. Material characterization of the brainstem from oscillatory shear tests. J Biomech 31, 801-807.

Beccani, M., Di Natali, C., Sliker, L., Schoen, J., Rentschler, M., Valdastri, P., 2013. Wireless Tissue Palpation for Intraoperative Detection of Lumps in Soft Tissue. IEEE Trans Biomed Eng.

Bilston, L.E., 2011. Brain Tissue Mechanical Properties, in: Miller, K. (Ed.), Biomechanics of the Brain. Springer Science & Business Media, pp. 69-89.

Brain Trauma, F., American Association of Neurological, S., Congress of Neurological, S., Joint Section on, N., Critical Care, A.C., Bratton, S.L., Chestnut, R.M., Ghajar, J., McConnell Hammond, F.F., Harris, O.A., Hartl, R., Manley, G.T., Nemecek, A., Newell, D.W., Rosenthal, G., Schouten, J., Shutter, L., Timmons, S.D., Ullman, J.S., Videtta, W., Wilberger, J.E., Wright, D.W., 2007. Guidelines for the management of severe traumatic brain injury. VIII. Intracranial pressure thresholds. J Neurotrauma 24 Suppl 1, S55-58.

Brands, D.W., Bovendeerd, P.H., Wismans, J.S., 2002. On the potential importance of non-linear viscoelastic material modelling for numerical prediction of brain tissue response: test and application. Stapp car crash journal 46, 103-121.

Branston, N.M., 1995. Neurogenic control of the cerebral circulation. Cerebrovascular and brain metabolism reviews 7, 338-349.

Brown, J.D., Rosen, J., Moreyra, M., Sinanan, M., Hannaford, B., 2002. Computer-controlled motorized endoscopic grasper for in vivo measurement of soft tissue biomechanical characteristics. Stud Health Technol Inform 85, 71-73.

Canada, Government of, 2002. Economic Burden of Illness in Canada, 1998, in: Canada, Public Health Agency of Canada (Ed.). Government of Canada, Canada.

Carter, T.J., Sermesant, M., Cash, D.M., Barratt, D.C., Tanner, C., Hawkes, D.J., 2005. Application of soft tissue modelling to image-guided surgery. Med Eng Phys 27, 893-909.

Chatelin, S., Vappou, J., Roth, S., Raul, J.S., Willinger, R., 2012. Towards child versus adult brain mechanical properties. J Mech Behav Biomed Mater 6, 166-173.

Cheng, S., Bilston, L.E., 2007. Unconfined compression of white matter. J Biomech 40, 117-124.

Cheng, S., Clarke, E.C., Bilston, L.E., 2008. Rheological properties of the tissues of the central nervous system: A review. Med Eng Phys.

Chinzei, K., Miller, K., Year Compression of swine brain tissue; experiment in vivo. In International Society of Biomechanics Tokyo Congress 97.

Chinzei, K., Miller, K., Year Modeling stress-strain relation of brain tissue. In 6th Annual Meeting of Japan Soc Comput Aided Surgery.

Chinzei, K., Miller, K., Year In vivo indentation experimentation of swine brain. In 7th Annual Conference of the JSCAS.

Chinzei, M., Homma, Hyodo, 1997. Experiments of brain tissue deformation; in vitro and in vivo. Japanese J Med Electronics Biol Eng 35, 316.

Cowin, S.C.D., S. B., 2007. Tissue Mechanics. Springer, New York.

Cutler, R.W., Page, L., Galicich, J., Watters, G.V., 1968. Formation and absorption of cerebrospinal fluid in man. Brain : a journal of neurology 91, 707-720.

Delingette, H., Cotin, S., Ayache, N., 1999. Efficient linear elastic models of soft tissues for real -time surgery simulation. Stud Health Technol Inform 62, 100 - 101.

Delorme, S., Laroche, D., DiRaddo, R., Del Maestro, R.F., 2012. NeuroTouch: a physics-based virtual simulator for cranial microneurosurgery training. Neurosurgery 71, 32-42.

Di Bona, S., Lutzemberger, L., Salvetti, O., 2003. A simulation model for analysing brain structure deformations. Phys. Med. Biol. 48, 4001-4022.

Di Ieva, A., Grizzi, F., Rognone, E., Tse, Z.T., Parittotokkaporn, T., Rodriguez, Y.B.F., Tschabitscher, M., Matula, C., Trattnig, S., Rodriguez, Y.B.R., 2010. Magnetic resonance elastography: a general overview of its current and future applications in brain imaging. Neurosurg Rev 33, 137-145; discussion 145.

Dodgson, M.C.H., 1962. Colloidal structure of brain. Biorheology 1, 21-30.

Donnelly, B.R., Medige, J., 1997. Shear properties of human brain tissue. J Biomech Eng 119, 423 -432.

Elder, J.B., Chiocca, E.A., 2012. Convection-enhanced delivery. J Neurosurg 117, 193-195; discussion 195-196.

Engin, A.E., Wang, H.C., 1970. A mathematical model to determine viscoelastic behavior of in vivo primate brain. J Biomech 3, 283-296.

Fallenstein, G.T., Hulce, V.D., Melvin, J.W., 1969. Dynamic mechanical properties of human brain tissue. J Biomech 2, 217-226.

Fan, Y., Jiang, T., Evans, D.J., 2002. Volumetric segmentation of brain images using parallel genetic algorithms. IEEE Transactions on Medical Imaging 21, 904-909.

Filosa, J.A., Iddings, J.A., 2013. Astrocyte regulation of cerebral vascular tone. American journal of physiology. Heart and circulatory physiology 305, H609-619.

Franke, E.K., 1954. The response of the human skull to mechanical vibrations, in: Bollerud, J. (Ed.), Wright Air Development Center Technical Report. Wright Air Development Center, Wright-Patterson Air Force Base, pp. 1-16.

Fukuhara, T., Gotoh, M., Asari, S., Ohmoto, T., Akioka, T., 1996. The relationship between brain surface elastance and brain reexpansion after evacuation of chronic subdural hematoma. Surg Neurol 45, 570-574.

Fukuhara, T., Nishio, S., Kawauchi, M., Asari, S., Ohmoto, T., Akioka, T., 1994. Experimental analysis of brain surface elastance in cats. Neurol Med Chir (Tokyo) 34, 734-737.

Fung, Y.-C., 1990. Biomechanics Motion, Flow, Stress, and Growth. Springer-Verlag, New York.

Fung, Y.C., 2004. Biomechanics: mechanical properties of living tissues, Second ed. Springer, New York.

Galford, J.E., McElhaney, J.H., 1970. A viscoelastic study of scalp, brain, and dura. J Biomech 3, 211-221.

Garo, A., Hrapko, M., van Dommelen, J.A., Peters, G.W., 2007. Towards a reliable characterisation of the mechanical behaviour of brain tissue: The effects of post-mortem time and sample preparation. Biorheology 44, 51-58.

Gefen, A., Margulies, S.S., 2004. Are in vivo and in situ brain tissues mechanically similar? J Biomech 37, 1339-1352.

Glaser, K.J., Manduca, A., Ehman, R.L., 2012. Review of MR elastography applications and recent developments. Journal of magnetic resonance imaging : JMRI 36, spcone.

Goldsmith, W., 2001. The state of head injury biomechanics: past, present, and future: part 1. Critical reviews in biomedical engineering 29, 441-600.

Guillaume, A., Osmont, D., Gaffie, D., Sarron, J.C., Quandieu, P., 1997. Effects of perfusion on the mechanical behavior of the brain-exposed to hypergravity. J Biomech 30, 383-389.

Guyton, A.C., Hall, J.E., 1996. Nervous regulation of the circulation, and rapid control of arterial pressure, Textbook of Medical Physiology, 9th ed. W.B. Saunders Company, Philidelphia, p. 1148.

Hagemann, A., Rohr, K., Stiehl, H.S., 2002. Coupling of fluid and elastic models for biomechanical simulations of brain deformations using FEM. Medical Image Analysis 6, 375-388.

Hansma, P., Yu, H., Schultz, D., Rodriguez, A., Yurtsev, E.A., Orr, J., Tang, S., Miller, J., Wallace, J., Zok, F., Li, C., Souza, R., Proctor, A., Brimer, D., Nogues-Solan, X., Mellbovsky, L., Pena, M.J., Diez-Ferrer, O., Mathews, P., Randall, C., Kuo, A., Chen, C., Peters, M., Kohn, D., Buckley, J., Li, X., Pruitt, L., Diez-Perez, A., Alliston, T., Weaver, V., Lotz, J., 2009. The tissue diagnostic instrument. The Review of scientific instruments 80, 054303.

Hartkens, T., Hill, D.L., Castellano -Smith, A.D., Hawkes, D.J., Maurer, C.R., Jr., Martin, A.J., Hall, W.A., Liu, H., Truwit, C.L., 2003. Measurement and analysis of brain deformation during neurosurgery. IEEE Trans Med Imaging 22, 82 -92.

Hickman, K.E., 1965. Rheological behavior of tissues subjected to external pressure. Case Institute of Technology.

Hosey, R.R., Liu, Y.K., 1982. A homeomorphic finite element model of the human head and neck, in: Galllagher, R.H. (Ed.), Finite Elements in Biomechanics. Vail-Ballou Press, Inc., Binghamton, U.S.A., pp. Pages 379-400.

Hrapko, M., van Dommelen, J.A., Peters, G.W., Wismans, J.S., 2008. Characterisation of the mechanical behaviour of brain tissue in compression and shear. Biorheology 45, 663-676.

Hurm, P.D., Traystman, R., 1997. Overview of Cerbrovascular Hemodynamics, in: Reis, D. (Ed.), Primer on Cerebrovascular Diseases. Elsevier, p. 823.

Itkis, M.L., Mchedlishvili, G.I., 1979. Method of determing the mechanical properties of the brain in vivo. Mekhanika Kompozitnykh Materialov 6, 1094-1099.

Ji, S., Margulies, S.S., 2005. In vivo pons motion within the skull. J Biomech, (in press).

Ji, S., Margulies, S.S., 2007. In vivo pons motion within the skull. J Biomech 40, 92-99.

Kiernan, J.A., 2005. Barr's The Human Nervous System., 8th ed. Lippincott Williams & Williams, Baltimore.

King, A.I., Ruan, J.S., Zhou, C., Hardy, W.N., Khalil, T.B., 1995. Recent advances in biomechanics of brain injury research: a review. J Neurotrauma 12, 651-658.

Koeneman, J.B., 1966. Viscoelastic properties of brain tissue. Case Institute of Technology.

Kuhnt, D., Bauer, M.H., Nimsky, C., 2012. Brain shift compensation and neurosurgical image fusion using intraoperative MRI: current status and future challenges. Critical reviews in biomedical engineering 40, 175-185.

Kuijpers, A.H.W.M., Claessens, M.H.A., Sauren, A.A.H.J., 1995. The influence of different boundary conditions on the response of the head to impact: a two-dimensionsl finite element study. Journal of Neurotrauma 12, 715-724.

Kurashina, T., Sakamaki, T., Yagi, A., Nakamura, T., Sakamoto, H., Nushiro, N., 1994. A new device for indirect blood pressure measurement in rabbits. Japanese circulation journal 58, 264-268.

Kyriacou, S.K., Mohamed, A., Miller, K., Neff, S., 2002. Brain mechanics For neurosurgery: modeling issues. Biomech Model Mechanobiol 1, 151-164.

Laksari, K., Shafieian, M., Darvish, K., 2012. Constitutive model for brain tissue under finite compression. J Biomech 45, 642-646.

Lanier, W.L., Warner, D.O., 1992. Intracranial elastance versus intracranial compliance: terminology should agree with that of other disciplines. Anesthesiology 77, 403-404.

Li, C.X., Patel, S., Auerbach, E.J., Zhang, X., 2013. Dose-dependent effect of isoflurane on regional cerebral blood flow in anesthetized macaque monkeys. Neuroscience letters 541, 58-62.

Lim, Y.J., Jones, D.B., De, S., 2005. Improved virtual surgical cutting based on physical experiments. Stud Health Technol Inform 111, 301-307.

Lu, Y.B., Franze, K., Seifert, G., Steinhauser, C., Kirchhoff, F., Wolburg, H., Guck, J., Janmey, P., Wei, E.Q., Kas, J., Reichenbach, A., 2006. Viscoelastic properties of individual glial cells and neurons in the CNS. Proceedings of the National Academy of Sciences of the United States of America 103, 17759-17764.

Majors, R., Schettini, A., Mahig, J., Nevis, A.H., 1972. Intracranial pressures measured with the coplanar pressure transducer. Med Biol Eng 10, 724-733.

Manduca, A., Oliphant, T.E., Dresner, M.A., Mahowald, J.L., Kruse, S.A., Amromin, E., Felmlee, J.P., Greenleaf, J.F., Ehman, R.L., 2001c. Magnetic resonance elastography: non-invasive mapping of tissue elasticity. Med Image Anal 5, 237-254.

Manning, P.J., Ringler, D.H., Newcomer, C.E., 1994. The Biology of the Laboratory Rabbit, 2nd ed. Academic Pres, San Diego.

Margulies, S.S., Thibault, K.L., 2000. Infant skull and suture properties: measurements and implications for mechanisms of pediatric brain injury. J Biomech Eng 122, 364-371.

Marmarou, A., Shulman, K., Rosende, R.M., 1978. A nonlinear analysis of the cerebrospinal fluid system and intracranial pressure dynamics. J Neurosurg 48, 332-344.

Marmarou, A.M., Beaumont, A., 2011. Physiology of the Cerebral Fluid and Intracranial Pressure, in: Winn, R.W. (Ed.), Youmans Neurological Surgery, 6th ed. Elsevier Saunders, Philidelphia, p. 1072.

McCraken, P.J., Manduca, A., Felmlee, J., Ehman, R.L., 2005. Mechanical transient-based magnetic resonance elastography. Magnetic Resonance Imaging 53, 628-639.

McHedlishvili, G., Itkis, M., Sikharulidze, N., 1989. Mechanical properties of brain tissue related to oedema development in rabbits. Acta neurochirurgica 96, 137-140.

Mchedlishvili, G.I., Itkis, M.L., Sikharulidze, N.V., 1981. [Effect of circulatory factors on the mechanical properties of the brain]. Mekhanika Kompozitnykh Materialov, 878-882.

McIntosh, A.S., Andersen, T.E., Bahr, R., Greenwald, R., Kleiven, S., Turner, M., Varese, M., McCrory, P., 2011. Sports helmets now and in the future. British journal of sports medicine 45, 1258-1265.

Mendis, K.K., Stalnaker, R.L., Advani, S.H., 1995. A constitutive relationship for large deformation finite element modeling of brain tissue. J Biomech Eng 117, 279 -285.

Metz, H., McElhaney, J., Ommaya, A.K., 1970. A comparison of the elasticity of live, dead, and fixed brain tissue. J Biomech 3, 453-458.

Miga, M.I., Paulsen, K.D., Hoopes, P.J., Kennedy, F.E., Jr., Hartov, A., Roberts, D.W., 2000b. In vivo quantification of a homogeneous brain deformation model for updating preoperative images during surgery. IEEE Transactions on Biomedical Engineering 47, 266-273.

Miller, C., Year Modelling of brain tissue mechanical properties: bi-phasic versus single-phase approach. In 3rd Intl Symp Comput Methods in Biomech & Biomed Eng.

Miller, C., 1999a. New UWA robot - possible application to robotic surgery. 135 - 140.

Miller, K., 1999b. Constitutive model of brain tissue suitable for finite element analysis of surgical procedures. J Biomech 32, 531-537.

Miller, K., 2000. Biomechanics of soft tissues. Med Sci Monit 6, 158-167.

Miller, K., 2001a. How to test very soft biological tissues in extension? J Biomech 34, 651-657.

Miller, K., 2001b. Non-linear computer simulation of brain deformation. Biomed Sci Instrum 37, 179-184.

Miller, K., 2005. Method of testing very soft biological tissues in compression. J Biomech 38, 153-158.

Miller, K., Chinzei, K., 1997. Constitutive modelling of brain tissue: experiment and theory. J Biomech 30, 1115-1121.

Miller, K., Chinzei, K., 2002. Mechanical properties of brain tissue in tension. Journal of Biomechanics 35, 483-490.

Miller, K., Chinzei, K., Orssengo, G., Bednarz, P., 2000. Mechanical properties of brain tissue in-vivo: experiment and computer simulation. J Biomech 33, 1369-1376.

Mohsenin, N.N., 1986. Mechanical Properties of Plant and Animal Materials. Gordon and Breach Science Publishers, New York.

Montemurro, D.G., Bruni, J.E., 1988. The Human Brain in Dissection, 2nd ed. Oxford University Press.

Morrison, B., 3rd, Meaney, D.F., Margulies, S.S., McIntosh, T.K., 2000. Dynamic mechanical stretch of organotypic brain slice cultures induces differential genomic expression: relationship to mechanical parameters. J Biomech Eng 122, 224-230.

Morrison, B., 3rd, Meaney, D.F., McIntosh, T.K., 1998. Mechanical characterization of an in vitro device designed to quantitatively injure living brain tissue. Ann Biomed Eng 26, 381 -390.

Murphy, M.C., Huston, J., 3rd, Glaser, K.J., Manduca, A., Meyer, F.B., Lanzino, G., Morris, J.M., Felmlee, J.P., Ehman, R.L., 2013a. Preoperative assessment of meningioma stiffness using magnetic resonance elastography. J Neurosurg 118, 643-648.

Murphy, M.C., Huston, J., 3rd, Jack, C.R., Jr., Glaser, K.J., Senjem, M.L., Chen, J., Manduca, A., Felmlee, J.P., Ehman, R.L., 2013b. Measuring the characteristic topography of brain stiffness with magnetic resonance elastography. PloS one 8, e81668.

Nathoo, N., Cavusoglu, M.C., Vogelbaum, M.A., Barnett, G.H., 2005a. In touch with robotics: neurosurgery for the future. Neurosurgery 56, 421-433.

Nicolle, S., Lounis, M., Willinger, R., Palierne, J.F., 2005. Shear linear behavior of brain tissue over a large frequency range. Biorheology 42, 209-223.

Ommaya, A.K., 1968. Mechanical properties of tissues of the nervous system. J Biomech 1, 127-138.

Ommaya, A.K., Goldsmith, W., Thibault, L., 2002. Biomechanics and neuropathology of adult and pediatric head injury. British Journal of Neurosurgery 16, 220-242.

Pamidi, M.R., Advani, S.H., 1978. Nonlinear constitutive relations for human brain tissue. J Biomech Eng 100, 44-48.

Penn, R.D., Lee, M.C., Linninger, A.A., Miesel, K., Lu, S.N., Stylos, L., 2005. Pressure gradients in the brain in an experimental model of hydrocephalus. J Neurosurg 102, 1069-1075.

Peters, G.W., Meulman, J.H., Sauren, A.A., 1997. The applicability of the time/temperature superposition principle to brain tissue. Biorheology 34, 127 - 138.

Prange, M.T., Coats, B., Duhaime, A.-C., Margulies, S.S., 2003. Anthropomorphic simulations of falls, shakes, and inflicted impacts in infants. Journal of Neurosurgery 99, 143-150.

Prange, M.T., Margulies, S.S., 2002. Regional, directional, and age -dependent properties of the brain undergoing large deformation. J Biomech Eng 124, 244 - 252.

Razumovsky, A.Y., Hanley, D.F., 1992. Intracranial pressure measurement/cranial vault mechanics: clinical and experimental observations. Current opinion in neurology and neurosurgery 5, 818-825.

Reicher, D., Bhalla, P., Rubinstein, E.H., 1987. Cholinergic cerebral vasodilator effect of ketamine in rabbits. Stroke; a journal of cerebral circulation 18, 445-449.

Ruan, J.S., Khalil, T., King, A.I., 1994. Dynamic response of the human head to impact by three-dimensional finite element analysis. J Biomech Eng 116, 44-50.

Scheller, M.S., Todd, M.M., Drummond, J.C., 1986. Isoflurane, halothane, and regional cerebral blood flow at various levels of PaCO2 in rabbits. Anesthesiology 64, 598-604.

Schettini, A., McKay, L., Mahig, J., Modell, J.H., 1972. The response of brain surface pressure to hypercapnic hypoxia and hyperventilation. Anesthesiology 36, 4-12.

Schettini, A., McKay, L., Majors, R., Mahig, J., Nevis, A.H., 1971. Experimental approach for monitoring surface brain pressure. J Neurosurg 34, 38-47.

Schettini, A., Walsh, E.K., 1974. Experimental identification of the subararachnoid and subpial compartments by intracranial pressure measurements. J Neurosurg 40, 609-616.

Schettini, A., Walsh, E.K., 1984. Brain elastic behavior in experimental brain compression: influence of steroid therapy. Brain Res 305, 141-143.

Schettini, A., Walsh, E.K., 1988. Brain tissue elastic behavior and experimental brain compression. Am J Physiol 255, R799-805.

Schiavone, P., Chassat, F., Boudou, T., Promayon, E., Valdivia, F., Payan, Y., 2009. In vivo measurement of human brain elasticity using a light aspiration device. Med Image Anal 13, 673-678.

Scholz, M., Noack, V., Pechlivanis, I., Engelhardt, M., Fricke, B., Linstedt, U., Brendel, B., Schmieder, K., Ermert, H., Harders, A., 2005. Vibrography during tumor neurosurgery. Journal of Ultrasound in Medicine 24, 985-992.

Shen, F., Tay, T.E., Li, J.Z., Nigen, S., Lee, P.V., Chan, H.K., 2006. Modified Bilston nonlinear viscoelastic model for finite element head injury studies. J Biomech Eng 128, 797-801.

Shulyakov, A.V., Buist, R.J., Del Bigio, M.R., 2012. Intracranial biomechanics of acute experimental hydrocephalus in live rats. Neurosurgery 71, 1032-1040.

Shulyakov, A.V., Cenkowski, S.S., Buist, R.J., Del Bigio, M.R., 2011. Age-dependence of intracranial viscoelastic properties in living rats. J Mech Behav Biomed Mater 4, 484-497.

Shulyakov, A.V., Fernando, F., Cenkowski, S.S., Del Bigio, M.R., 2009. Simultaneous determination of mechanical properties and physiologic parameters in living rat brain. Biomech Model Mechanobiol 8, 415-425.

Sirovskii, E.B., Pal'tsev, E.I., Manevich, A.Z., Fedorov, S.N., Makhmudov, U.B., 1981. [Pressure-volume relation in the craniospinal cavity in the presence of supra- and subtentorial pathology. II. Changes in local intracerebral pressure subsequent to cerebrospinal fluid compression and decompression of the brain]. Zhurnal voprosy neirokhirurgii imeni N. N, 33-39.

Soza, G., Grosso, R., Nimsky, C., Hastreiter, P., Fahlbusch, R., Greiner, G., 2005. Determination of the elasticity parameters of brain tissue with combined simulation and registration. Int J Med Robot 1, 87-95.

Suckow, M.A., Douglas, F.A., 1996. The Laboratory Rabbit. CRC Press, Danvers.

Tan, C.T., Khurana, V.G., Benarroch, E.E., Meyer, F.B., 2011. Cerebral Blood Flow and Metabolism and Cerebral Ischemia, in: Winn, R.W. (Ed.), Youmans Neurological Surgery, 6 ed. Elsevier Saunders, Philadelphia, pp. 3548-3549.

Tanna, N.K., Kohn, M.I., Horwich, D.N., Jolles, P.R., Zimmerman, R.A., Alves, W.M., Alavi, A., 1991. Analysis of brain and cerebrospinal fluid volumes with MR imaging: impact on PET data correction for atrophy. Part II. Aging and Alzheimer dementia. Radiology 178, 123-130.

Taylor, Z., Miller, K., 2004. Reassessment of brain elasticity for analysis of biomechanisms of hydrocephalus. J Biomech 37, 1263-1269.

Tenti, G., Sivaloganathan, S., Drake, J.M., 2008. Mathematical modeling of the brain: principles and challenges. Neurosurgery 62, 1146-1156; discussion 1156-1162.

ter Laan, M., van Dijk, J.M., Elting, J.W., Staal, M.J., Absalom, A.R., 2013. Sympathetic regulation of cerebral blood flow in humans: a review. British journal of anaesthesia 111, 361-367.

Thiele, R.H., Nemergut, E.C., Lynch, C., 3rd, 2011. The clinical implications of isolated alpha(1) adrenergic stimulation. Anesthesia and analgesia 113, 297-304.

Trapp, B.D., Herrup, K., 2011. Neurons and Neuroglia, in: Winn, R.W. (Ed.), Youmans Neurological Surgery, 6th ed. Elsevier Saunders, Philidelphia, p. 1072.

Traystman, R.J., 1997. Regulation of cerebral blood flow by carbon dioxide, in: Welch, K.M.A., Cahill Jr, G.F., Reis, D.J. (Eds.), Primer on Cerebrovascular Disease. Academic Press, San Diego, pp. 21-25.

Ueno, T., Macias, B.R., Yost, W.T., Hargens, A.R., 2005. Noninvasive assessment of intracranial pressure waveforms by using pulsed phase lock loop technology. J Neurosurg 103, 361-367.

Van Aken, H., Fitch, W., Graham, D.I., Brussel, T., Themann, H., 1986. Cardiovascular and cerebrovascular effects of isoflurane-induced hypotension in the baboon. Anesthesia and analgesia 65, 565-574.

Voo, L., Kumaresan, S., Pintar, F.A., Yoganandan, N., Sances, A., Jr., 1996. Finite-element models of the human head. Medical & Biological Engineering & Computing 34, 375-381.

Walsh, E.K., Schettini, A., 1976. Elastic behavior of brain tissue in vivo. Am J Physiol 230, 1058-1062.

Walsh, E.K., Schettini, A., 1984. Calculation of brain elastic parameters in vivo. Am J Physiol 247, R693-700.

Walsh, E.K., Schettini, A., 1990. Brain tissue elasticity and CSF elastance. Neurol Res 12, 123-127.

Wang, H.C., Wineman, A.S., 1972. A mathematical model for the determination of viscoelastic behavior of brain in vivo. I. Oscillatory response. J Biomech 5, 431 -446.

Wu, J.Z., Dong, R.G., Schopper, A.W., 2004a. Analysis of effects of friction on the deformation behavior of soft tissues in unconfined compression tests. J Biomech 37, 147 -155.

Wu, J.Z., Dong, R.G., Smutz, W.P., 2004b. Elimination of the friction effects in unconfined compression tests of biomaterials and soft tissues. Proc Inst Mech Eng [H] 218, 35 -40.

Yamamoto, Y., Moritake, K., Nagai, H., Sato, M., 2004. Quantitative estimation of brain stiffness measured using a tactile biosensor in animal models. Neurological Research 26, 622-627.

Zheng, Y., Mak, A.F., Lue, B., 1999. Objective assessment of limb tissue elasticity: development of a manual indentation procedure. Journal of rehabilitation research and development 36, 71-85.

Zong, Z., Lee, H.P., Lu, C., 2006. A three-dimensional human head finite element model and power flow in a human head subject to impact loading. J Biomech 39, 284-292.

APPENDIX 1 – Technical specifics of the indenter apparatus and method

The indenter used is a customized open platform Micro Hardness Tester (MHT) (CSM Instruments SA; Peseux, Switzerland). Aspects of its application have been previously described (Shulyakov et al., 2011; Shulyakov et al., 2009). The MHT and its control unit are entirely computer controlled and menu driven. The instrument is load controlled, and therefore measures depth as a function of load. The load is generated from an actuator / voice-coil (VC), and measured via a force transducer that is located immediately above the indenter tip holder.

The instrument is capable of a load range from approximately 1 mN to 30 N, with a load resolution of 0.3 mN. The depth sensor is a linear variable differential transformer (LVDT) sensor that consists of a hollow tube with a permanent magnet core in the center that is attached to the indenter tip. The movement of the magnetic core in relation to the LVDT coil generates a voltage, which is converted to depth. The measurement range available is to a maximum of 2000 μm, which is calibrated to the -10 to 10 V range of the LVDT. In reality, ~10% of measurement range may be used during the "approach phase" of an actual indentation test. The approach distance is the distance from the beginning of the data being recorded to the start of the actual indentation. The depth resolution of the instrument is 0.3 nm. Calibrations of the normal force (Fn) and the penetration depth (Dz) are performed with a standardized external reference load cell and LVDT sensor respectively.

The calibration coefficient of the coarse depth range (2000 μm) is 105.364 μm/V, and can be used to calculate the total distance traveled by the VC (which is greater than the recording range). To do this, during calibration the LVDT is physically reset, followed by measuring the total number of volts on the LVDT required to move the VC through its entire measuring range. This value is ~37V, and the maximum travel of the VC (0 to 10 V) correlates to 3897 μm of indenter tip travel (the absolute physical depth range of the instrument). The linear correlation of depth to voltage through the entire range is $R^2 = 0.997$.

Indenter tips are interchangeable with the MHT. An indenter tip is secured in the vertical shaft of the indenter head, and fixed with tightening of a set screw.

Via a position control function of the software, the instrument platform can be moved in the x, y, and z directions. The platform is first moved to the front of the instrument to facilitate the attachment of the rabbit head holder and body support platform.

An *Adjust Depth Offset* (ADO), as termed by CSM software, is a procedure performed for the purpose of obtaining a reference of the sample height in the z dimension, and is always conducted before an indentation test is performed on a sample, and after every time the sample is moved. This information allows the instrument to run the actual indentation more efficiently, by speeding the approximation of the brain and indenter tip surfaces.

Upon initiating the ADO procedure, the indenter tip lowers. The amount that it lowers is pre-defined by the user, and is referred to as "Command" in the software. Command is the percent of the entire travel range that the indenter tip

is to descend before reaching the measurement range, and for our experiments has been set as 50%. After Command quickly runs to 50% (reflecting the indenter head lowering 50% of 3897 μm), the table begins to steadily rise until a predefined force is detected by the force transducer. Therefore, in addition to table height, the ADO also gathers information regarding the move of the voice-coil in relation to the current Command. The force detected is intended to reflect the point of contact between the cortical surface and the indenter tip. This threshold value is set by the user, and if set too low, "contact" will be detected due to noise or small vibrations, or even fluid on the brain surface which exhibits oscillatory changes. If the detection force is set higher than necessary, indentation of brain surface will begin before the indentation is initiated by the software. The lowest practical set detection force for the MHT in the laboratory environment is 4.6 mN. Forces lower than 4.6 mN are set not to be recorded.

Inertia is the limiting factor in actually attaining an “instantaneous” step-loaded indentation, and the maximum physical limit of depth is encountered before the set maximum force can be reached. The set maximum force is an arbitrarily high number, which is meaningless when testing brain as it is not achievable before the maximum physical limit of depth is reached.

Upon initiation of an indentation test, the table rises and stops, bringing the brain surface to close proximity of the indenter tip. The indenter tip then slowly lowers. Next, initial contact between the cortical surface and indenter tip surface is directly observed. This always approximates the detection force. The Command at this time approaches 50%. At 50% Command, the live-time

software function that displays the indenter tip depth begins (starts at 0 μm). The position the rises slowly and linearly. Once 4.6 mN is detected, the indenter tip lowers into the sample in a step-loaded fashion, which approximates 1 second as limited by inertia.

Once measurement range depth is exceeded, which is within the absolute physical range, depth saturation is deemed to have occurred and the indenter tip is held steady.

APPENDIX 2 – MATLAB code used to fit generalized Maxwell model and solve for stress-relaxation coefficients.

```
%% In-vivo rabbit brain indentation for stress-relaxation analysis.
%Stress-time curve fit to stress-relaxation using maxwell model with
%two viscoelastic elements and an equilibrium stress.
%
% Equation. sigma(t)=sigma_n*exp(-t/tau)+sigma_e where sigma_n is
% equivalent to (sigma_0-sigma_e). If n=2 there is a second sigma_n*exp
% term.  sigma_e is the equilibrium stress, sigma_0 is the instantaneous stress.
% Text. Peak Stress = A1*e(-t/TRel1) + A2*e(-t/TRel2) + AEq

% dt=0.1;
% time=0:dt:length(stress)*dt-dt;
% time=time';

%Create initial conditions for parameters;
%e.g.,
C0=[1 1000 1 1000 1000];

%Inline function created for the equations
fit=inline('C(2)*exp(-time/C(1))+C(4)*exp(-time/C(3))+C(5)','C','time');

%lsqcurvefit options
options=optimset('MaxIter',1000,'TolFun',1e-15,'MaxFunEvals',1000,'TolX',1e-9,'FinDiffType','Central');

%Use lsqcurvefit to find the best value for the parameters.
[C, resSSC]=lsqcurvefit(fit,C0,time,stress,[],[],options);

%Calculated predicted values of y
yhatC=fit(C,time);

plot(time,stress,'.r',time,yhatC,'b')
xlabel('Time (s)')
ylabel('Stress (Pa)')
legend('Experiment','Model')
title('In-vivo rabbit brain stress relaxation')

%Statistical Calculations
SSS=resSSC;
TSS=sum((stress-mean(stress)).^2);
RSS=sum((yhatC-mean(stress)).^2);

R2=RSS/TSS;

PeakStress=C(2)+C(4)+C(5)

```

Fit Y by X Group
Oneway Analysis of pCO2 By Indent

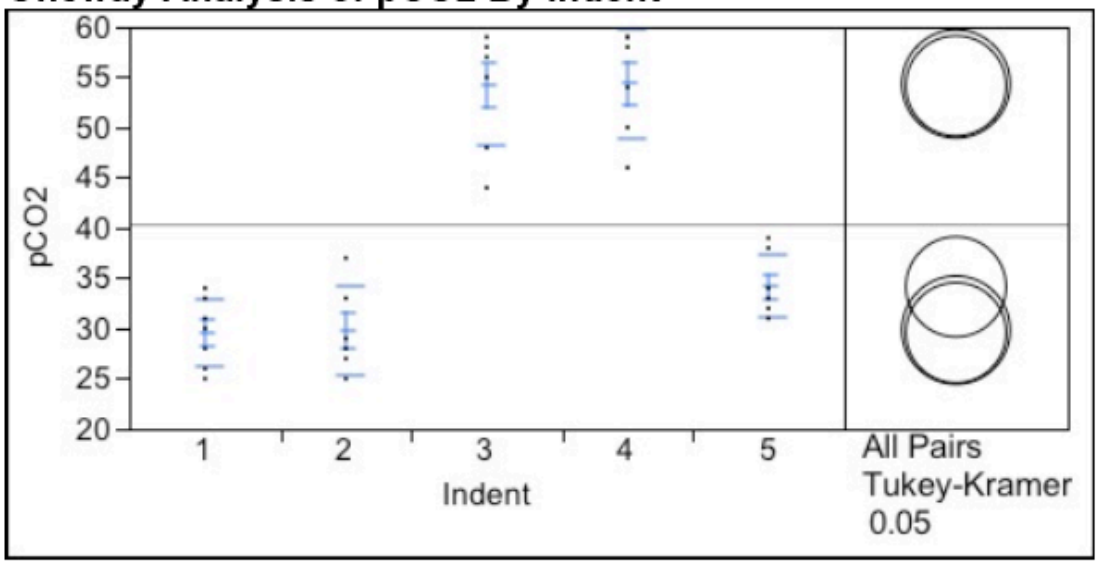

Excluded Rows
2

Means and Std Deviations

Level	Number	Mean	Std Dev	Std Err Mean	Lower 95%	Upper 95%
1	7	29.5714	3.40867	1.2884	26.419	32.724
2	6	29.8333	4.40076	1.7966	25.215	34.452
3	7	54.1429	5.81460	2.1977	48.765	59.520
4	6	54.3333	5.39135	2.2010	48.675	59.991
5	7	34.1429	3.13202	1.1838	31.246	37.039

Means Comparisons
Comparisons for all pairs using Tukey-Kramer HSD
Confidence Quantile

q*	Alpha
2.91349	0.05

Ordered Differences Report

Level	- Level	Difference	Std Err Dif	Lower CL	Upper CL	p-Value
4	1	24.76190	2.518087	17.4255	32.09834	<.0001*
3	1	24.57143	2.419300	17.5228	31.62005	<.0001*
4	2	24.50000	2.613143	16.8866	32.11338	<.0001*
3	2	24.30952	2.518087	16.9731	31.64596	<.0001*
4	5	20.19048	2.518087	12.8540	27.52691	<.0001*
3	5	20.00000	2.419300	12.9514	27.04862	<.0001*
5	1	4.57143	2.419300	-2.4772	11.62005	0.3459
5	2	4.30952	2.518087	-3.0269	11.64596	0.4435
2	1	0.26190	2.518087	-7.0745	7.59834	1.0000
4	3	0.19048	2.518087	-7.1460	7.52691	1.0000

Oneway Analysis of MAP By Indent

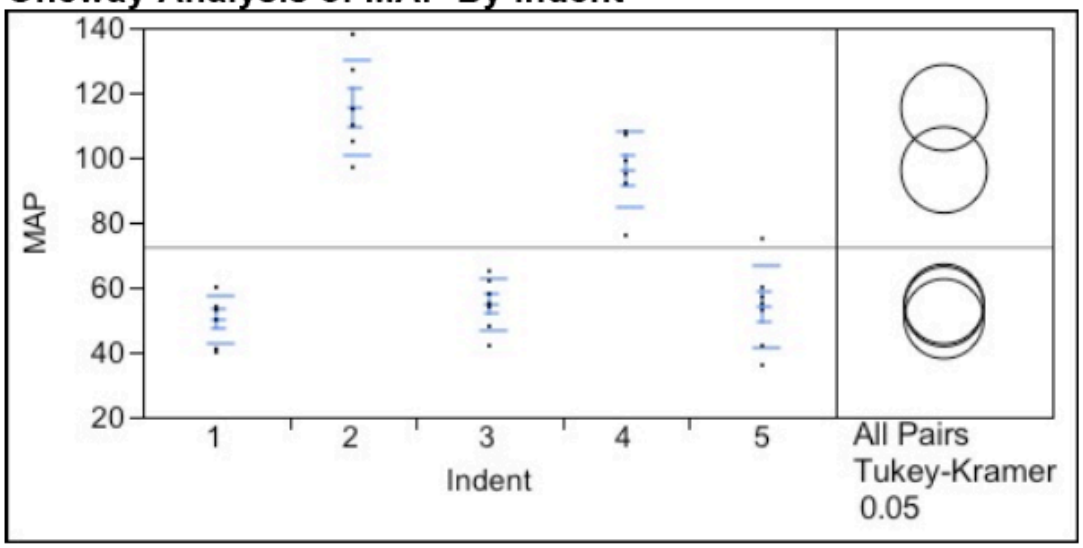

Excluded Rows
2

Means and Std Deviations

Level	Number	Mean	Std Dev	Std Err Mean	Lower 95%	Upper 95%
1	7	50.286	7.3193	2.7664	43.517	57.05
2	6	115.333	14.9755	6.1137	99.617	131.05
3	7	54.857	7.9252	2.9955	47.528	62.19
4	6	96.167	11.7544	4.7987	83.831	108.50
5	7	54.000	12.6227	4.7709	42.326	65.67

Means Comparisons

Comparisons for all pairs using Tukey-Kramer HSD

Confidence Quantile

q*	Alpha
2.91349	0.05

Ordered Differences Report

Level	- Level	Difference	Std Err Dif	Lower CL	Upper CL	p-Value
2	1	65.04762	6.190285	47.0123	83.08298	<.0001*
2	5	61.33333	6.190285	43.2980	79.36869	<.0001*
2	3	60.47619	6.190285	42.4408	78.51155	<.0001*
4	1	45.88095	6.190285	27.8456	63.91631	<.0001*
4	5	42.16667	6.190285	24.1313	60.20203	<.0001*
4	3	41.30952	6.190285	23.2742	59.34489	<.0001*
2	4	19.16667	6.423962	0.4505	37.88285	0.0427*
3	1	4.57143	5.947433	-12.7564	21.89924	0.9375
5	1	3.71429	5.947433	-13.6135	21.04210	0.9699
3	5	0.85714	5.947433	-16.4707	18.18496	0.9999

Fit Y by X Group
Oneway Analysis of peak stress By Indent

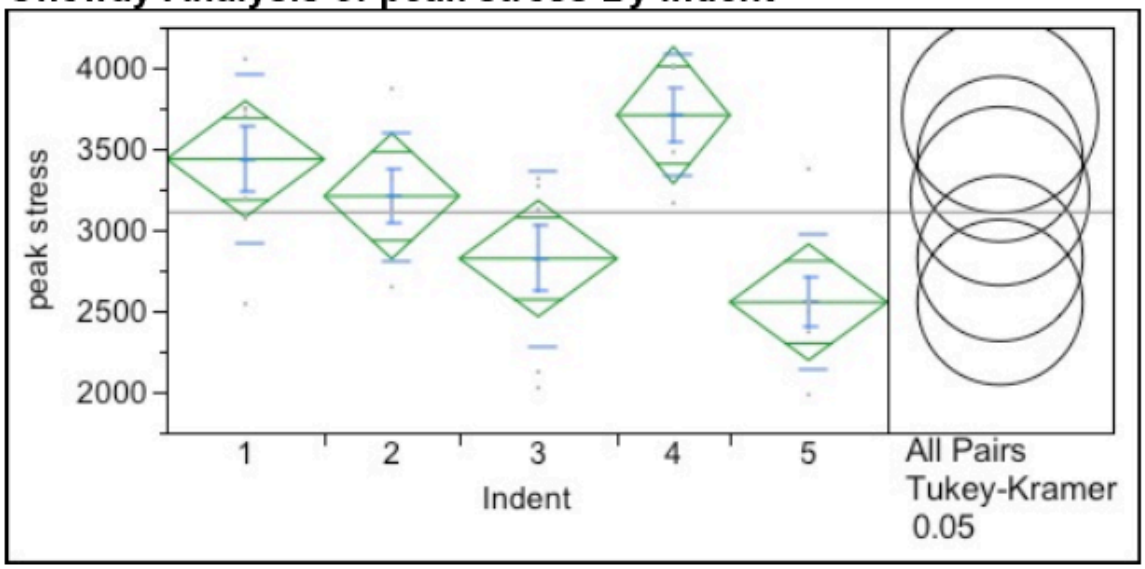

Excluded Rows
3

Oneway Anova
Summary of Fit

Rsquare	0.480665
Adj Rsquare	0.403727
Root Mean Square Error	461.8279
Mean of Response	3108.344
Observations (or Sum Wgts)	32

Analysis of Variance

Source	DF	Sum of Squares	Mean Square	F Ratio	Prob > F
Indent	4	5329908	1332477	6.2474	0.0011*
Error	27	5758695	213285		
C. Total	31	11088603			

Means for Oneway Anova

Level	Number	Mean	Std Error	Lower 95%	Upper 95%
1	7	3436.14	174.55	3078.0	3794.3
2	6	3207.67	188.54	2820.8	3594.5
3	7	2822.71	174.55	2464.6	3180.9
4	5	3707.00	206.54	3283.2	4130.8
5	7	2553.43	174.55	2195.3	2911.6

Std Error uses a pooled estimate of error variance

Means and Std Deviations

Level	Number	Mean	Std Dev	Std Err Mean	Lower 95%	Upper 95%
1	7	3436.14	521.715	197.19	2953.6	3918.6
2	6	3207.67	395.902	161.63	2792.2	3623.1
3	7	2822.71	539.378	203.87	2323.9	3321.6
4	5	3707.00	372.885	166.76	3244.0	4170.0
5	7	2553.43	416.361	157.37	2168.4	2938.5

Means Comparisons

Comparisons for all pairs using Tukey-Kramer HSD

Confidence Quantile

q*	Alpha
2.92068	0.05

Ordered Differences Report

Level	- Level	Difference	Std Err Dif	Lower CL	Upper CL	p-Value
4	5	1153.571	270.4187	363.764	1943.379	0.0019*
4	3	884.286	270.4187	94.478	1674.093	0.0225*
1	5	882.714	246.8574	161.722	1603.707	0.0108*
2	5	654.238	256.9373	-96.195	1404.671	0.1099
1	3	613.429	246.8574	-107.564	1334.421	0.1240
4	2	499.333	279.6507	-317.438	1316.105	0.4021

Level	- Level	Difference	Std Err Dif	Lower CL	Upper CL	p-Value
2	3	384.952	256.9373	-365.480	1135.385	0.5724
4	1	270.857	270.4187	-518.951	1060.665	0.8523
3	5	269.286	246.8574	-451.707	990.278	0.8096
1	2	228.476	256.9373	-521.957	978.909	0.8984

Oneway Analysis of Inst E By Indent

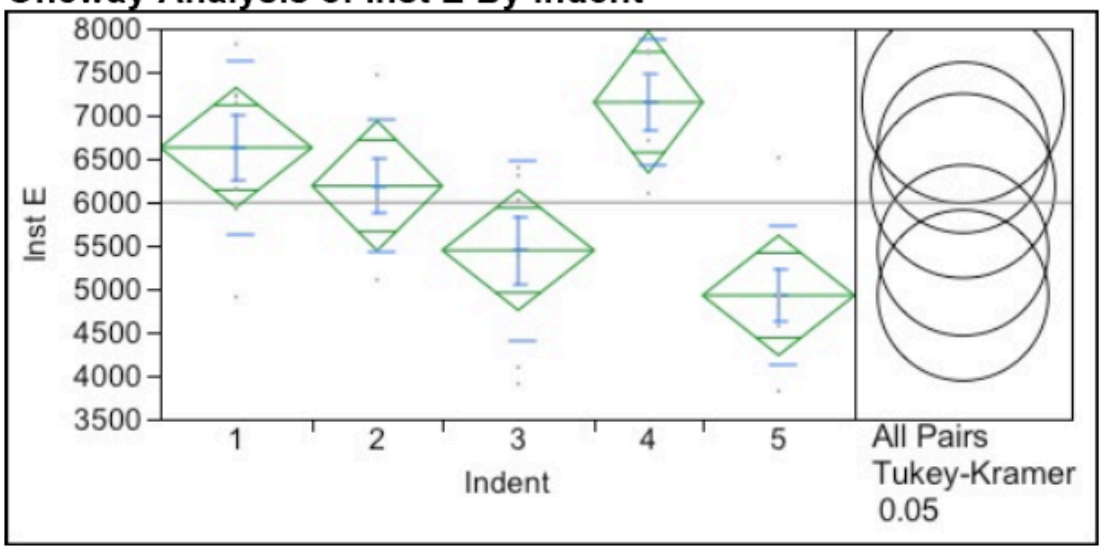

Excluded Rows
3

Oneway Anova
Summary of Fit

Rsquare	0.480682
Adj Rsquare	0.403747
Root Mean Square Error	890.6866
Mean of Response	5995.125
Observations (or Sum Wgts)	32

Analysis of Variance

Source	DF	Sum of Squares	Mean Square	F Ratio	Prob > F
Indent	4	19826172	4956543	6.2478	0.0011*
Error	27	21419710	793323		
C. Total	31	41245882			

Means for Oneway Anova

Level	Number	Mean	Std Error	Lower 95%	Upper 95%
1	7	6627.29	336.65	5936.5	7318.0
2	6	6186.67	363.62	5440.6	6932.8
3	7	5444.29	336.65	4753.5	6135.0
4	5	7149.80	398.33	6332.5	7967.1
5	7	4924.86	336.65	4234.1	5615.6

Std Error uses a pooled estimate of error variance

Means and Std Deviations

Level	Number	Mean	Std Dev	Std Err Mean	Lower 95%	Upper 95%
1	7	6627.29	1006.18	380.30	5696.7	7557.8
2	6	6186.67	763.59	311.73	5385.3	6988.0
3	7	5444.29	1040.19	393.15	4482.3	6406.3
4	5	7149.80	719.46	321.75	6256.5	8043.1
5	7	4924.86	802.87	303.46	4182.3	5667.4

Means Comparisons

Comparisons for all pairs using Tukey-Kramer HSD

Ordered Differences Report

Level	- Level	Difference	Std Err Dif	Lower CL	Upper CL	p-Value
4	5	2224.943	521.5327	701.71	3748.175	0.0019*
4	3	1705.514	521.5327	182.28	3228.747	0.0225*

Level	- Level	Difference	Std Err Dif	Lower CL	Upper CL	p-Value
1	5	1702.429	476.0920	311.91	3092.943	0.0108*
2	5	1261.810	495.5323	-185.48	2709.103	0.1099
1	3	1183.000	476.0920	-207.51	2573.515	0.1240
4	2	963.133	539.3375	-612.10	2538.368	0.4020
2	3	742.381	495.5323	-704.91	2189.674	0.5724
4	1	522.514	521.5327	-1000.72	2045.747	0.8522
3	5	519.429	476.0920	-871.09	1909.943	0.8095
1	2	440.619	495.5323	-1006.67	1887.912	0.8984

Oneway Analysis of exp A1 By Indent

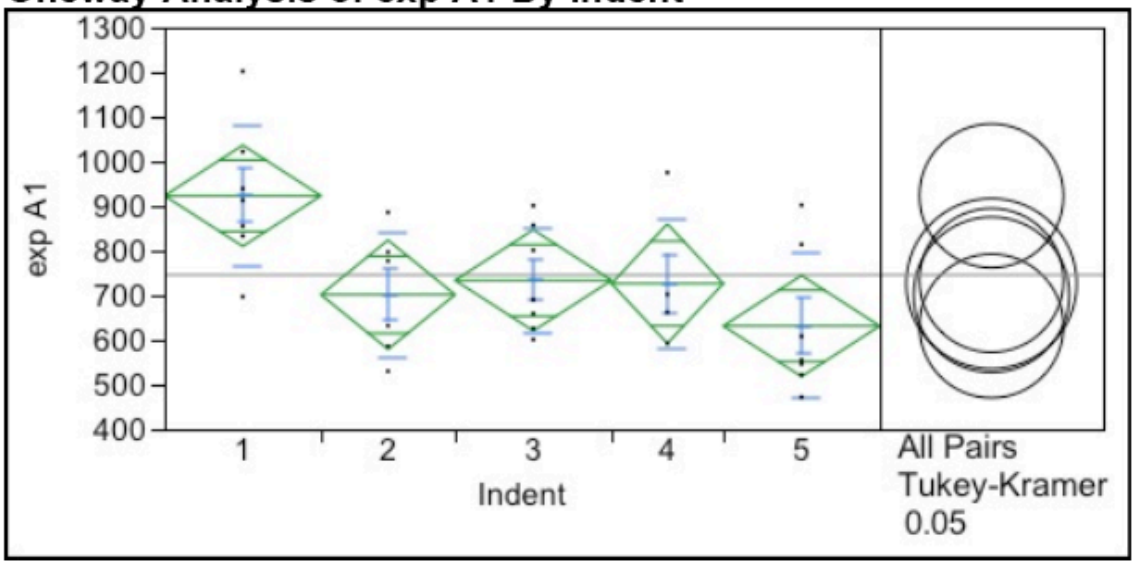

Excluded Rows
3

Oneway Anova
Summary of Fit

Rsquare	0.361882

Adj Rsquare	0.267346
Root Mean Square Error	146.007
Mean of Response	745.4375
Observations (or Sum Wgts)	32

Analysis of Variance

Source	DF	Sum of Squares	Mean Square	F Ratio	Prob > F
Indent	4	326420.60	81605.1	3.8280	0.0137*
Error	27	575587.28	21318.0		
C. Total	31	902007.88			

Means for Oneway Anova

Level	Number	Mean	Std Error	Lower 95%	Upper 95%
1	7	923.000	55.185	809.77	1036.2
2	6	701.333	59.607	579.03	823.6
3	7	733.571	55.185	620.34	846.8
4	5	726.200	65.296	592.22	860.2
5	7	631.286	55.185	518.05	744.5

Std Error uses a pooled estimate of error variance

Means and Std Deviations

Level	Number	Mean	Std Dev	Std Err Mean	Lower 95%	Upper 95%
1	7	923.000	159.059	60.119	775.90	1070.1
2	6	701.333	138.884	56.699	555.58	847.1
3	7	733.571	118.617	44.833	623.87	843.3
4	5	726.200	146.035	65.309	544.87	907.5
5	7	631.286	162.081	61.261	481.39	781.2

Means Comparisons

Comparisons for all pairs using Tukey-Kramer HSD

Ordered Differences Report

Level	- Level	Difference	Std Err Dif	Lower CL	Upper CL	p-Value
1	5	291.7143	78.04403	63.772	519.6563	0.0072*
1	2	221.6667	81.23080	-15.583	458.9162	0.0756
1	4	196.8000	85.49295	-52.898	446.4979	0.1752
1	3	189.4286	78.04403	-38.513	417.3706	0.1387
3	5	102.2857	78.04403	-125.656	330.2277	0.6871
4	5	94.9143	85.49295	-154.784	344.6122	0.7997
2	5	70.0476	81.23080	-167.202	307.2972	0.9081
3	2	32.2381	81.23080	-205.011	269.4876	0.9944
4	2	24.8667	88.41164	-233.356	283.0892	0.9985
3	4	7.3714	85.49295	-242.327	257.0694	1.0000

Oneway Analysis of Exp Trel1 2 By Indent

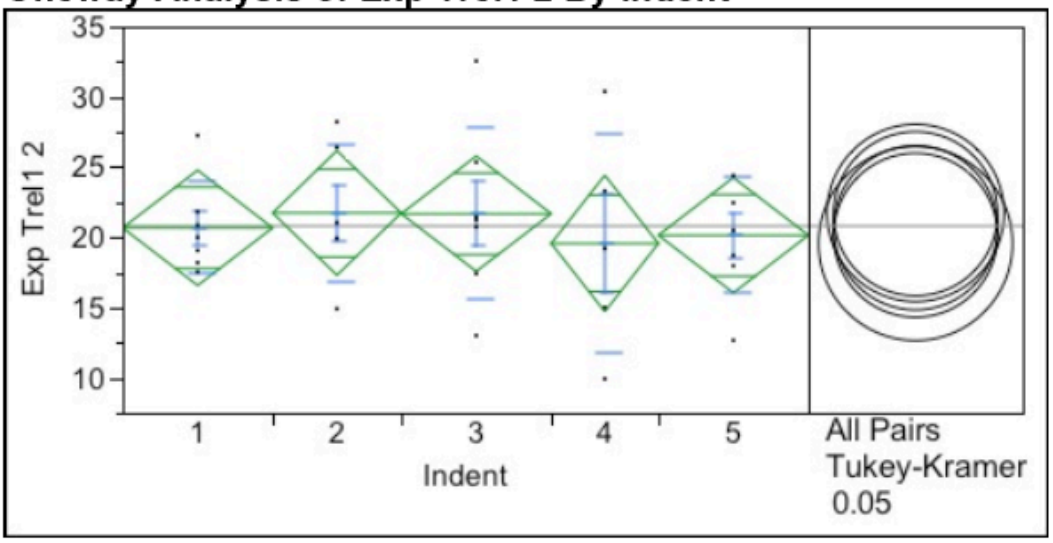

Excluded Rows
3

Oneway Anova
Summary of Fit

Rsquare	0.027485
Adj Rsquare	-0.11659
Root Mean Square Error	5.29284
Mean of Response	20.80125
Observations (or Sum Wgts)	32

Analysis of Variance

Source	DF	Sum of Squares	Mean Square	F Ratio	Prob > F
Indent	4	21.37644	5.3441	0.1908	0.9411
Error	27	756.38211	28.0142		
C. Total	31	777.75855			

Means for Oneway Anova

Level	Number	Mean	Std Error	Lower 95%	Upper 95%
1	7	20.6714	2.0005	16.567	24.776
2	6	21.7317	2.1608	17.298	26.165
3	7	21.6757	2.0005	17.571	25.780
4	5	19.5600	2.3670	14.703	24.417
5	7	20.1457	2.0005	16.041	24.250

Std Error uses a pooled estimate of error variance

Means and Std Deviations

Level	Number	Mean	Std Dev	Std Err Mean	Lower 95%	Upper 95%
1	7	20.6714	3.25663	1.2309	17.660	23.683
2	6	21.7317	4.85077	1.9803	16.641	26.822
3	7	21.6757	6.14058	2.3209	15.997	27.355
4	5	19.5600	7.82354	3.4988	9.846	29.274
5	7	20.1457	4.16388	1.5738	16.295	23.997

Means Comparisons
Comparisons for all pairs using Tukey-Kramer HSD

Ordered Differences Report

Level	- Level	Difference	Std Err Dif	Lower CL	Upper CL	p-Value
2	4	2.171667	3.204974	-7.18905	11.53238	0.9596
3	4	2.115714	3.099170	-6.93598	11.16741	0.9585
2	5	1.585952	2.944664	-7.01448	10.18639	0.9824
3	5	1.530000	2.829142	-6.73303	9.79303	0.9822
1	4	1.111429	3.099170	-7.94027	10.16313	0.9962
2	1	1.060238	2.944664	-7.54020	9.66067	0.9962
3	1	1.004286	2.829142	-7.25874	9.26732	0.9964
5	4	0.585714	3.099170	-8.46598	9.63741	0.9997
1	5	0.525714	2.829142	-7.73732	8.78874	0.9997
2	3	0.055952	2.944664	-8.54448	8.65639	1.0000

Oneway Analysis of Exp E1 By Indent

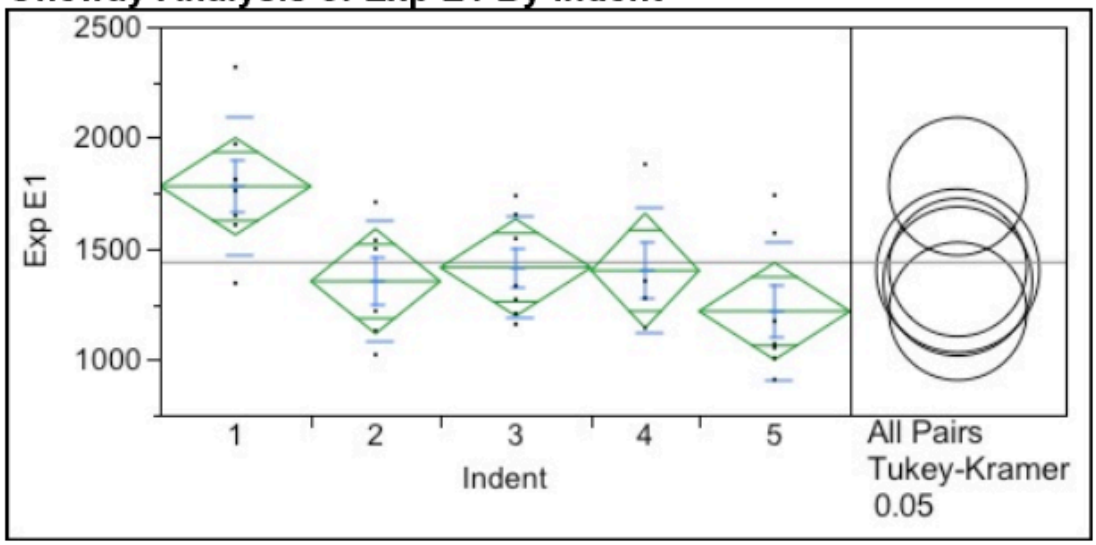

Excluded Rows

Oneway Anova
Summary of Fit

Rsquare	0.361771
Adj Rsquare	0.267219
Root Mean Square Error	281.641
Mean of Response	1437.719
Observations (or Sum Wgts)	32

Analysis of Variance

Source	DF	Sum of Squares	Mean Square	F Ratio	Prob > F
Indent	4	1213984.5	303496	3.8261	0.0137*
Error	27	2141684.0	79322		
C. Total	31	3355668.5			

Means for Oneway Anova

Level	Number	Mean	Std Error	Lower 95%	Upper 95%
1	7	1780.14	106.45	1561.7	1998.6
2	6	1352.67	114.98	1116.7	1588.6
3	7	1414.86	106.45	1196.4	1633.3
4	5	1400.60	125.95	1142.2	1659.0
5	7	1217.57	106.45	999.2	1436.0

Std Error uses a pooled estimate of error variance

Means and Std Deviations

Level	Number	Mean	Std Dev	Std Err Mean	Lower 95%	Upper 95%
1	7	1780.14	306.712	115.93	1496.5	2063.8
2	6	1352.67	268.012	109.42	1071.4	1633.9
3	7	1414.86	228.934	86.53	1203.1	1626.6
4	5	1400.60	281.384	125.84	1051.2	1750.0
5	7	1217.57	312.763	118.21	928.3	1506.8

Means Comparisons
Comparisons for all pairs using Tukey-Kramer HSD

Ordered Differences Report

Level	- Level	Difference	Std Err Dif	Lower CL	Upper CL	p-Value
1	5	562.5714	150.5434	122.882	1002.261	0.0072*
1	2	427.4762	156.6906	-30.168	885.120	0.0757
1	4	379.5429	164.9121	-102.113	861.199	0.1754
1	3	365.2857	150.5434	-74.404	804.976	0.1389
3	5	197.2857	150.5434	-242.404	636.976	0.6872
4	5	183.0286	164.9121	-298.628	664.685	0.7999
2	5	135.0952	156.6906	-322.548	592.739	0.9081
3	2	62.1905	156.6906	-395.453	519.834	0.9944
4	2	47.9333	170.5421	-450.166	546.033	0.9985
3	4	14.2571	164.9121	-467.399	495.913	1.0000

Oneway Analysis of exp visc1 By Indent

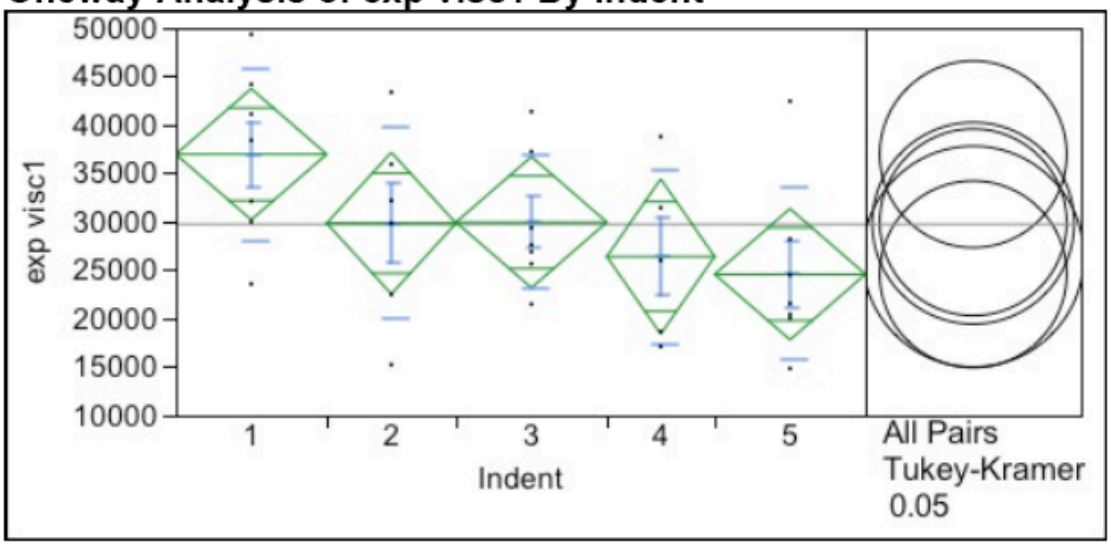

Excluded Rows
3

Oneway Anova
Summary of Fit

Rsquare	0.228069
Adj Rsquare	0.113708
Root Mean Square Error	8729.445
Mean of Response	29736.5
Observations (or Sum Wgts)	32

Analysis of Variance

Source	DF	Sum of Squares	Mean Square	F Ratio	Prob > F
Indent	4	607888707	151972177	1.9943	0.1238
Error	27	2057486903	76203219		
C. Total	31	2665375610			

Means for Oneway Anova

Level	Number	Mean	Std Error	Lower 95%	Upper 95%
1	7	36965.4	3299.4	30196	43735
2	6	29848.7	3563.8	22536	37161
3	7	29948.7	3299.4	23179	36719
4	5	26404.6	3903.9	18394	34415
5	7	24579.1	3299.4	17809	31349

Std Error uses a pooled estimate of error variance

Means and Std Deviations

Level	Number	Mean	Std Dev	Std Err Mean	Lower 95%	Upper 95%
1	7	36965.4	8909.78	3367.6	28725	45206
2	6	29848.7	9931.24	4054.4	19426	40271
3	7	29948.7	6937.24	2622.0	23533	36365
4	5	26404.6	9014.86	4031.6	15211	37598

Level	Number	Mean	Std Dev	Std Err Mean	Lower 95%	Upper 95%
5	7	24579.1	8890.17	3360.2	16357	32801

Means Comparisons
Comparisons for all pairs using Tukey-Kramer HSD

Ordered Differences Report

Level	- Level	Difference	Std Err Dif	Lower CL	Upper CL	p-Value
1	5	12386.29	4666.085	-1241.9	26014.45	0.0882
1	4	10560.83	5111.440	-4368.1	25489.73	0.2635
1	2	7116.76	4856.615	-7067.9	21301.40	0.5926
1	3	7016.71	4666.085	-6611.4	20644.88	0.5690
3	5	5369.57	4666.085	-8258.6	18997.73	0.7784
2	5	5269.52	4856.615	-8915.1	19454.16	0.8126
3	4	3544.11	5111.440	-11384.8	18473.02	0.9562
2	4	3444.07	5285.942	-11994.5	18882.63	0.9649
4	5	1825.46	5111.440	-13103.4	16754.36	0.9963
3	2	100.05	4856.615	-14084.6	14284.69	1.0000

Oneway Analysis of exp A2 By Indent

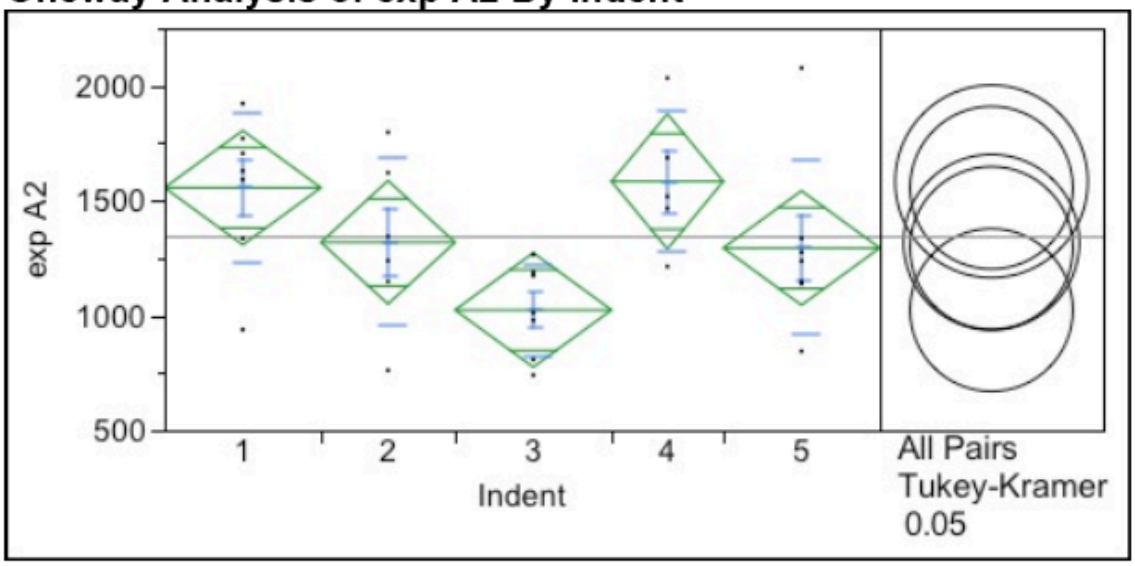

Excluded Rows
3

Oneway Anova
Summary of Fit

Rsquare	0.325468
Adj Rsquare	0.225537
Root Mean Square Error	320.7737
Mean of Response	1341.594
Observations (or Sum Wgts)	32

Analysis of Variance

Source	DF	Sum of Squares	Mean Square	F Ratio	Prob > F
Indent	4	1340500.9	335125	3.2569	0.0265*
Error	27	2778184.9	102896		
C. Total	31	4118685.7			

Means for Oneway Anova

Level	Number	Mean	Std Error	Lower 95%	Upper 95%
1	7	1555.71	121.24	1306.9	1804.5
2	6	1318.00	130.96	1049.3	1586.7
3	7	1023.43	121.24	774.7	1272.2
4	5	1583.00	143.45	1288.7	1877.3
5	7	1293.43	121.24	1044.7	1542.2

Std Error uses a pooled estimate of error variance

Means and Std Deviations

Level	Number	Mean	Std Dev	Std Err Mean	Lower 95%	Upper 95%
1	7	1555.71	326.413	123.37	1253.8	1857.6
2	6	1318.00	365.356	149.16	934.6	1701.4
3	7	1023.43	198.549	75.04	839.8	1207.1
4	5	1583.00	303.337	135.66	1206.4	1959.6
5	7	1293.43	380.111	143.67	941.9	1645.0

Means Comparisons

Comparisons for all pairs using Tukey-Kramer HSD

Ordered Differences Report

Level	- Level	Difference	Std Err Dif	Lower CL	Upper CL	p-Value
4	3	559.5714	187.8258	10.991	1108.151	0.0439*
1	3	532.2857	171.4607	31.503	1033.068	0.0331*
2	3	294.5714	178.4620	-226.660	815.803	0.4797
4	5	289.5714	187.8258	-259.009	838.151	0.5456
5	3	270.0000	171.4607	-230.783	770.783	0.5255
4	2	265.0000	194.2381	-302.308	832.308	0.6547
1	5	262.2857	171.4607	-238.497	763.068	0.5530
1	2	237.7143	178.4620	-283.517	758.945	0.6743
4	1	27.2857	187.8258	-521.294	575.866	0.9999

Oneway Analysis of exp Trel2 By Indent

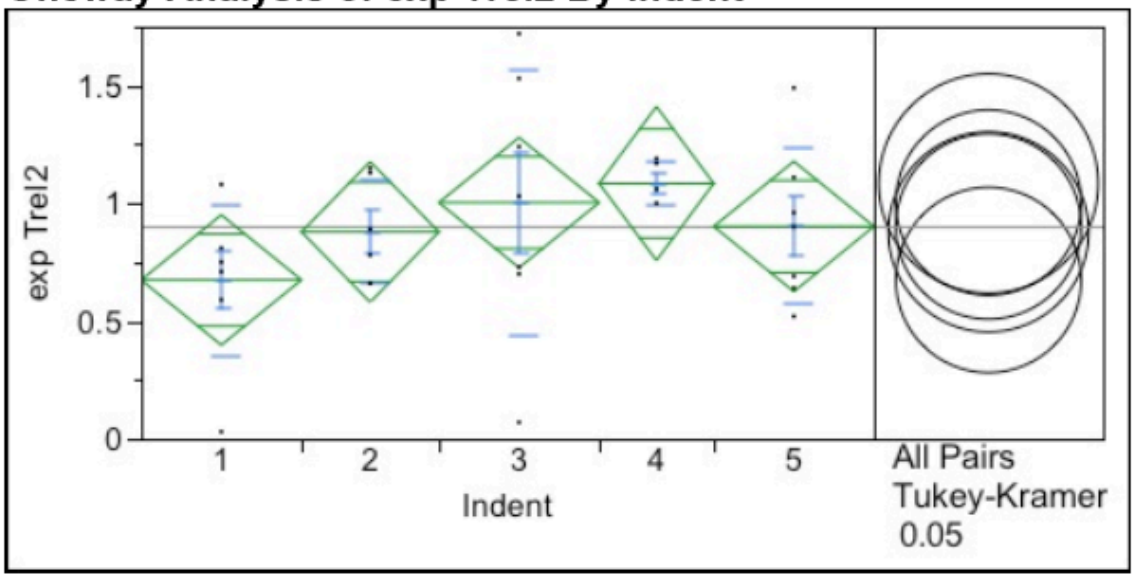

Excluded Rows
3

Oneway Anova
Summary of Fit

Rsquare	0.149413
Adj Rsquare	0.0234
Root Mean Square Error	0.356475
Mean of Response	0.898125
Observations (or Sum Wgts)	32

Analysis of Variance

Source	DF	Sum of Squares	Mean Square	F Ratio	Prob > F
Indent	4	0.6026842	0.150671	1.1857	0.3395
Error	27	3.4310033	0.127074		

Source	DF	Sum of Squares	Mean Square	F Ratio	Prob > F
C. Total	31	4.0336875			

Means for Oneway Anova

Level	Number	Mean	Std Error	Lower 95%	Upper 95%
1	7	0.67429	0.13473	0.39783	0.9507
2	6	0.87833	0.14553	0.57973	1.1769
3	7	1.00286	0.13473	0.72640	1.2793
4	5	1.08400	0.15942	0.75690	1.4111
5	7	0.90143	0.13473	0.62498	1.1779

Std Error uses a pooled estimate of error variance

Means and Std Deviations

Level	Number	Mean	Std Dev	Std Err Mean	Lower 95%	Upper 95%
1	7	0.67429	0.320929	0.12130	0.37748	0.9711
2	6	0.87833	0.220129	0.08987	0.64732	1.1093
3	7	1.00286	0.560586	0.21188	0.48440	1.5213
4	5	1.08400	0.091269	0.04082	0.97067	1.1973
5	7	0.90143	0.329617	0.12458	0.59658	1.2063

Means Comparisons

Comparisons for all pairs using Tukey-Kramer HSD

Ordered Differences Report

Level	- Level	Difference	Std Err Dif	Lower CL	Upper CL	p-Value
4	1	0.4097143	0.2087302	-0.199921	1.019349	0.3104
3	1	0.3285714	0.1905437	-0.227947	0.885090	0.4366
5	1	0.2271429	0.1905437	-0.329375	0.783661	0.7557
4	2	0.2056667	0.2158561	-0.424781	0.836114	0.8734
2	1	0.2040476	0.1983242	-0.375195	0.783290	0.8398

Level	- Level	Difference	Std Err Dif	Lower CL	Upper CL	p-Value
4	5	0.1825714	0.2087302	-0.427064	0.792206	0.9037
3	2	0.1245238	0.1983242	-0.454719	0.703766	0.9692
3	5	0.1014286	0.1905437	-0.455090	0.657947	0.9832
4	3	0.0811429	0.2087302	-0.528492	0.690778	0.9949
5	2	0.0230952	0.1983242	-0.556147	0.602338	1.0000

Oneway Analysis of exp E2 By Indent

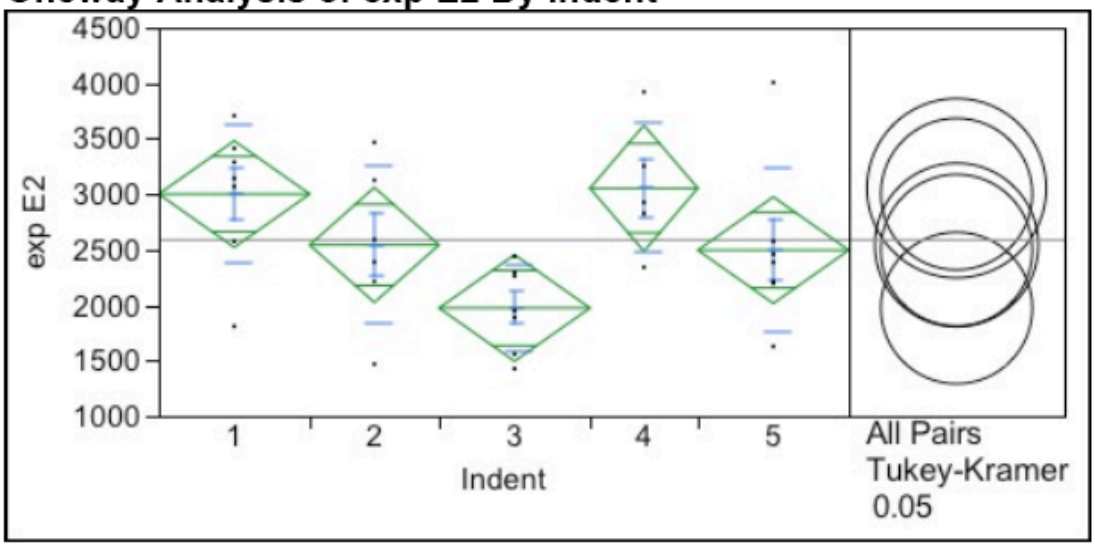

Excluded Rows
3

Oneway Anova
Summary of Fit

Rsquare	0.325557
Adj Rsquare	0.22564
Root Mean Square Error	618.6287
Mean of Response	2587.5
Observations (or Sum Wgts)	32

Analysis of Variance

Source	DF	Sum of Squares	Mean Square	F Ratio	Prob > F
Indent	4	4987769	1246942	3.2583	0.0265*
Error	27	10332939	382701		
C. Total	31	15320708			

Means for Oneway Anova

Level	Number	Mean	Std Error	Lower 95%	Upper 95%
1	7	3000.43	233.82	2520.7	3480.2
2	6	2542.00	252.55	2023.8	3060.2
3	7	1973.71	233.82	1494.0	2453.5
4	5	3053.20	276.66	2485.5	3620.9
5	7	2494.71	233.82	2015.0	2974.5

Std Error uses a pooled estimate of error variance

Means and Std Deviations

Level	Number	Mean	Std Dev	Std Err Mean	Lower 95%	Upper 95%
1	7	3000.43	629.470	237.92	2418.3	3582.6
2	6	2542.00	704.544	287.63	1802.6	3281.4
3	7	1973.71	383.023	144.77	1619.5	2328.0
4	5	3053.20	584.936	261.59	2326.9	3779.5
5	7	2494.71	733.121	277.09	1816.7	3172.7

Means Comparisons

Comparisons for all pairs using Tukey-Kramer HSD

Ordered Differences Report

Level	- Level	Difference	Std Err Dif	Lower CL	Upper CL	p-Value
4	3	1079.486	362.2319	21.52	2137.451	0.0438*
1	3	1026.714	330.6709	60.93	1992.500	0.0330*

Level	- Level	Difference	Std Err Dif	Lower CL	Upper CL	p-Value
2	3	568.286	344.1732	-436.94	1573.507	0.4794
4	5	558.486	362.2319	-499.48	1616.451	0.5456
5	3	521.000	330.6709	-444.79	1486.785	0.5249
4	2	511.200	374.5983	-582.88	1605.283	0.6545
1	5	505.714	330.6709	-460.07	1471.500	0.5532
1	2	458.429	344.1732	-546.79	1463.650	0.6743
4	1	52.771	362.2319	-1005.19	1110.736	0.9999
2	5	47.286	344.1732	-957.94	1052.507	0.9999

Oneway Analysis of exp visc2 By Indent

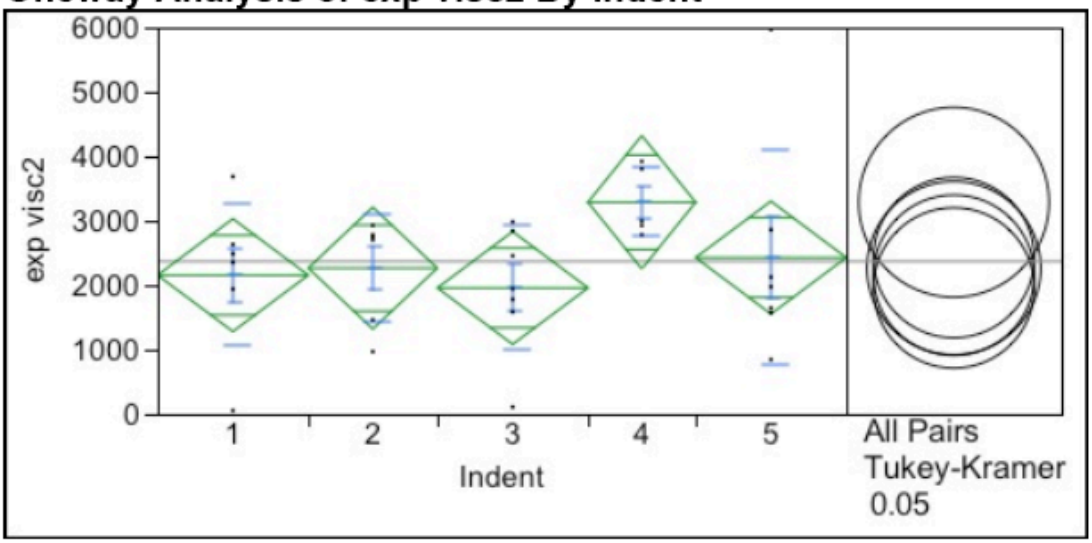

Excluded Rows
3

Oneway Anova
Summary of Fit

Rsquare	0.144556
Adj Rsquare	0.017823
Root Mean Square Error	1128.178
Mean of Response	2368.781

Observations (or Sum Wgts) 32

Analysis of Variance

Source	DF	Sum of Squares	Mean Square	F Ratio	Prob > F
Indent	4	5807139	1451785	1.1406	0.3586
Error	27	34365216	1272786		
C. Total	31	40172355			

Means for Oneway Anova

Level	Number	Mean	Std Error	Lower 95%	Upper 95%
1	7	2155.00	426.41	1280.1	3029.9
2	6	2264.83	460.58	1319.8	3209.9
3	7	1957.14	426.41	1082.2	2832.1
4	5	3286.60	504.54	2251.4	4321.8
5	7	2427.71	426.41	1552.8	3302.6

Std Error uses a pooled estimate of error variance

Means and Std Deviations

Level	Number	Mean	Std Dev	Std Err Mean	Lower 95%	Upper 95%
1	7	2155.00	1097.88	414.96	1139.6	3170.4
2	6	2264.83	831.36	339.40	1392.4	3137.3
3	7	1957.14	972.38	367.53	1057.8	2856.4
4	5	3286.60	533.32	238.51	2624.4	3948.8
5	7	2427.71	1676.63	633.71	877.1	3978.3

Means Comparisons

Comparisons for all pairs using Tukey-Kramer HSD

Ordered Differences Report

Level	- Level	Difference	Std Err Dif	Lower CL	Upper CL	p-Value
4	3	1329.457	660.5934	-599.93	3258.842	0.2872
4	1	1131.600	660.5934	-797.79	3060.985	0.4432
4	2	1021.767	683.1458	-973.49	3017.020	0.5739
4	5	858.886	660.5934	-1070.50	2788.271	0.6933
5	3	470.571	603.0366	-1290.71	2231.851	0.9341
2	3	307.690	627.6603	-1525.51	2140.888	0.9876
5	1	272.714	603.0366	-1488.57	2033.994	0.9909
1	3	197.857	603.0366	-1563.42	1959.137	0.9973
5	2	162.881	627.6603	-1670.32	1996.079	0.9989
2	1	109.833	627.6603	-1723.36	1943.031	0.9998

Oneway Analysis of exp Aeq By Indent

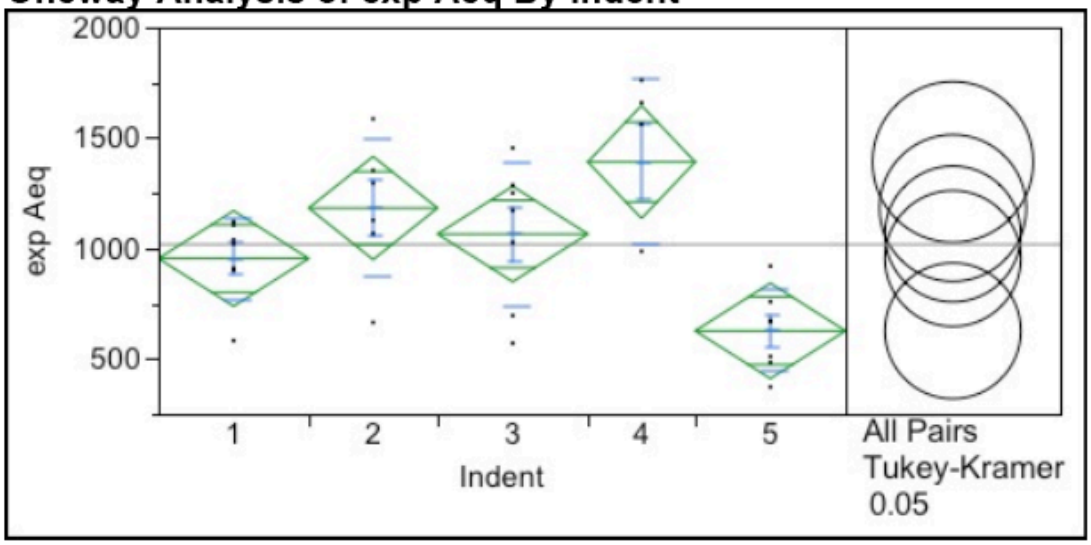

Excluded Rows
3

Oneway Anova
Summary of Fit

Rsquare	0.484994

Adj Rsquare	0.408696
Root Mean Square Error	278.6661
Mean of Response	1017.375
Observations (or Sum Wgts)	32

Analysis of Variance

Source	DF	Sum of Squares	Mean Square	F Ratio	Prob > F
Indent	4	1974492.3	493623	6.3566	0.0010*
Error	27	2096679.2	77655		
C. Total	31	4071171.5			

Means for Oneway Anova

Level	Number	Mean	Std Error	Lower 95%	Upper 95%
1	7	953.71	105.33	737.6	1169.8
2	6	1182.00	113.76	948.6	1415.4
3	7	1064.57	105.33	848.5	1280.7
4	5	1390.60	124.62	1134.9	1646.3
5	7	626.14	105.33	410.0	842.3

Std Error uses a pooled estimate of error variance

Means and Std Deviations

Level	Number	Mean	Std Dev	Std Err Mean	Lower 95%	Upper 95%
1	7	953.71	184.986	69.92	782.63	1124.8
2	6	1182.00	312.986	127.78	853.54	1510.5
3	7	1064.57	323.797	122.38	765.11	1364.0
4	5	1390.60	376.439	168.35	923.19	1858.0
5	7	626.14	185.143	69.98	454.91	797.4

Means Comparisons

Comparisons for all pairs using Tukey-Kramer HSD

Ordered Differences Report

Level	- Level	Difference	Std Err Dif	Lower CL	Upper CL	p-Value
4	5	764.4571	163.1701	287.889	1241.026	0.0006*
2	5	555.8571	155.0355	103.047	1008.667	0.0105*
3	5	438.4286	148.9533	3.383	873.474	0.0476*
4	1	436.8857	163.1701	-39.683	913.454	0.0841
1	5	327.5714	148.9533	-107.474	762.617	0.2105
4	3	326.0286	163.1701	-150.540	802.597	0.2939
2	1	228.2857	155.0355	-224.524	681.095	0.5883
4	2	208.6000	168.7407	-284.238	701.438	0.7308
2	3	117.4286	155.0355	-335.381	570.238	0.9405
3	1	110.8571	148.9533	-324.188	545.903	0.9440

Oneway Analysis of insp A1 By Indent

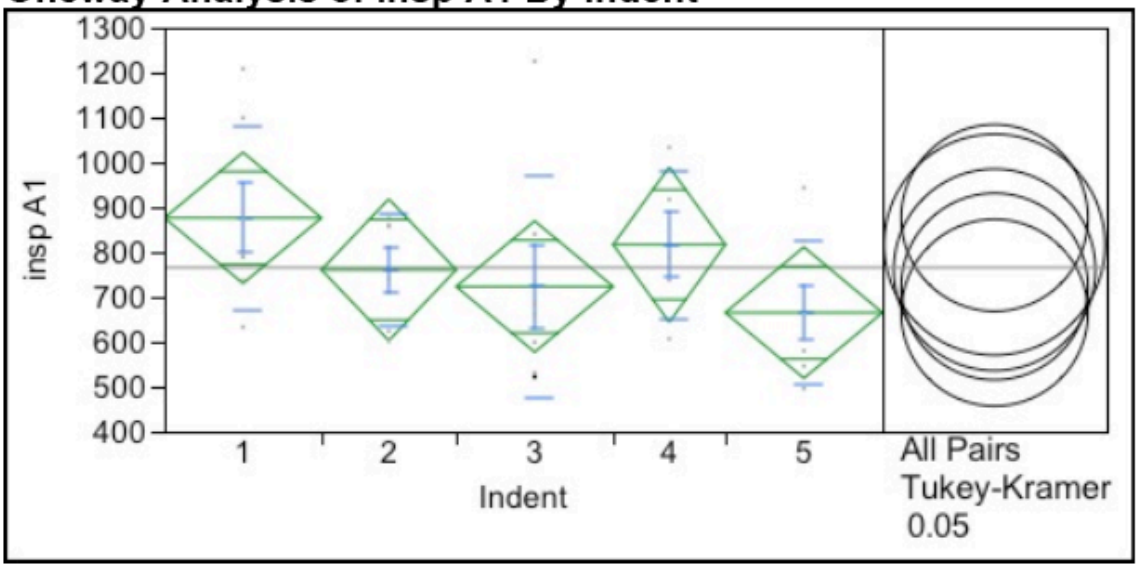

Excluded Rows
3

Oneway Anova
Summary of Fit

Rsquare	0.159633

Adj Rsquare	0.035134
Root Mean Square Error	188.4591
Mean of Response	765.5
Observations (or Sum Wgts)	32

Analysis of Variance

Source	DF	Sum of Squares	Mean Square	F Ratio	Prob > F
Indent	4	182159.6	45539.9	1.2822	0.3015
Error	27	958954.4	35516.8		
C. Total	31	1141114.0			

Means for Oneway Anova

Level	Number	Mean	Std Error	Lower 95%	Upper 95%
1	7	876.143	71.231	729.99	1022.3
2	6	760.500	76.938	602.64	918.4
3	7	723.143	71.231	576.99	869.3
4	5	816.600	84.281	643.67	989.5
5	7	665.000	71.231	518.85	811.2

Std Error uses a pooled estimate of error variance

Means and Std Deviations

Level	Number	Mean	Std Dev	Std Err Mean	Lower 95%	Upper 95%
1	7	876.143	205.193	77.556	686.37	1065.9
2	6	760.500	125.080	51.064	629.24	891.8
3	7	723.143	246.204	93.056	495.44	950.8
4	5	816.600	164.193	73.429	612.73	1020.5
5	7	665.000	161.538	61.056	515.60	814.4

Means Comparisons

Comparisons for all pairs using Tukey-Kramer HSD

Ordered Differences Report

Level	- Level	Difference	Std Err Dif	Lower CL	Upper CL	p-Value
1	5	211.1429	100.7356	-83.074	505.3598	0.2508
1	3	153.0000	100.7356	-141.217	447.2170	0.5597
4	5	151.6000	110.3503	-170.699	473.8985	0.6489
1	2	115.6429	104.8490	-190.588	421.8736	0.8035
2	5	95.5000	104.8490	-210.731	401.7307	0.8902
4	3	93.4571	110.3503	-228.841	415.7557	0.9133
1	4	59.5429	110.3503	-262.756	381.8414	0.9823
3	5	58.1429	100.7356	-236.074	352.3598	0.9773
4	2	56.1000	114.1176	-277.202	389.4016	0.9875
2	3	37.3571	104.8490	-268.874	343.5879	0.9963

Oneway Analysis of insp Trel1 By Indent

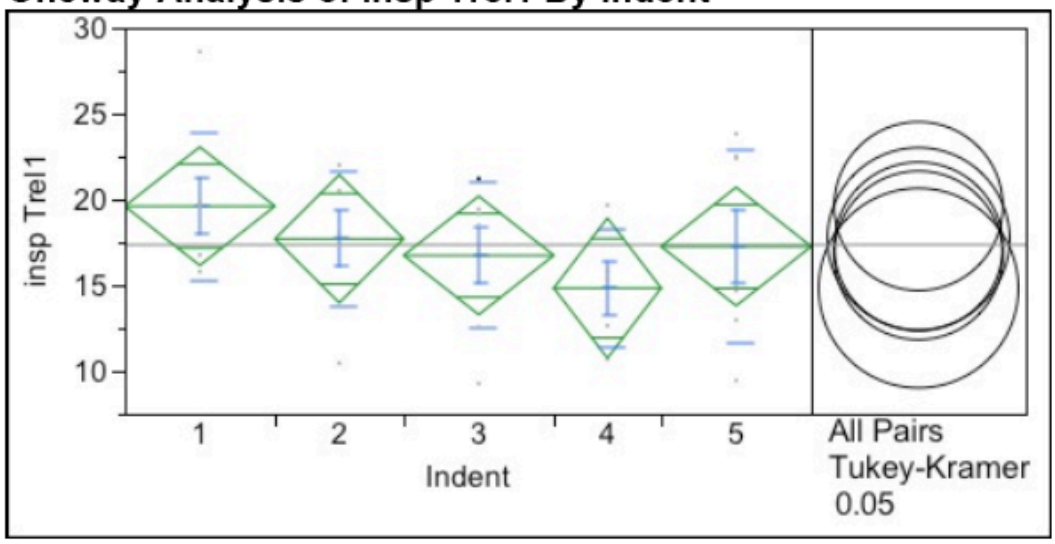

Excluded Rows
3

Oneway Anova
Summary of Fit

Rsquare	0.116722
Adj Rsquare	-0.01413
Root Mean Square Error	4.452418
Mean of Response	17.36
Observations (or Sum Wgts)	32

Analysis of Variance

Source	DF	Sum of Squares	Mean Square	F Ratio	Prob > F
Indent	4	70.73098	17.6827	0.8920	0.4822
Error	27	535.24862	19.8240		
C. Total	31	605.97960			

Means for Oneway Anova

Level	Number	Mean	Std Error	Lower 95%	Upper 95%
1	7	19.6029	1.6829	16.150	23.056
2	6	17.7033	1.8177	13.974	21.433
3	7	16.7357	1.6829	13.283	20.189
4	5	14.8300	1.9912	10.744	18.916
5	7	17.2543	1.6829	13.801	20.707

Std Error uses a pooled estimate of error variance

Means and Std Deviations

Level	Number	Mean	Std Dev	Std Err Mean	Lower 95%	Upper 95%
1	7	19.6029	4.31941	1.6326	15.608	23.598
2	6	17.7033	3.97933	1.6246	13.527	21.879
3	7	16.7357	4.26956	1.6137	12.787	20.684
4	5	14.8300	3.40938	1.5247	10.597	19.063
5	7	17.2543	5.60148	2.1172	12.074	22.435

Means Comparisons
Comparisons for all pairs using Tukey-Kramer HSD

Ordered Differences Report

Level	- Level	Difference	Std Err Dif	Lower CL	Upper CL	p-Value
1	4	4.772857	2.607069	-2.84157	12.38728	0.3776
2	4	2.873333	2.696073	-5.00104	10.74771	0.8221
1	3	2.867143	2.379917	-4.08384	9.81813	0.7487
5	4	2.424286	2.607069	-5.19014	10.03871	0.8828
1	5	2.348571	2.379917	-4.60242	9.29956	0.8589
3	4	1.905714	2.607069	-5.70871	9.52014	0.9473
1	2	1.899524	2.477097	-5.33529	9.13434	0.9379
2	3	0.967619	2.477097	-6.26720	8.20244	0.9948
5	3	0.518571	2.379917	-6.43242	7.46956	0.9995
2	5	0.449048	2.477097	-6.78577	7.68386	0.9997

Oneway Analysis of insp E1 By Indent

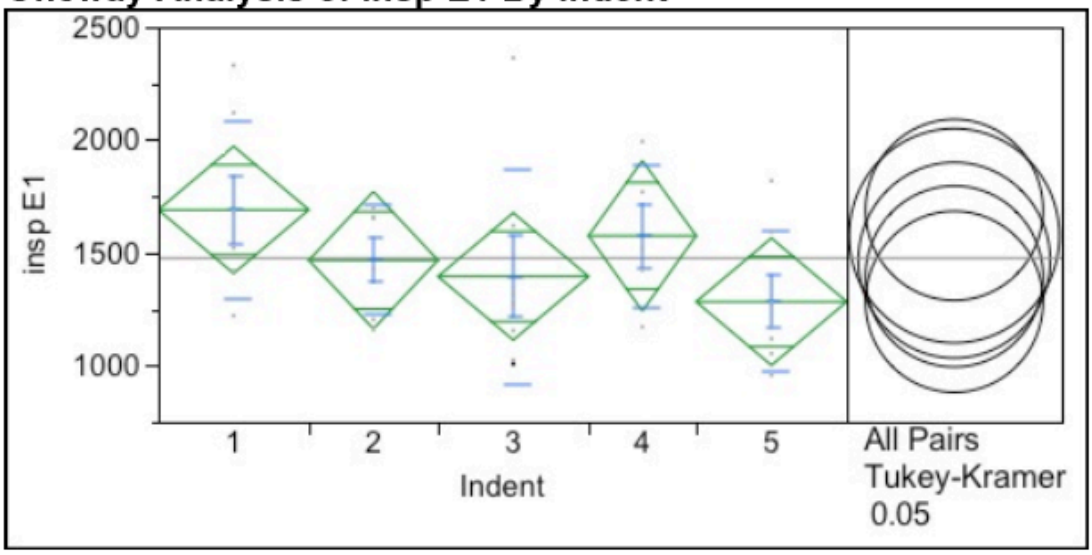

Oneway Anova
Summary of Fit

Rsquare	0.159582
Adj Rsquare	0.035076
Root Mean Square Error	363.5018
Mean of Response	1476.438
Observations (or Sum Wgts)	32

Analysis of Variance

Source	DF	Sum of Squares	Mean Square	F Ratio	Prob > F
Indent	4	677432.8	169358	1.2817	0.3017
Error	27	3567607.0	132134		
C. Total	31	4245039.9			

Means for Oneway Anova

Level	Number	Mean	Std Error	Lower 95%	Upper 95%
1	7	1689.86	137.39	1408.0	1971.8
2	6	1466.67	148.40	1162.2	1771.2
3	7	1394.71	137.39	1112.8	1676.6
4	5	1575.00	162.56	1241.4	1908.6
5	7	1282.71	137.39	1000.8	1564.6

Std Error uses a pooled estimate of error variance

Means and Std Deviations

Level	Number	Mean	Std Dev	Std Err Mean	Lower 95%	Upper 95%
1	7	1689.86	395.888	149.63	1323.7	2056.0
2	6	1466.67	241.058	98.41	1213.7	1719.6
3	7	1394.71	474.975	179.52	955.4	1834.0
4	5	1575.00	316.571	141.58	1181.9	1968.1
5	7	1282.71	311.507	117.74	994.6	1570.8

Means Comparisons
Comparisons for all pairs using Tukey-Kramer HSD

Ordered Differences Report

Level	- Level	Difference	Std Err Dif	Lower CL	Upper CL	p-Value
1	5	407.1429	194.2999	-160.346	974.6316	0.2511
1	3	295.1429	194.2999	-272.346	862.6316	0.5596
4	5	292.2857	212.8449	-329.367	913.9385	0.6493
1	2	223.1905	202.2338	-367.471	813.8515	0.8031
2	5	183.9524	202.2338	-406.709	774.6134	0.8907
4	3	180.2857	212.8449	-441.367	801.9385	0.9133
1	4	114.8571	212.8449	-506.796	736.5099	0.9823
3	5	112.0000	194.2999	-455.489	679.4887	0.9774
4	2	108.3333	220.1113	-534.542	751.2090	0.9874
2	3	71.9524	202.2338	-518.709	662.6134	0.9964

Oneway Analysis of insp Visc1 By Indent

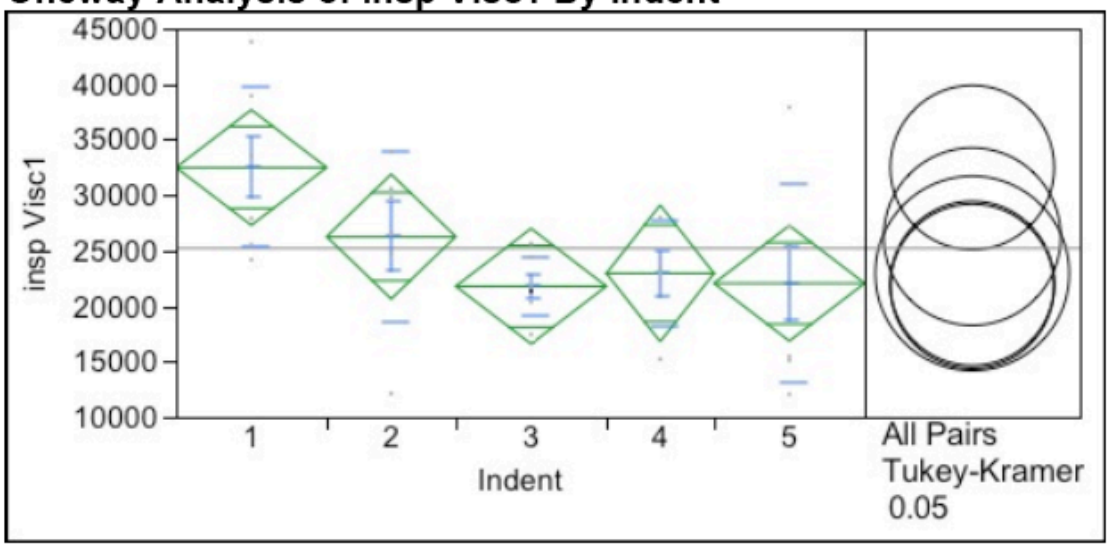

Oneway Anova
Summary of Fit

Rsquare	0.313384
Adj Rsquare	0.211663
Root Mean Square Error	6706.856
Mean of Response	25199.31
Observations (or Sum Wgts)	32

Analysis of Variance

Source	DF	Sum of Squares	Mean Square	F Ratio	Prob > F
Indent	4	554325560	138581390	3.0808	0.0327*
Error	27	1214511767	44981917		
C. Total	31	1768837327			

Means for Oneway Anova

Level	Number	Mean	Std Error	Lower 95%	Upper 95%
1	7	32477.6	2535.0	27276	37679
2	6	26255.0	2738.1	20637	31873
3	7	21781.7	2535.0	16580	26983
4	5	22941.2	2999.4	16787	29095
5	7	22046.7	2535.0	16845	27248

Std Error uses a pooled estimate of error variance

Means and Std Deviations

Level	Number	Mean	Std Dev	Std Err Mean	Lower 95%	Upper 95%
1	7	32477.6	7192.55	2718.5	25826	39130
2	6	26255.0	7631.81	3115.7	18246	34264
3	7	21781.7	2679.01	1012.6	19304	24259
4	5	22941.2	4745.23	2122.1	17049	28833

Level	Number	Mean	Std Dev	Std Err Mean	Lower 95%	Upper 95%
5	7	22046.7	8942.05	3379.8	13777	30317

Means Comparisons
Comparisons for all pairs using Tukey-Kramer HSD

Ordered Differences Report

Level	- Level	Difference	Std Err Dif	Lower CL	Upper CL	p-Value
1	3	10695.86	3584.965	225.3	21166.41	0.0435*
1	5	10430.86	3584.965	-39.7	20901.41	0.0512
1	4	9536.37	3927.133	-1933.5	21006.29	0.1384
1	2	6222.57	3731.350	-4675.5	17120.67	0.4697
2	3	4473.29	3731.350	-6424.8	15371.38	0.7520
2	5	4208.29	3731.350	-6689.8	15106.38	0.7906
2	4	3313.80	4061.203	-8547.7	15175.29	0.9234
4	3	1159.49	3927.133	-10310.4	12629.40	0.9982
4	5	894.49	3927.133	-10575.4	12364.40	0.9994
5	3	265.00	3584.965	-10205.6	10735.55	1.0000

Oneway Analysis of insp A2 By Indent

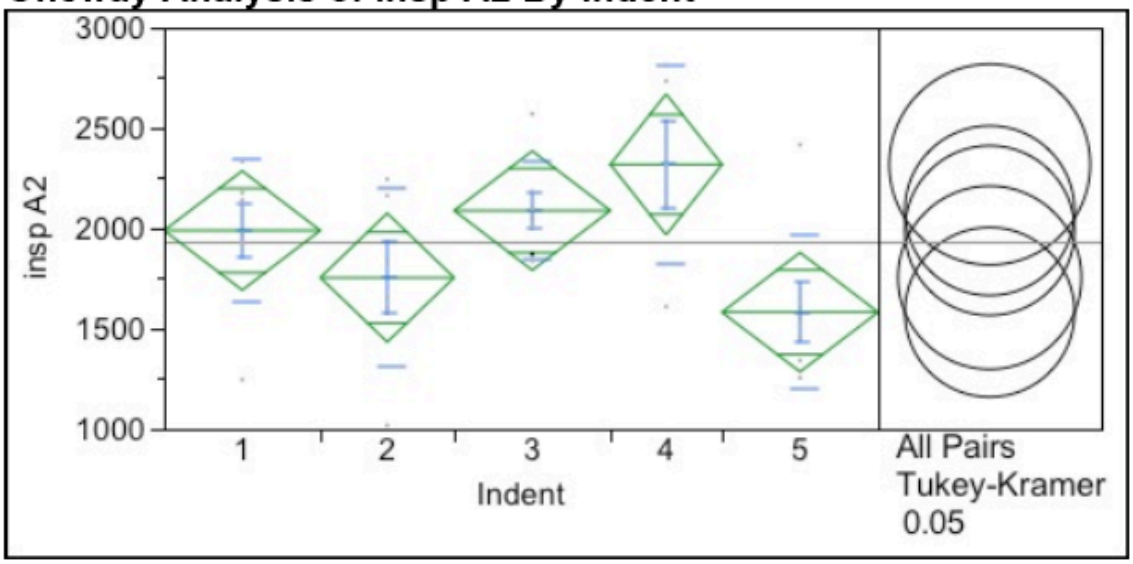

Excluded Rows
3

Oneway Anova
Summary of Fit

Rsquare	0.334003
Adj Rsquare	0.235336
Root Mean Square Error	382.9784
Mean of Response	1929
Observations (or Sum Wgts)	32

Analysis of Variance

Source	DF	Sum of Squares	Mean Square	F Ratio	Prob > F
Indent	4	1986047.5	496512	3.3852	0.0228*
Error	27	3960156.5	146672		
C. Total	31	5946204.0			

Means for Oneway Anova

Level	Number	Mean	Std Error	Lower 95%	Upper 95%
1	7	1989.00	144.75	1692.0	2286.0
2	6	1754.17	156.35	1433.4	2075.0
3	7	2088.14	144.75	1791.1	2385.1
4	5	2318.00	171.27	1966.6	2669.4
5	7	1581.86	144.75	1284.9	1878.9

Std Error uses a pooled estimate of error variance

Means and Std Deviations

Level	Number	Mean	Std Dev	Std Err Mean	Lower 95%	Upper 95%
1	7	1989.00	354.071	133.83	1661.5	2316.5
2	6	1754.17	444.858	181.61	1287.3	2221.0
3	7	2088.14	244.921	92.57	1861.6	2314.7
4	5	2318.00	490.804	219.49	1708.6	2927.4
5	7	1581.86	386.219	145.98	1224.7	1939.1

Means Comparisons

Comparisons for all pairs using Tukey-Kramer HSD

Ordered Differences Report

Level	- Level	Difference	Std Err Dif	Lower CL	Upper CL	p-Value
4	5	736.1429	224.2492	81.182	1391.104	0.0219*
4	2	563.8333	231.9049	-113.488	1241.155	0.1376
3	5	506.2857	204.7106	-91.609	1104.181	0.1269
1	5	407.1429	204.7106	-190.752	1005.038	0.2981
3	2	333.9762	213.0695	-288.333	956.285	0.5299
4	1	329.0000	224.2492	-325.961	983.961	0.5916
1	2	234.8333	213.0695	-387.475	857.142	0.8039
4	3	229.8571	224.2492	-425.104	884.818	0.8416
2	5	172.3095	213.0695	-449.999	794.618	0.9257

Oneway Analysis of insp Trel2 By Indent

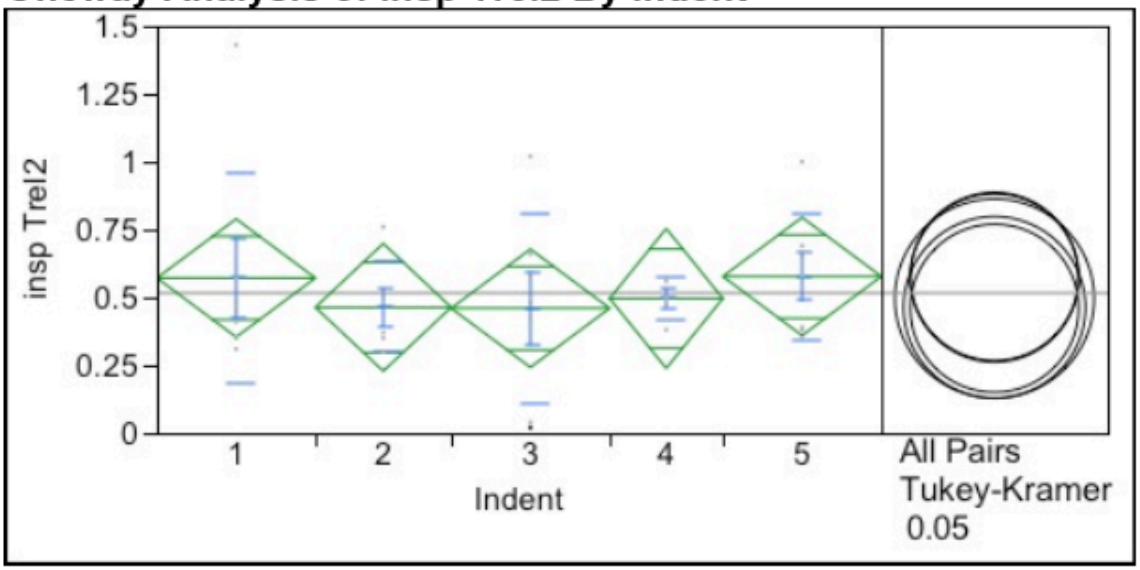

Excluded Rows
3

Oneway Anova
Summary of Fit

Rsquare	0.039815
Adj Rsquare	-0.10243
Root Mean Square Error	0.280785
Mean of Response	0.51625
Observations (or Sum Wgts)	32

Analysis of Variance

Source	DF	Sum of Squares	Mean Square	F Ratio	Prob > F
Indent	4	0.0882681	0.022067	0.2799	0.8884
Error	27	2.1286819	0.078840		

Source	DF	Sum of Squares	Mean Square	F Ratio	Prob > F
C. Total	31	2.2169500			

Means for Oneway Anova

Level	Number	Mean	Std Error	Lower 95%	Upper 95%
1	7	0.571429	0.10613	0.35367	0.78918
2	6	0.463333	0.11463	0.22813	0.69853
3	7	0.460000	0.10613	0.24225	0.67775
4	5	0.496000	0.12557	0.23835	0.75365
5	7	0.577143	0.10613	0.35939	0.79490

Std Error uses a pooled estimate of error variance

Means and Std Deviations

Level	Number	Mean	Std Dev	Std Err Mean	Lower 95%	Upper 95%
1	7	0.571429	0.388091	0.14668	0.21250	0.93035
2	6	0.463333	0.166693	0.06805	0.28840	0.63827
3	7	0.460000	0.351188	0.13274	0.13520	0.78480
4	5	0.496000	0.077006	0.03444	0.40038	0.59162
5	7	0.577143	0.231784	0.08761	0.36278	0.79151

Means Comparisons
Comparisons for all pairs using Tukey-Kramer HSD

Ordered Differences Report

Level	- Level	Difference	Std Err Dif	Lower CL	Upper CL	p-Value
5	3	0.1171429	0.1500858	-0.321210	0.5554960	0.9341
5	2	0.1138095	0.1562142	-0.342443	0.5700619	0.9479
1	3	0.1114286	0.1500858	-0.326925	0.5497817	0.9444
1	2	0.1080952	0.1562142	-0.348157	0.5643476	0.9565
5	4	0.0811429	0.1644107	-0.399049	0.5613347	0.9873

Level	- Level	Difference	Std Err Dif	Lower CL	Upper CL	p-Value
1	4	0.0754286	0.1644107	-0.404763	0.5556204	0.9904
4	3	0.0360000	0.1644107	-0.444192	0.5161918	0.9995
4	2	0.0326667	0.1700236	-0.463919	0.5292520	0.9997
5	1	0.0057143	0.1500858	-0.432639	0.4440674	1.0000
2	3	0.0033333	0.1562142	-0.452919	0.4595857	1.0000

Oneway Analysis of insp E2 By Indent

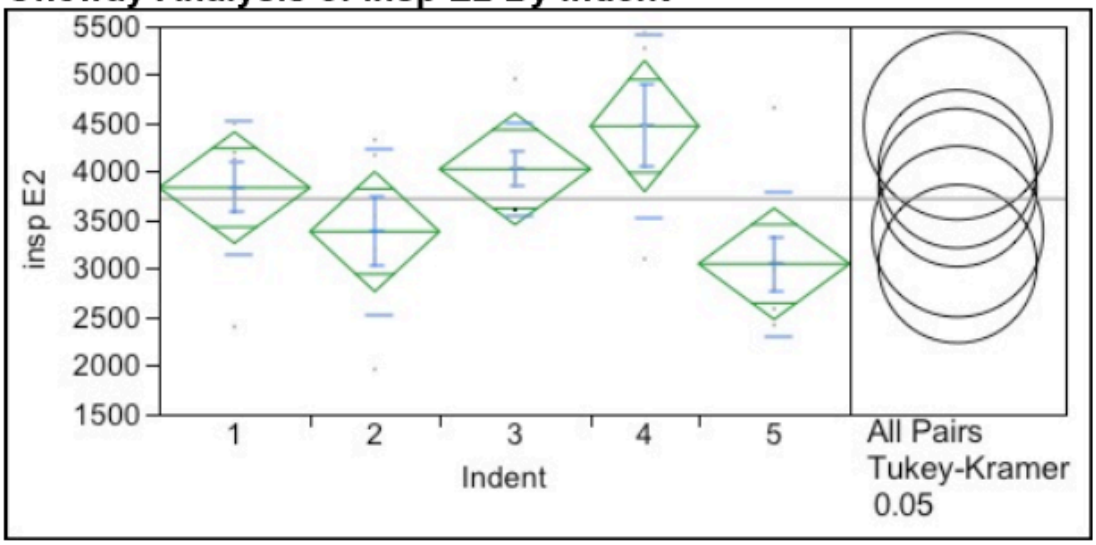

Excluded Rows
3

Oneway Anova
Summary of Fit

Rsquare	0.333937
Adj Rsquare	0.23526
Root Mean Square Error	738.7338
Mean of Response	3720.438
Observations (or Sum Wgts)	32

Analysis of Variance

Source	DF	Sum of Squares	Mean Square	F Ratio	Prob > F
Indent	4	7387338	1846834	3.3842	0.0228*
Error	27	14734646	545728		
C. Total	31	22121984			

Means for Oneway Anova

Level	Number	Mean	Std Error	Lower 95%	Upper 95%
1	7	3836.14	279.22	3263.2	4409.0
2	6	3383.33	301.59	2764.5	4002.1
3	7	4027.43	279.22	3454.5	4600.3
4	5	4470.60	330.37	3792.7	5148.5
5	7	3050.86	279.22	2478.0	3623.8

Std Error uses a pooled estimate of error variance

Means and Std Deviations

Level	Number	Mean	Std Dev	Std Err Mean	Lower 95%	Upper 95%
1	7	3836.14	682.975	258.14	3204.5	4467.8
2	6	3383.33	858.170	350.35	2482.7	4283.9
3	7	4027.43	472.377	178.54	3590.6	4464.3
4	5	4470.60	946.640	423.35	3295.2	5646.0
5	7	3050.86	745.016	281.59	2361.8	3739.9

Means Comparisons

Comparisons for all pairs using Tukey-Kramer HSD

Ordered Differences Report

Level	- Level	Difference	Std Err Dif	Lower CL	Upper CL	p-Value	
4	5	1419.743	432.5582	156.377	2683.109	0.0219*	⊏
4	2	1087.267	447.3255	-219.230	2393.763	0.1378	⊏

Level	- Level	Difference	Std Err Dif	Lower CL	Upper CL	p-Value
3	5	976.571	394.8698	-176.719	2129.862	0.1269
1	5	785.286	394.8698	-368.004	1938.576	0.2982
3	2	644.095	410.9935	-556.287	1844.478	0.5301
4	1	634.457	432.5582	-628.909	1897.823	0.5918
1	2	452.810	410.9935	-747.573	1653.192	0.8041
4	3	443.171	432.5582	-820.195	1706.538	0.8418
2	5	332.476	410.9935	-867.906	1532.859	0.9256
3	1	191.286	394.8698	-962.004	1344.576	0.9882

Oneway Analysis of insp Visc2 By Indent

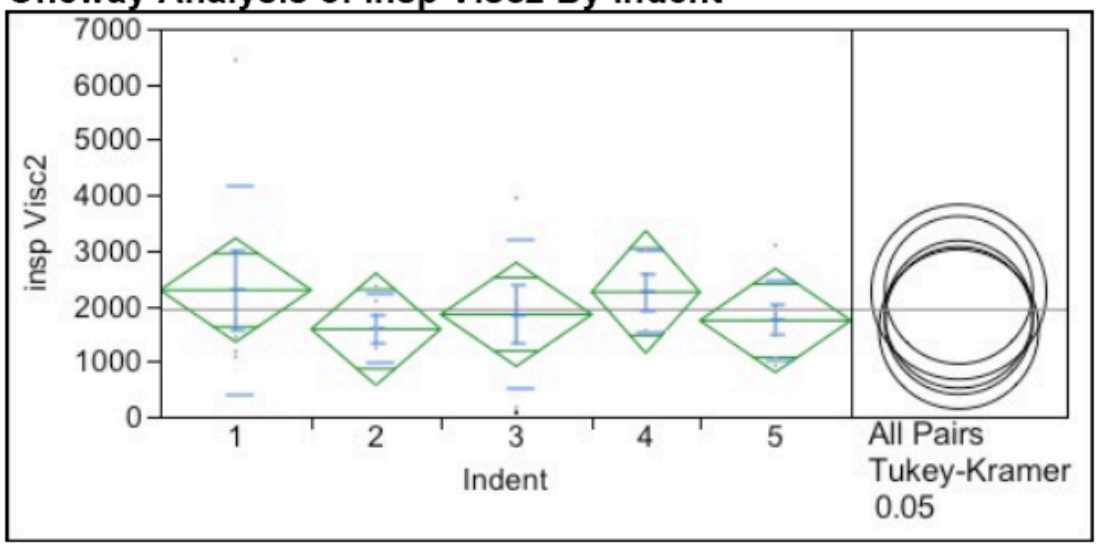

Excluded Rows
3

Oneway Anova
Summary of Fit

Rsquare	0.058672
Adj Rsquare	-0.08078
Root Mean Square Error	1207.094
Mean of Response	1930.031

Analysis of Variance

Source	DF	Sum of Squares	Mean Square	F Ratio	Prob > F
Indent	4	2452103	613026	0.4207	0.7922
Error	27	39341078	1457077		
C. Total	31	41793181			

Means for Oneway Anova

Level	Number	Mean	Std Error	Lower 95%	Upper 95%
1	7	2284.29	456.24	1348.2	3220.4
2	6	1577.67	492.79	566.5	2588.8
3	7	1845.00	456.24	908.9	2781.1
4	5	2249.60	539.83	1142.0	3357.2
5	7	1734.57	456.24	798.4	2670.7

Std Error uses a pooled estimate of error variance

Means and Std Deviations

Level	Number	Mean	Std Dev	Std Err Mean	Lower 95%	Upper 95%
1	7	2284.29	1879.21	710.28	546.3	4022.3
2	6	1577.67	623.97	254.74	922.8	2232.5
3	7	1845.00	1349.16	509.94	597.2	3092.8
4	5	2249.60	740.65	331.23	1330.0	3169.2
5	7	1734.57	717.63	271.24	1070.9	2398.3

Means Comparisons

Comparisons for all pairs using Tukey-Kramer HSD

Ordered Differences Report

Level	- Level	Difference	Std Err Dif	Lower CL	Upper CL	p-Value
1	2	706.6190	671.5653	-1254.81	2668.050	0.8287
4	2	671.9333	730.9320	-1462.89	2806.755	0.8870
1	5	549.7143	645.2191	-1334.77	2434.196	0.9116
4	5	515.0286	706.8021	-1549.32	2579.375	0.9479
1	3	439.2857	645.2191	-1445.20	2323.767	0.9589
4	3	404.6000	706.8021	-1659.75	2468.946	0.9780
3	2	267.3333	671.5653	-1694.10	2228.764	0.9944
5	2	156.9048	671.5653	-1804.53	2118.335	0.9993
3	5	110.4286	645.2191	-1774.05	1994.910	0.9998
1	4	34.6857	706.8021	-2029.66	2099.032	1.0000

Oneway Analysis of insp Aeq By Indent

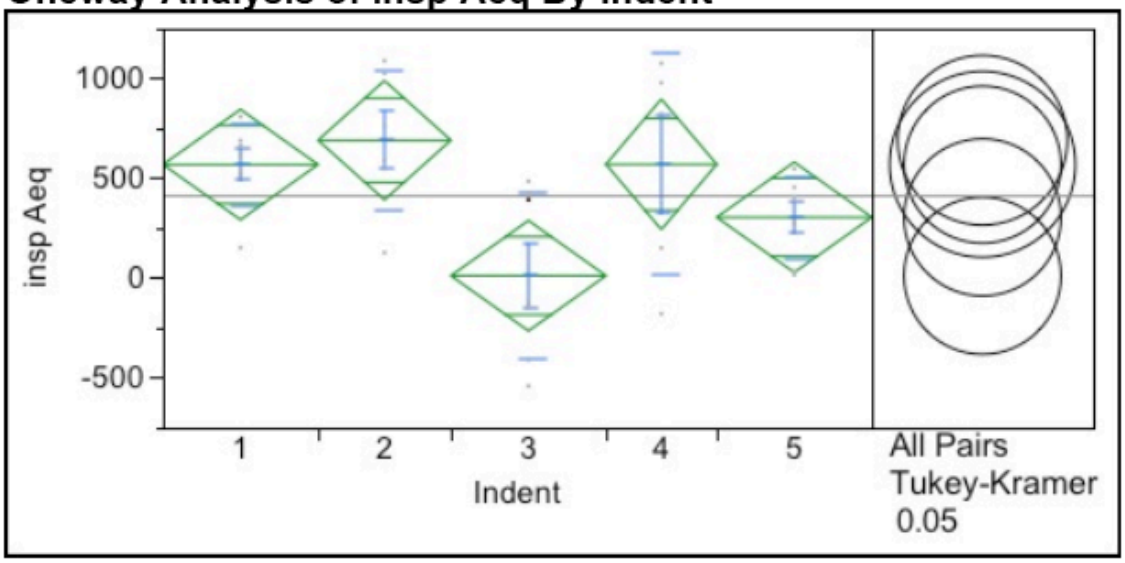

Excluded Rows
3

Oneway Anova
Summary of Fit

Rsquare	0.364016
Adj Rsquare	0.269796
Root Mean Square Error	356.6724
Mean of Response	412.0313
Observations (or Sum Wgts)	32

Analysis of Variance

Source	DF	Sum of Squares	Mean Square	F Ratio	Prob > F
Indent	4	1965970.8	491493	3.8635	0.0131*
Error	27	3434810.2	127215		
C. Total	31	5400781.0			

Means for Oneway Anova

Level	Number	Mean	Std Error	Lower 95%	Upper 95%
1	7	568.571	134.81	292.0	845.18
2	6	690.667	145.61	391.9	989.44
3	7	11.571	134.81	-265.0	288.18
4	5	570.000	159.51	242.7	897.28
5	7	304.286	134.81	27.7	580.89

Std Error uses a pooled estimate of error variance

Means and Std Deviations

Level	Number	Mean	Std Dev	Std Err Mean	Lower 95%	Upper 95%
1	7	568.571	209.063	79.02	375.2	761.9
2	6	690.667	353.617	144.36	319.6	1061.8
3	7	11.571	421.747	159.41	-378.5	401.6
4	5	570.000	553.077	247.34	-116.7	1256.7
5	7	304.286	206.777	78.15	113.0	495.5

Means Comparisons
Comparisons for all pairs using Tukey-Kramer HSD

Ordered Differences Report

Level	- Level	Difference	Std Err Dif	Lower CL	Upper CL	p-Value
2	3	679.0952	198.4342	99.532	1258.659	0.0157*
4	3	558.4286	208.8460	-51.545	1168.402	0.0848
1	3	557.0000	190.6494	0.173	1113.827	0.0499*
2	5	386.3810	198.4342	-193.183	965.945	0.3180
5	3	292.7143	190.6494	-264.112	849.541	0.5495
4	5	265.7143	208.8460	-344.259	875.687	0.7098
1	5	264.2857	190.6494	-292.541	821.112	0.6413
2	1	122.0952	198.4342	-457.468	701.659	0.9714
2	4	120.6667	215.9759	-510.131	751.464	0.9799
4	1	1.4286	208.8460	-608.545	611.402	1.0000

APPENDIX 4 - Experimental data force-time curves of the selected peak expiration force data points of all of the indentations analyzed

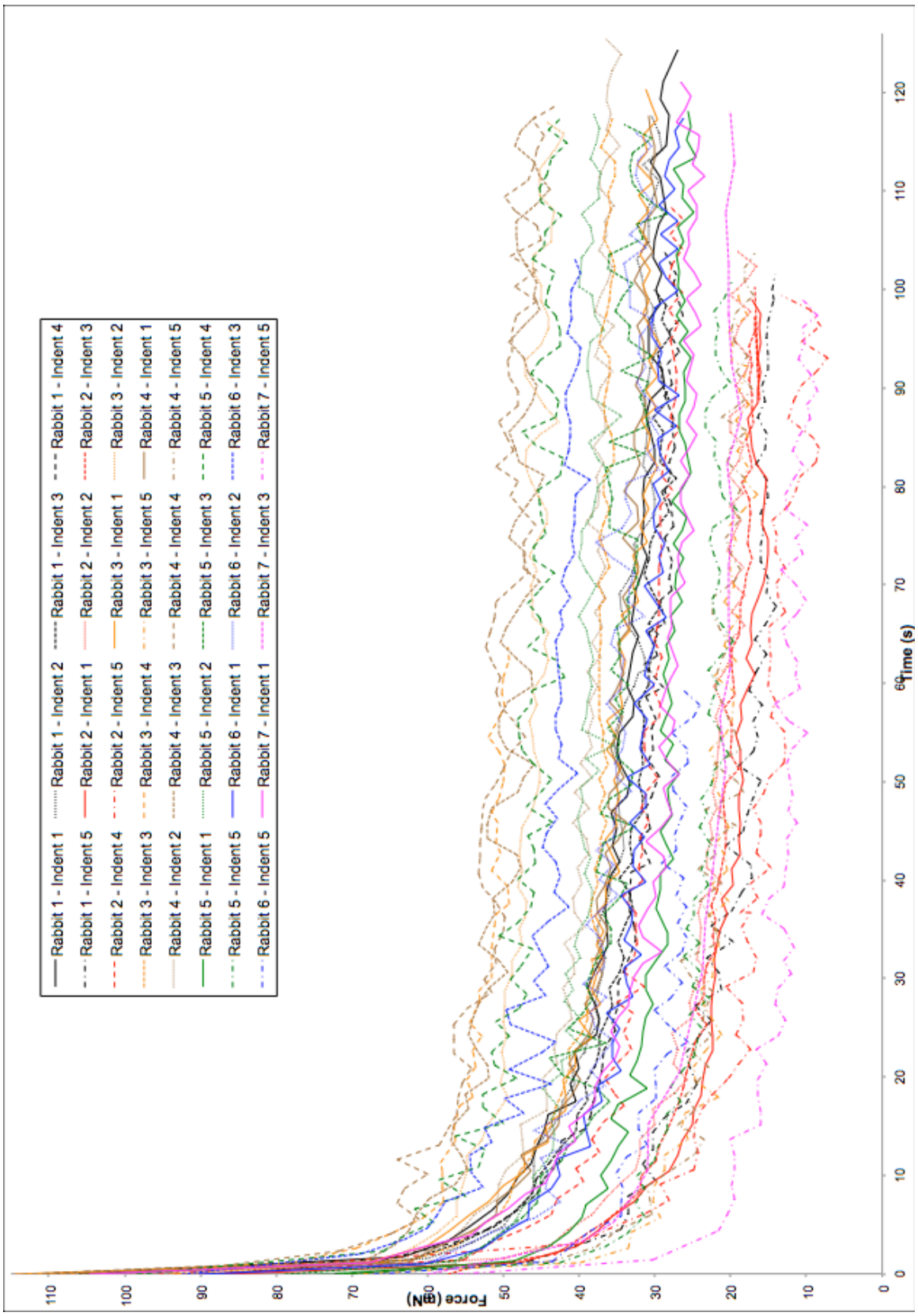
Rabbit 1 - Indent 1
Rabbit 1 - Indent 2
Rabbit 1 - Indent 3
Rabbit 1 - Indent 4
Rabbit 1 - Indent 5
Rabbit 2 - Indent 1
Rabbit 2 - Indent 2
Rabbit 2 - Indent 3
Rabbit 2 - Indent 4
Rabbit 2 - Indent 5
Rabbit 3 - Indent 1
Rabbit 3 - Indent 2
Rabbit 3 - Indent 3
Rabbit 3 - Indent 4
Rabbit 3 - Indent 5
Rabbit 4 - Indent 1
Rabbit 4 - Indent 2
Rabbit 4 - Indent 3
Rabbit 4 - Indent 4
Rabbit 4 - Indent 5
Rabbit 5 - Indent 1
Rabbit 5 - Indent 2
Rabbit 5 - Indent 3
Rabbit 5 - Indent 4
Rabbit 5 - Indent 5
Rabbit 6 - Indent 1
Rabbit 6 - Indent 2
Rabbit 6 - Indent 3
Rabbit 6 - Indent 5
Rabbit 7 - Indent 1
Rabbit 7 - Indent 3
Rabbit 7 - Indent 5
Force (mN)
Time (s)
0
10
20
30
40
50
60
70
80
90
100
110
120

APPENDIX 5 - Experimental data force-time curves of the selected maximal inspiration force data points of all of the indentations analyzed

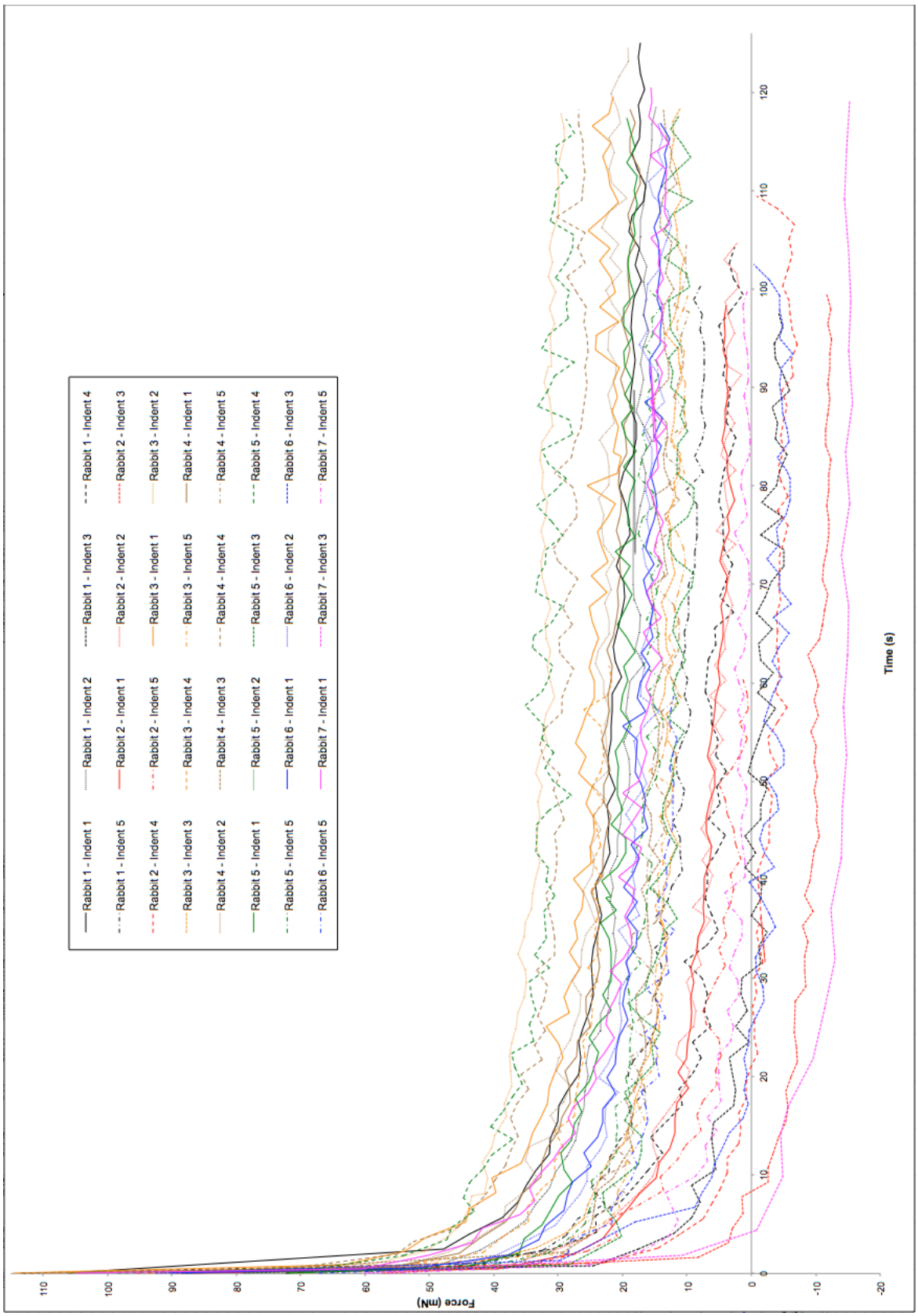
Rabbit 1 - Indent 1
Rabbit 1 - Indent 2
Rabbit 1 - Indent 3
Rabbit 1 - Indent 4
Rabbit 1 - Indent 5
Rabbit 2 - Indent 1
Rabbit 2 - Indent 2
Rabbit 2 - Indent 3
Rabbit 2 - Indent 4
Rabbit 2 - Indent 5
Rabbit 3 - Indent 1
Rabbit 3 - Indent 2
Rabbit 3 - Indent 3
Rabbit 3 - Indent 4
Rabbit 3 - Indent 5
Rabbit 4 - Indent 1
Rabbit 4 - Indent 2
Rabbit 4 - Indent 3
Rabbit 4 - Indent 4
Rabbit 4 - Indent 5
Rabbit 5 - Indent 1
Rabbit 5 - Indent 2
Rabbit 5 - Indent 3
Rabbit 5 - Indent 4
Rabbit 5 - Indent 5
Rabbit 6 - Indent 1
Rabbit 6 - Indent 2
Rabbit 6 - Indent 3
Rabbit 6 - Indent 5
Rabbit 7 - Indent 1
Rabbit 7 - Indent 3
Rabbit 7 - Indent 5
Force (mN)
Time (s)